October 1, 1994

Modeling of Rolling Element

Bearing Mechanics
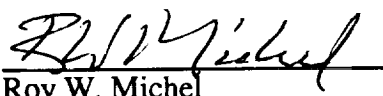
Contract NAS 8-38607
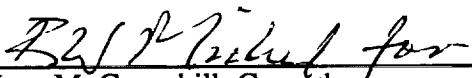
Theoretical Manual

Prepared For:

National Aeronautics and Space Administration
George C. Marshall Space Flight Center
Marshall Space Flight Center, AL 35812

Prepared By:

David H. Merchant, Principal Author
Senior Engineering Specialist
Product Analysis

Approved By:

Roy W. Michel
Program Manager
Strategic & Space Propulsion

Lyn M. Greenhill, Co-author
Chief Engineer
Rotordynamics-Seal Research
3628 Madison Avenue
North Highlands, CA 95660

GenCorp Aerojet
P.O. Box 13222
Sacramento, CA 95813-6000

RPT/I0062.149

10/17/94

TABLE OF CONTENTS

TABLE OF CONTENTS, CONTINUED

1. INTRODUCTION

This is the initial release of a theoretical manual for Version 1.10 of the NASA Rolling Element Bearing ANalysis System (REBANS) family of computer programs. Compared to other bearing analysis codes, REBANS offers improved capability to determine the quasi-static response to external loads or displacements for three types of high-speed rolling element bearings:

- angular contact ball bearings (single ball row),

- duplex angular contact ball bearings (dual ball row), and

- cylindrical roller bearings,

by including the effects of bearing ring and support structure flexibility. A finite element representation, prepared using Version 4.4 of ANSYS, is used for structure modeling. The current analysis system is composed of two main programs, the operation of which are referred to separately in a companion user's manual, are briefly described as follows:

PREBAN – PREprocessor for Bearing ANalysis, used to create and modify the two necessary input files for FEREBA, the main analysis program. This interactive code provides extensive on-line help for all model definition commands and examines input data for validity.

FEREBA – Flexibility Enhanced Rolling Element Bearing Analysis, the main analysis code, reads the files prepared by PREBAN and performs the requested analysis. The program may be run either interactively (with command line arguments) or batch, and prints a complete output file of results from the analysis.

The primary focus of this technical manual is the description of the theory that enables the flexibility enhanced quasi-static analysis. As such, all discussion in this manual is relative to the main analysis code FEREBA, a complete operating description of PREBAN is given in the User's Manual.

1.1 Development History

The genesis of FEREBA is taken from one the more recent computer programs developed to perform rolling element bearing quasi-static analysis – SHABERTH [1]*. This code was chosen as the development platform for several reasons:

- modular organization of source,
- availability of program documentation,
- use of standard bearing kinematic relations, and
- ability to analyze the types of bearings required.

SHABERTH, which is an acronym for **SH**aft and **BE**a**R**ing **TH**ermal analysis, has a long history of development, starting from the theory originally described by Jones [2], and subsequently modified by Harris [3]. In addition to the fundamental bearing mechanics analysis, SHABERTH also provides the capability for determining the load and temperature distribution for a shaft and bearing system, including the effects of lubrication and friction. These additional analysis features were not part of the development scope of FEREBA.

Although SHABERTH provides a sophisticated treatment of a shaft-bearing system, the only flexibility in the bearing analysis is due to contact (Hertzian) deformation. For bearings that are mounted into rigid housings, without any clearance radially or axially, considering only contact deformation is probably reasonable. However, seldom is a bearing installed with such an arrangement, and thus the question is raised regarding the influence of clearance and flexible rings on the load-deflection characteristics.

Recognizing the limitations of the rigid-ring theory, several authors have developed extended analyses that include the effect of ring flexibility. Filetti and Rumbarger [4] modeled the outer ring of a roller bearing with what is essentially curved-beam finite elements. Their calculations and experiments showed marked differences in roller load distribution between rigid and flexible ring models. Davis and Vallance [5], in a precursor effort to REBANS, developed a method using a finite element representation of the outer ring. Their results, for axial preload conditions only, showed increased axial motion of the inner ring, compared with rigid-ring calculations.

REBANS extends these previous efforts to consider general race and housing flexibility, including such effects as dead-band and preload springs. The intent of the analysis is to determine the load-deflection relationship for system comprised of shafting, the inner and outer rings, the rolling elements, and any significant supporting structure, all represented with 3D finite element models. In a sense, this system can be thought of as a "control volume" for bearing analysis.

---

* Numbers in brackets refer to the reference list given in Chapter 9 of this manual

1.2 Nomenclature

Throughout this theoretical description, the following symbols are used to describe physical quantities. A brief definition of the terms is also provided. Where possible, common notation used in traditional bearing mechanics has been retained.

A_{1j} Axial distance between *ORCC* and *IRCC* under load at ball *j*

A_{2j} Radial distance between *ORCC* and *IRCC* under load at ball *j*

B Total curvature for ball bearings

BD Initial distance between *IRCC* and *ORCC* in the unloaded mounted configuration

CD_k Crown drop (including roller crown and raceway crown) of kth slice of all rollers measured normal to roller

CS_1 Global coordinate system fixed in inertial space with origin at the center of an unloaded bearing, with Cartesian axes of *X-Y-Z*, cylindrical axes of *X-R-Φ*

CS_2 Primary bearing coordinate system which moves with the inner ring and shaft relative to the global inertial coordinate system (CS_1) with five degrees of freedom (Δx, Δy, Δz, θy, θz), with Cartesian axes of *x-y-z*, cylindrical axes of *x-r-ϕ*

D Unloaded rolling element diameter

D_m Diametral distance between rolling element centers in unmounted configuration (pitch diameter)

E_b, E_w Elastic (young's) modulus for ball and raceway, respectively

F_{cj} Centrifugal force on the jth ball directed along the positive *R* axis

F_{cxj} Component of F_{cj} directed along the *x*-axis

F_{crj} Component of F_{cj} directed along the *r*-axis

F_{ilj}, F_{irj} Radial force applied to left, right node in j^{th} azimuthal plane of inner raceway in inner ring elastic model

F_{olj}, F_{orj} Radial force applied to left, right node in j^{th} azimuthal plane of outer raceway in outer ring elastic model

F_{pre} Specified total axial preload force

G Vector of gap separation distances (either axial or radial dimension)

$IRCC$ Curvature center of a ball bearing inner raceway groove

K_d Jones axial deflection constant

K_{ij}, K_{oj} Hertzian contact stiffness between the jth ball or roller and the inner, outer raceway

L_i, L_o Effective roller length at inner, outer roller bearing raceway contact

M_{ij}, M_{oj} Total tilt moment about centroid of jth roller due to local roller contact forces at inner, outer raceway

n Number of rolling elements in a single, primary or duplex bearing

$ORCC$ Curvature center of a ball bearing outer raceway groove

P_{ij}, P_{oj} Total radial force applied to centroid of jth roller by inner, outer raceway

P_d Initial diametral clearance

Q_{ikj}, Q_{okj} Local radial force applied to k^{th} slice of jth roller by inner, outer raceway

r_i, r_o Radius of curvature of a ball bearing inner, outer raceway grooves

R_{cj} Radial component of constraint relation that determines if inner race is unloaded

R_i, R_o In the initially unloaded condition, locus radius of $IRCC$'s, $ORCC$'s for a ball bearing; radial distance from bearing center to inner, outer raceway for a roller bearing

x_{ok}, x_{ik} Distance along roller axis from roller centroid to center of kth slice measured along inner, outer raceway

X_{cj} Axial component of constraint relation that determines if inner race is unloaded

X_{cd} Inertial axial distance from the CS_1 origin to the $ORCC$ of a duplex bearing in the unloaded condition (the duplex bearing is initially located a positive distance X_{cd} along the X axis relative to the primary bearing)

X_{1j} Axial distance between ball center and $ORCC$ under load

X_{2j} Radial distance between ball center and $ORCC$ under load

α^o Initial (positive) contact angle for the primary bearing in the unloaded mounted configuration defined in CS_2

α_{ij}, α_{oj} Inner, outer race loaded contact angle at the jth azimuthal ball location defined in CS_2

α_p Initial (positive) contact angle for the primary bearing in the unloaded mounted configuration, defined in CS_2, under the action of specified axial preload

δd_{ij}, δd_{oj} Hertzian contact deflection of the ball and inner and outer race at the jth azimuthal ball location defined in CS_2

δn Hertzian contact deflection along the line of contact due to axial preload

δr_{ij} Radial elastic displacement of the $IRCC$ at the jth ball location defined in CS_2

δr_{pi}, δr_{po} Radial elastic displacement of inner, outer ring due to axial preload averaged around all ball locations

δr_{oj} Radial elastic displacement of the $ORCC$ at the jth ball location defined in CS_1

δx_{ij} Axial elastic displacement of the $IRCC$ at the jth ball location defined in CS_2

δx_{oj} Axial elastic displacement of the $ORCC$ at the jth ball location defined in CS_1

δx_{pi}, δx_{po} Axial elastic displacement of inner, outer ring due to axial preload averaged around all ball locations

δq_{ikj}, δq_{okj} Radial interference between inner, outer contact point at the kth slice on the jth roller and radially adjacent point on inner, outer raceway

δu_{ij}, δu_{oj} Elastic radial displacement of inner, outer raceway in j^{th} azimuthal plane

δr_{ij}, δr_{oj} Radial interference between center inner, outer contact point on j^{th} roller and radially adjacent point on inner raceway

δr_{ilj}, δr_{irj} Elastic radial deflection of left, right node in j^{th} azimuthal plane of inner raceway in roller bearing inner ring elastic model

δr_{olj}, δr_{orj} Elastic radial deflection of left, right node in j^{th} azimuthal plane of outer raceway in roller bearing outer ring elastic model

Nomenclature, continued

Δe — Inertial axial displacement of the CS_2 origin, relative to the CS_1 origin, required to bring a ball into contact with both races during mounting (also the inertial axial distance from the $ORCC$ to the $IRCC$ in the unloaded mounted condition)

Δp — Fixed axial displacement of inner ring due to axial preload

ΔP_d — Change in radial clearance due to temperature effects

Δr_j — Inertial radial displacement of centroid of jth roller in j^{th} azimuthal plane

Δu_{rj} — Total radial displacement of inner raceway in j^{th} azimuthal plane including elastic radial displacement

Δx — Rigid-body displacement of the CS_2 origin in the X-direction related to shaft/inner ring response to applied forces and moments

Δy — Rigid-body displacement of the CS_2 origin in the Y-direction related to shaft/inner ring response to applied forces and moments

ΔY — Inertial Y-axis displacement of inner ring and shaft

Δz — Rigid-body displacement of the CS_2 origin in the Z-direction related to shaft/inner ring response to applied forces and moments

ΔZ — Inertial Z-axis displacement of inner ring and shaft

$\Delta\theta_j$ — Total tilt rotation of inner raceway at j^{th} azimuthal plane (elastic plus imposed)

μ_b, μ_w — Poisson's ratio for ball and raceway, respectively

ϕ_j — Inertial tilt rotation of centroid of jth roller in j^{th} azimuthal plane

Φ_j — Azimuthal angle to the jth ball or roller location in the quasi-static analysis measured from the global inertial Y-axis (the planar kinematics used in the quasi-static analysis permits Φ to be considered identical in CS_1 and CS_2)

θ_{ij}, θ_{oj} — Elastic tilt rotation of inner, outer raceway in j^{th} azimuthal plane

$\theta y, \theta z$ — Rigid-body rotation of the CS_2 axes about the Y- or Z-axis related to shaft/inner ring response to applied forces and moments

$\theta Y, \theta Z$ — Rigid-body rotation of the inner ring and shaft about inertial Y- or Z-axis

subscript d — Appended to any symbol related to the primary bearing, the subscript d distinguishes the variable as being related to the duplex bearing

subscript p — Appended to any symbol, the subscript p indicates the variable is related to axial preload calculations

1–5

2. ASSUMPTIONS AND LIMITATIONS

The theoretical development described in this manual makes assumptions on the bearing system behavior and places limits on the extent of applicability as defined below:

1. The single ball/roller bearing or duplex angular contact ball bearing being studied has a nonrotating carrier with fixed supports and a single rotating shaft. The shaft rotates with constant angular velocity as required for a quasi-static analysis.

2. The shaft interfaces with the inner ring by means of a shrink fit with no clearance. Except for bearing systems with hollow shafts, elastic displacements of the inner ring and shaft are generally considered to contribute negligibly to bearing kinematics.

3. Inner ring relative structural displacements are obtained from a linear flexibility matrix constrained at the interface between the shaft and inner ring in the axial and tangential directions. If the shaft finite-element model is sufficiently detailed, potentially significant local radial deformations of a hollow shaft are accurately represented. Tangential elastic deflections of the inner ring are considered negligibly small.

4. Force-displacement relations for the outer ring and carrier are described by a single stiffness matrix with the associated assumptions such as small deflections and linear elastic material properties. The outer ring is connected to the carrier by soft springs joining coincident nodes across radial and axial gaps. These soft springs must have stiffnesses which guarantee that the spurious forces generated across open gaps will be negligible, and that the single stiffness matrix describing the outer ring and carrier can be inverted to form a flexibility matrix $[CO]$. Outer ring "rigid-body" displacements result from distortions of these soft springs.

5. Nonlinear effects due to radial and axial contact between the outer ring and the carrier are treated with the flexibility matrix using kinematic constraint relations. Due to chamfering, any point on the exterior of the outer ring can contact the carrier either in the radial direction or in the axial direction, but not in both directions simultaneously.

6. All forces generated by the cage and all dissipative forces are neglected for the quasi-static analysis. The quasi-static analysis, based on the classical approach of Jones [2] and Harris [3], determines elastic forces and deflections with balls located in their evenly spaced idealized positions.

7. No transient thermal effects will be considered. Steady-state thermal effects are considered in the quasi-static analysis only to the extent of dimensional change.

Permitted motions of the inner ring consist of five degree-of-freedom (DOF) rigid-body motion combined with elastic structural deflections of the inner ring relative to the shaft motions. Rigid-body motion of the inner ring is described by small displacements (Δx, Δy, Δz) and small rotations (θy, θz) of a reference frame (CS_2) fixed at the shaft center and able to move relative to the fixed global inertial reference frame (CS_1). These five rigid-body freedoms are considered to result

from general shaft bending and axial displacement. Elastic displacements of the inner ring relative to (CS_2) are determined from a flexibility matrix [CI].

2.1   Solution Methodology

The SHABERTH quasi-static iteration determines rolling element equilibrium and inner ring deflections to match applied forces. To incorporate general structural flexibility into the analysis, an iterative solution methodology is used that involves dividing the analysis into three sequential steps:

1. With the outer ring fixed in inertial space and the elastic deflection of the inner ring specified, ball forces on the inner and outer races are calculated in terms of assumed values of the five rigid-body displacements of the inner ring and shaft. This step follows essentially the classical quasi-static bearing analysis of Jones [2] and Harris [3] except that all displacements, except for the Hertzian ball-race contact deflections, are considered fixed during each iteration. The nonlinear equations are solved using a Newton-Raphson technique with the required partial derivatives expressed numerically.

2. Calculated ball forces on the inner race are applied to the flexibility matrix of the inner ring and shaft [CI] to determine the corresponding elastic deflections of the inner race curvature centers. These ball forces on the inner race are also summed to determine total forces and moments, at the origin of the global inertial reference frame (CS_1), for comparison in Step 3 with the input applied forces and moments. Calculated ball forces on the outer race are applied to the flexibility matrix of the outer ring and carrier [CO], using a nonlinear iterative procedure to identify points of contact. The result of this iterative procedure is the "rigid-body" and elastic deflections of the outer race curvature centers corresponding to the forces applied to the outer race.

3. Given the deflections of the inner and outer rings corresponding to the ball forces applied to the inner and outer races, the differences between the input applied forces and moments and the previously calculated forces and moments are used to revise the values of the five rigid-body displacements of the inner ring and shaft. This step follows essentially the tangent-compliance method of Davis and Vallance [5] except that the system compliance matrix does not contain the outer ring flexibilities. Increments of the five displacements of the inner ring and shaft corresponding to outer ring displacements are determined from "rigid-body" displacements of the outer ring in terms of a least-squares fit.

Examining the flexibility enhanced iteration, as described by these three steps, at least one and possibly two more iterative loops are required to obtain a solution. The outermost loop is described by Step 3. If a nonlinear outer race model is used, another loop is required to determine displacements with gaps. Thus a total of 4 nested iterations are performed by FEREBA. Note that the elastic deflections of the inner ring and outer ring lag the calculated ball-race forces by one iteration. If a reasonable error is given to the elastic displacement iteration, this difference is minor.

2.2 Kinematic Relations

The kinematics of static contact between a rolling element and race require that, for a ball bearing, each race curvature center be on a straight line extending from the ball-race contact point through the ball center. A similar relationship holds for a roller bearing. For small displacements in the tangential (azimuth) direction, a planar relation of both contact forces directed through the rolling element center must hold. This planar kinematic relation is basic to the classical quasi-static analysis, and is illustrated in Figure 2-1 for a ball bearing.
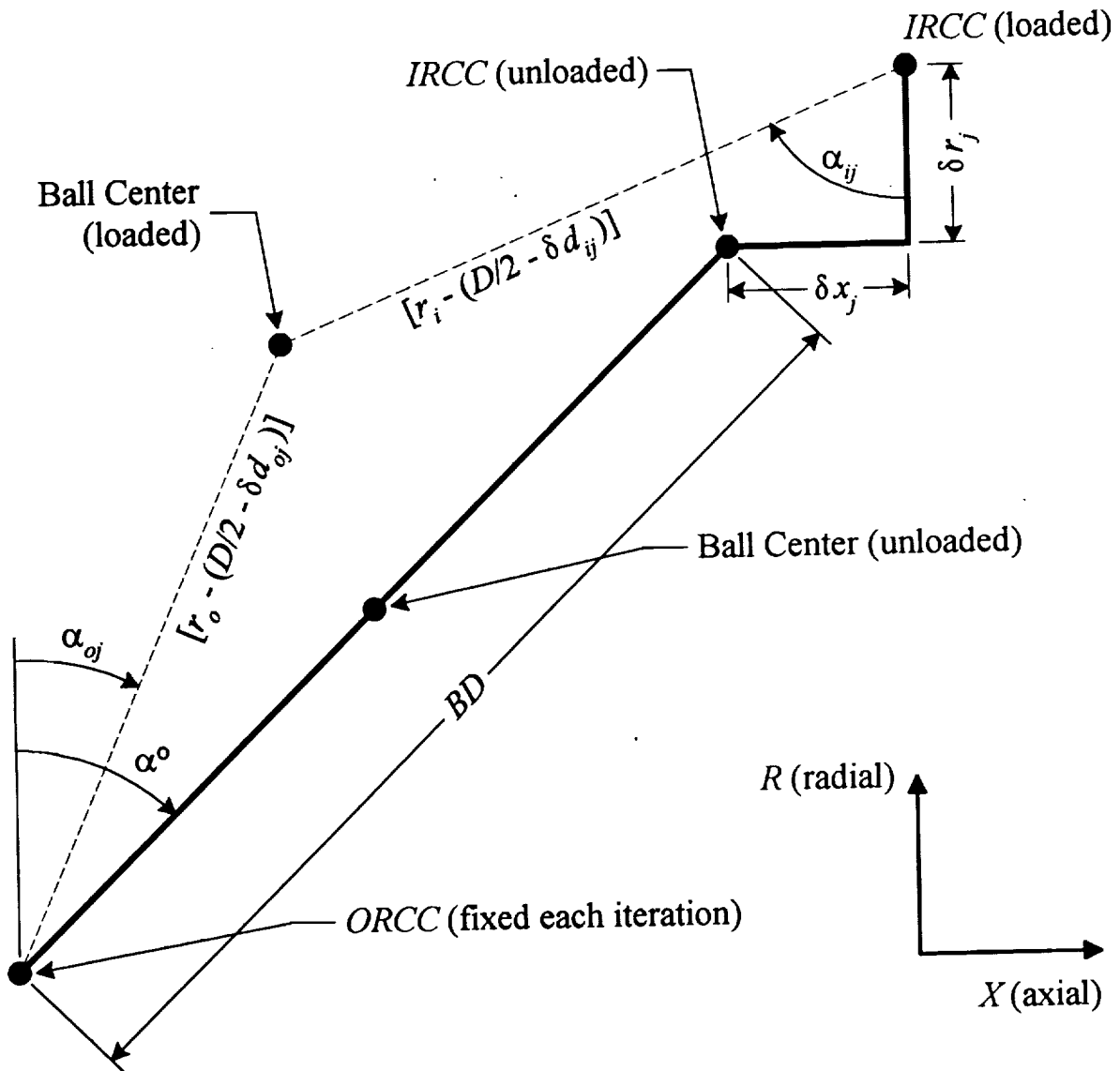
Figure 2-1 Planar kinematic diagram for ball bearings

Therefore, there are no first-order effects on kinematics of small motions in the tangential direction. There are, however, second-order effects by which tangential displacements of the inner ring affect slightly the radial and axial locations of the outer race curvature center in inertial space when determined from the inner ring. The radial incremental displacement due to the inner

The basic approach of Jones [2] and Harris [3] can therefore be followed with regard to the two-dimensional kinematic relations expressed in their planar diagram. However, for the present quasi-static analysis, several additional small terms involving rigid-body displacements and structural deflections must be included among the primary δx and δr displacement effects.

2.3 Use of Finite Element Models

Flexibility effects of the inner ring and shaft and of the outer ring and carrier are represented by structural finite-element models (FEMs) generated by Version 4.4 of ANSYS [5]. The FEMs are input to the bearing mechanics code in the form of stiffness matrices in *cylindrical* coordinates. The stiffness matrices are manipulated as required and inverted in the bearing mechanics code to form the desired flexibility matrices in cylindrical coordinates.

The elastic deflections of the inner ring are determined from a flexibility matrix $[CI]$ in which points at the ring/shaft interface are constrained in the tangential and axial directions. The resulting calculations for inner ring deflections due to ball-race contact forces are straightforward and linear. Assuming a shrink fit without clearance for the ring/shaft interface precludes any complicated nonlinear effects for this structural model.

The elastic deflections of the outer ring are determined from a flexibility matrix $[CO]$ of the outer ring and carrier constrained at the bearing supports. Three different models are considered for the radial and axial interfaces between the outer ring and carrier:
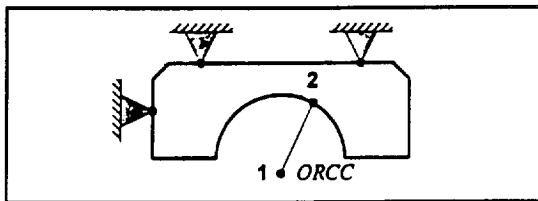
Figure 2-2 Outer Ring/Carrier Model 1
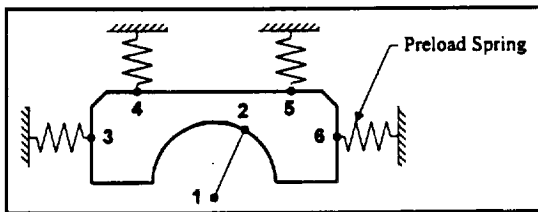
Figure 2-3 Outer Ring/Carrier Model 2
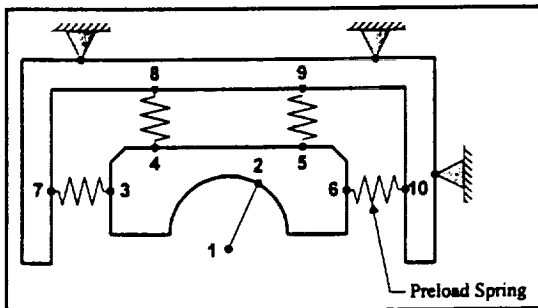
Figure 2-4 Outer Ring/Carrier Model 3

1. A linear model has the outer ring rigidly connected to the carrier at the radial and axial interface nodes, as shown in Figure 2-2 for a ball bearing. The outer ring undergoes elastic motions influenced by the carrier flexibility.

2. The first nonlinear model, illustrated in Figure 2-3, has the outer ring connected to a rigid carrier at the interface nodes by soft springs, except for an optional preload spring. The outer ring can undergo general "rigid-body" and elastic motions relative to the rigid carrier.

3. The general nonlinear model, as shown in Figure 2-4, has the outer ring connected to the flexible carrier at the interface nodes by soft springs, except for an optional preload spring. The outer ring then undergoes general "rigid-body" and elastic motions influenced by the carrier flexibility.

2-4

For all three models, the outer ring and carrier FEMs are modeled with separate nodes across the gaps at the interfaces. The first model has the outer ring and carrier FEMs rigidly connected (i.e. grounded) at the interface nodes. The second model has the outer ring FEM connected to ground by soft springs at the interfaces, except for the use of an optional preload spring. The third model has the outer ring and carrier FEMs connected by soft springs at the interface nodes, with the possible use of finite stiffness preload spring. Clearances between the outer ring and carrier are input to the bearing mechanics code for the two nonlinear models. Gaps are positive clearances, and interferences are negative clearances.

For the general nonlinear structural model, the solution technique, as described in section 1 of this chapter, initially identifies contact points in the radial or axial directions between the outer ring and carrier. Using the contact points, linear outer-ring deflections are calculated from the ball-race contact forces using the $[CO]$ flexibility matrix with appropriate constraint relations using an iterative procedure. This general method directly accommodates axial preload effects, centrifugal force effects, and nonlinear effects due to clearance between the outer ring and carrier (deadband). Interference fits are evaluated by using negative clearance distances.

3. REPRESENTATION OF BEARING FLEXIBILITIES

The structural flexibility characteristics of the bearing inner ring(s), outer ring(s) and carrier are developed using Version 4.4 of the ANSYS structural analysis code [5]. A total of nine configurations are defined for the outer ring(s) and carrier for single ball bearing, duplex ball bearing set, and cylindrical roller bearing. A total of three configurations are defined for the inner ring(s) and shaft of the same ball and roller bearings.

Stiffness matrices for the ball bearing configuations have a separate node for each outer race curvature center (ORCC) in the outer ring model and for each inner race curvature center (IRCC) in the inner ring model. These ORCC and IRCC nodes are connected to the ANSYS structural model for the appropriate ring by two 3-D spar elements (STIF8) in each azimuthal plane. This modeling concept allows a statically-determinate three-hinged arch to approximate the ORCC and IRCC planar kinematics due to elastic distortions of the rings. The ORCC and IRCC elastic deflections computed in this manner are then essentially independent of the local Hertzian contact deflections at the ball/raceway contact points. With this approach, the total bearing flexibility is properly determined by combining the separate effects of Hertzian contact deflections with ORCC/IRCC elastic structural deflections.

Stiffness matrices for the cylindrical roller bearing configuration have two radial degrees of freedom (DOFs) for each rolling element on its lines of contact with each raceway. These two radial DOFs are the points of application of the equivalent roller Hertzian line contact forces and the points where radial structural deflections are determined. At each azimuthal plane, the two radial structural elastic deflections are converted to an elastic radial deflection and an elastic tilt angle for subsequent use in kinematic constraint relations and roller contact force calculations. To separate the effects of Hertzian line contact deflections from raceway structural deflections, multiple adjacent nodes along the contact line near each retained raceway DOF are "coupled" in ANSYS to move together in the radial direction.

For the inner ring(s) and shaft, stiffness matrices are generated in ANSYS using cylindrical coordinates having the order $(R_A \; \theta_A \; Z_A)$. These stiffness matrices have appropriate fixed constraints imposed in ANSYS at the inner ring/shaft interface to permit the shaft/inner ring flexibility influence coefficient matrix to be formed. A set of master nodes are specified and the substructure option is run to obtain a reduced matrix. In FEREBA, the constrained ANSYS and substructured stiffness matrix is then transformed into the FEREBA cylindrical coordinates system $(X_F \; R_F \; \theta_F)$ prior to eliminating unnecessary DOFs by another matrix condensation. After the stiffness matrix is reduced, it is inverted to form the flexibility matrix [CI] which is then partitioned for convenient use in subsequent computations.

Stiffness matrices for the outer ring(s) and carrier are generated in ANSYS in cylindrical coordinates with outer ring(s) unconstrained. The carrier stiffness matrix, where applicable, is supported with appropriate fixed constraints consistent with the design. After being substructured, the total ANSYS stiffness matrix is read into FEREBA and then transformed into FEREBA cylindrical coordinates. The stiffness matrix for the outer ring(s) is connected to ground or to the carrier by soft springs (3 DOF/node) at each candidate contact point except preload spring locations and, where applicable, by axial preload springs at the preload location in

3-1

each azimuthal plane. The constrained stiffness matrix is then reduced to eliminate unnecessary DOFs and inverted to form the flexibility matrix $[CO]$. This matrix is then separated into four partitions, in general, for convenient use in subsequent computations.

The substructure information written by ANSYS is in binary format, and in general, is ordered along the wavefront pattern. The REBANS preprocessor PREBAN reads the binary data, and sorts the information in ascending order. This substructure matrix is output from PREBAN in ASCII format, using the highest precision available for 32-bit computers. The ASCII format was selected to enable the stiffness matrix to be transferred between different computing platforms.

3.1 Bearing/Support Configurations

The nine bearing/support configurations for the outer ring and carrier are designated by IBSCOR (index) values one through nine. The three bearing/support configurations for the inner ring and shaft are designated by IBSCIR values one through three. In the following figures which define these 12 configurations, master DOFs in both ANSYS and FEREBA are listed with n referring to the number of rolling element azimuthal planes. Node ordering and, where applicable, gap ordering in each azimuthal plane are also indicated. These specified node and gap orderings associated with the IBSCOR/IBSCIR indices are used in several subsequent numerical computations.

1. Single ball bearing with flexible outer ring and/or carrier and no deadband (IBSCOR = 1). This model is linear. There are no gaps between the outer ring rigid housing, and at each azimuthal position, 2 master nodes are required. After reduction in FEREBA, four DOFs remain at each ball location (2 axial, 2 radial).
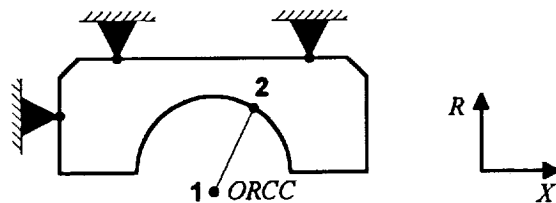
Active DOFs

ANSYS $6 \cdot n$ (X, Y, Z)

FEREBA $4 \cdot n$ (X, R)

Active Nodes (DOFs)

X: 1, 2 (1, 4)

R: 1, 2 (2, 5)

Reduced DOFs

3*, 6

* DOF 3 is deleted

2. Single ball bearing, flexible outer ring with deadband, carrier assumed rigid (IBSCOR = 2). This model is nonlinear due to deadband contact, which is dependent on ball loads applied to the outer race. There are four gaps between the outer ring and rigid housing, and at each azimuthal position, 6 master nodes are required. After reduction in FEREBA, eight DOFs remain at each ball location (4 axial, 4 radial).
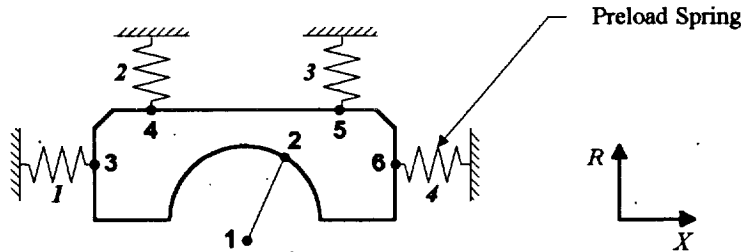
Active DOFs

ANSYS $18 \cdot n$ (X, Y, Z)

FEREBA $8 \cdot n$ (X, R)

Active Nodes (DOFs)

X: 1, 2, 3, 6 (1, 4, 7, 16)

R: 1, 2, 4, 5 (2, 5, 11, 14)

Reduced DOFs

3*, 6, 8, 9, 10, 12, 13, 15, 17, 18

* DOF 3 is deleted

3. Single ball bearing with flexible outer ring and carrier with deadband (IBSCOR = 3). This model is nonlinear due to deadband contact, which is dependent on ball loads applied to the outer race, and also due to the preload spring (nodes 6 - 10), which can bottom. There are four gaps between the outer ring and carrier, and at each azimuthal position, 10 master nodes are required (6 on the outer ring, 4 on the carrier). After reduction in FEREBA, twelve DOFs remain at each ball location (6 axial, 6 radial).
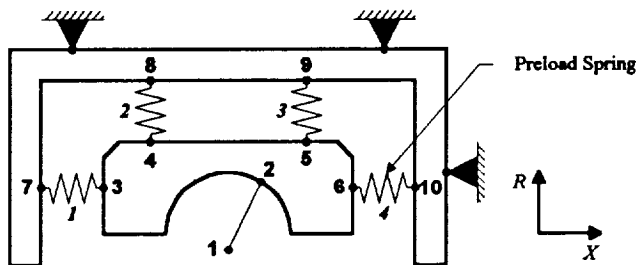
Active DOFs

ANSYS $30 \cdot n$ (X, Y, Z)
FEREBA $12 \cdot n$ (X, R)

Active Nodes (DOFs)

X: 1, 2, 3, 6, 7, 10
    (1, 4, 7, 16, 19, 28)

R: 1, 2, 4, 5, 8, 9
    (2, 5, 11, 14, 23, 26)

Reduced DOFs

3*, 6, 8, 9, 10, 12, 13, 15, 17, 18, 20, 21, 22, 24, 25, 27, 29, 30
* DOF 3 is deleted

4. Duplex ball bearing set with flexible outer rings and carrier with no deadband (IBSCOR = 4). The analysis is restricted to having n equal in both bearings. This model is nonlinear because the preload spring (3 - 6) could bottom. There is only one gap between the outer rings, with the primary bearing free to move axially (but not radially). At each azimuthal position, 6 master nodes are required (3 for each ring). After reduction in FEREBA, ten DOFs remain at each ball location (6 axial, 4 radial).
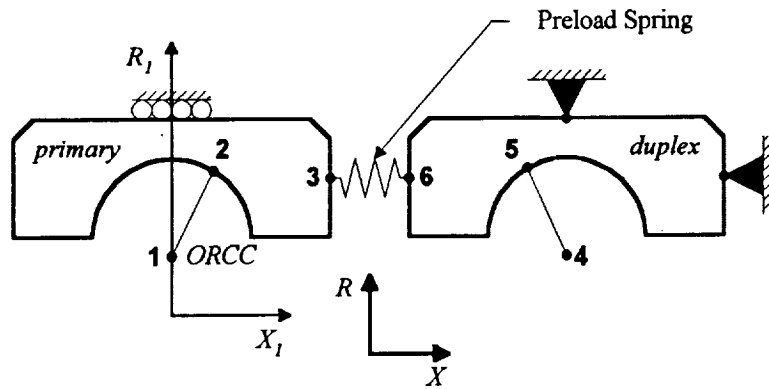
Active DOFs

ANSYS $18 \cdot n$ (X, Y, Z)

FEREBA $10 \cdot n$ (X, R)

Active Nodes (DOFs)

X: 1 - 6 (1, 4, 7, 10, 13, 16)

R: 1, 2, 4, 5 (2, 5, 11, 14)

Reduced DOFs

3*, 6, 8, 9, 12*, 15, 17, 18

* DOFs 3 & 12 are deleted

Note the relative positions of "*primary*" and "*duplex*" bearings.

5. Duplex ball bearing set with flexible outer rings with deadband and with carrier assumed rigid (IBSCOR = 5). The analysis is restricted to having n equal in both bearings. This model is nonlinear due to deadband contact and the possibility that the preload spring (6 - 9) could bottom. There are seven gaps between the outer ring and rigid housing, and at each azimuthal position, 12 master nodes are required (6 on each bearing). After reduction in FEREBA, sixteen DOFs remain at each ball location (8 axial, 8 radial).
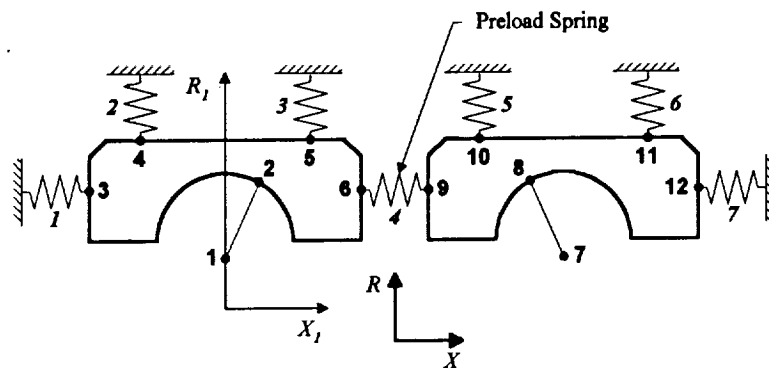
Active DOFs

ANSYS $36 \cdot n$ (X, Y, Z)

FEREBA $16 \cdot n$ (X, R)

Active Nodes (DOFs)

X: 1, 2, 3, 6, 7, 8, 9, 12
    (1, 4, 7, 16, 19, 22, 25, 34)

R: 1, 2, 4, 5, 7, 8, 10, 11
    (2, 5, 11, 14, 20, 23, 29, 32)

Reduced DOFs

3*, 6, 8, 9, 10, 12, 13, 15, 17, 18, 21*, 24, 26, 27, 28, 30, 31, 33, 35, 36

* DOFs 3 & 21 are deleted

The relative positions of the "*primary*" and "*duplex*" bearings is the same as configuration 4.

3–4

6. Duplex ball bearing set with flexible outer rings and carrier with deadband (IBSCOR = 6). The analysis is restricted to having n equal in both bearings. This model is nonlinear due to deadband contact and the possibility that the preload spring (6 - 9) could bottom. There are seven gaps between the outer ring and carrier, and at each azimuthal position, 18 master nodes are required (6 on each bearing and 6 on the carrier). After reduction in FEREBA, twenty two DOFs remain at each ball location (10 axial, 12 radial).
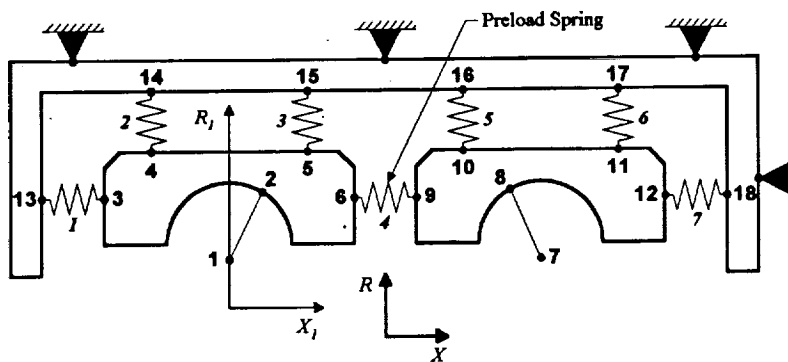
Active DOFs

ANSYS   54·n (X, Y, Z)

FEREBA   22·n (X, R)

Active Nodes (DOFs)

X: 1, 2, 3, 6, 7, 8, 9, 12, 13, 18
    (1, 4, 7, 16, 19, 22, 25, 34,
    37, 52)

R: 1, 2, 4, 5, 7, 8, 10, 11, 14,
    15, 16, 17 (2, 5, 11, 14,
    20, 23, 29, 32, 41, 44, 47,
    50)

Reduced DOFs

3*, 6, 8, 9, 10, 12, 13, 15, 17,
18, 21*, 24, 26, 27, 28, 30, 31,
33, 35, 36, 38, 39, 40, 42, 43,
45, 46, 48, 49, 51, 53, 54

* DOFs 3 & 21 are deleted

The relative positions of the "*primary*" and "*duplex*" bearings is the same as configuration 4.

7. Cylindrical roller bearing with flexible outer ring and carrier, no deadband (IBSCOR = 7). This model is linear. There are no gaps between the outer ring rigid housing, and at each azimuthal position, 2 master nodes are required. After reduction in FEREBA, two radial DOFs remain at each roller location.
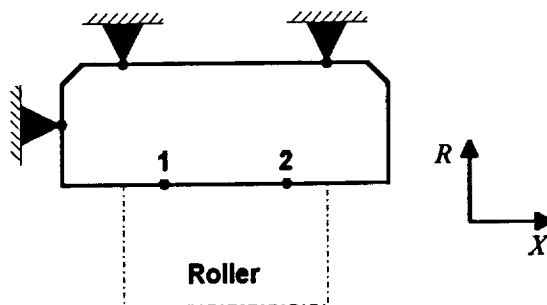
Active DOFs

ANSYS   6·n (X, Y, Z)

FEREBA   2·n (R)

Active Nodes (DOFs)

X: none

R: 1, 2 (2, 5)

Reduced DOFs

1, 3, 4, 6

The radial force and corresponding moment about the axial centerline will be represented by two unequal radial forces at master nodes 1 & 2.

8. Cylindrical roller bearing with flexible outer ring with deadband and with carrier assumed rigid (IBSCOR = 8). This model is nonlinear due to deadband contact. There are two gaps between the outer ring and rigid housing, and at each azimuthal position, 4 master nodes are required. After reduction in FEREBA, four radial DOFs remain at each roller location.
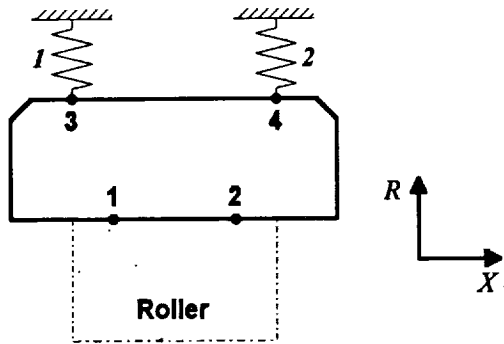
Active DOFs

ANSYS $12 \cdot n$ (X, Y, Z)

FEREBA $4 \cdot n$ (R)

Active Nodes (DOFs)

X: none

R: 1, 2, 3, 4 (2, 5, 8, 11)

Reduced DOFs

1, 3, 4, 6, 7, 9, 10, 12

9. Cylindrical roller bearing with flexible outer ring and carrier with deadband (IBSCOR = 9). This model is nonlinear due to deadband contact. There are two gaps between the outer ring and carrier, and at each azimuthal position, 6 master nodes are required (4 on the bearing and 2 on the carrier). After reduction in FEREBA, six radial DOFs remain at each roller location.
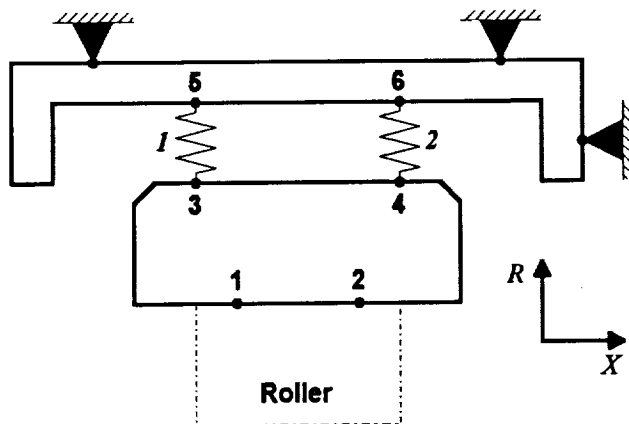
Active DOFs

ANSYS $18 \cdot n$ (X, Y, Z)

FEREBA $6 \cdot n$ (R)

Active Nodes (DOFs)

X: none

R: 1 - 6 (2, 5, 8, 11, 14, 17)

Reduced DOFs

1, 3, 4, 6, 7, 9, 10, 12,

13, 15, 16, 18

10. Single ball bearing with flexible or rigid shaft (IBSCIR = 1). This model is linear. The inner ring is assumed to be fixed to the shaft. After reduction in FEREBA, four DOFs remain at each ball location (2 axial, 2 radial).
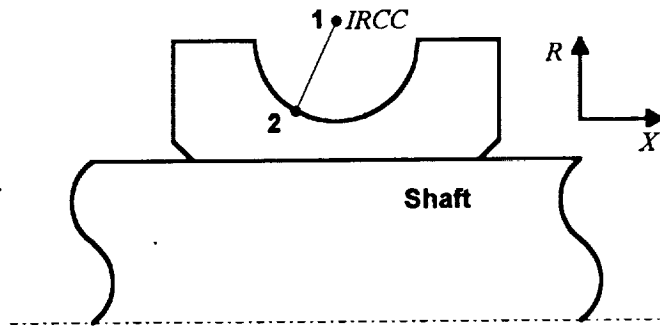
Active DOFs

ANSYS $6 \cdot n$ (X, Y, Z)

FEREBA $4 \cdot n$ (X, R)

Active Nodes (DOFs)

X: 1, 2 (1, 4)

R: 1, 2 (2, 5)

Reduced DOFs

3*, 6

* DOF 3 is deleted

11. Duplex ball bearing set with flexible or rigid shaft (IBSCIR = 2). The analysis is restricted to having n equal in both bearings. This model is linear, with the inner rings fixed to the shaft. After reduction in FEREBA, eight DOFs remain at each ball location (4 axial, 4 radial).
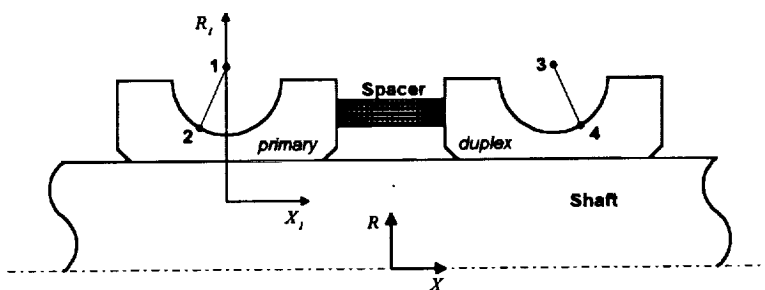
Active DOFs

ANSYS $12 \cdot n$ (X, Y, Z)

FEREBA $8 \cdot n$ (X, R)

Active Nodes (DOFs)

X: 1, 2, 3, 4 (1, 4, 7, 10)

R: 1, 2, 3, 4 (2, 5, 8, 11)

Reduced DOFs

3*, 6, 9*, 12

* DOFs 3 & 9 are deleted

Note the relative positions of "*primary*" and "*duplex*" bearings.

12. Cylindrical roller bearing with flexible or rigid shaft (IBSCIR = 3). This model is linear. The inner ring is assumed to be fixed to the shaft.
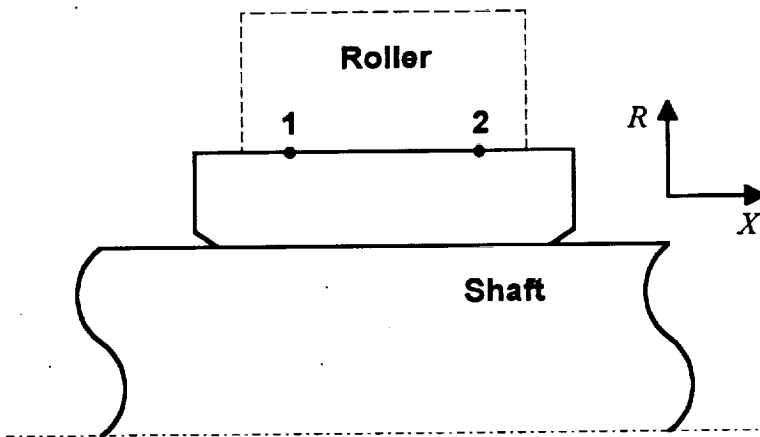
Active DOFs

ANSYS $6 \cdot n$ (X, Y, Z)

FEREBA $2 \cdot n$ (R)

Active Nodes (DOFs)

X: none

R: 1, 2 (2, 5)

Reduced DOFs

1, 3, 4, 6

The radial force and corresponding moment about the axial centerline will be represented by two unequal radial forces.

3.2 Inner Ring/Shaft Finite-Element Models

The ANSYS structural model of the inner ring(s) and shaft is generated in cylindrical coordinates having the ANSYS order $(R_A \; \theta_A \; Z_A)$. The shaft/inner ring free-free stiffness matrix must be constrained such that the relative elastic deflections from the flexibility matrix $[CI]$ can subsequently be added properly to the rigid-body inertial displacements defined in the shaft coordinate system CS_2. For single ball or roller bearings or primary bearings of a duplex set, the axial and tangential DOFs are fixed against displacement at the interface between the shaft and inner rings. To represent a solid shaft without a finite-element model of the shaft, the radial DOFs could also be constrained.

If the local radial flexibility effects of a hollow shaft are significant, the shaft must be modeled with ANSYS general shell elements (STIF63) or equivalent. If elastic straight pipe elements (such as ANSYS STIF16) or equivalent beam elements are used, local radial deformations are not available. The shaft would be modeled most accurately with the same radial definition of elements as used for the inner ring. This would probably require two to four shell elements between each rolling element for each axial section. In the axial direction, the mesh refinement must be compatible with the radial definition of elements.

The master or retained DOFs from the ANSYS inner ring/shaft stiffness matrix must be those defined for the specific bearing/support configurations. Unnecessary DOFs not constrained at the shaft/inner ring interface or those coupled along the roller/raceway contact line are eliminated in ANSYS by static condensation.

For ball bearings, the inner raceway groove is a circular section for containing the spherical balls. The candidate ball contact points within this circular race are defined by nodes corresponding to

3-8

an assumed constant contact angle of, for example, ±20°. Although the range of typical ball contact angles is 0° to ±40°, applying the ball contact force components to a single node is sufficiently accurate for determining elastic deflections of the inner rings. By definition, the positive contact angle for ball bearings corresponds to a single bearing or to the "primary" bearing in a duplex set; the negative contact angle corresponds to the "duplex" bearing in a duplex set.

With regard to the ball bearing kinematic relations, the most important displacements generated by the shaft/inner ring flexibility matrix are those describing the locations of the inner-race curvature centers (IRCCs). It is therefore necessary to include a node for the IRCC at each ball location. The three DOFs for each IRCC node are then connected rigidly to inner race nodes adjacent to the ball contact node in the azimuthal plane using ANSYS 3-D spar elements (STIF8). Note that the tangential DOF at each IRCC node has no stiffness normal to the azimuthal plane.

For ball bearings, forces applied to the inner race flexibility matrix [CI] are calculated in CS_2 components at each rolling element contact point. The desired elastic deflections are then the product of matrix [CI] times the vector of forces applied to the inner raceways. Matrix [CI] is used only to determine the elastic deflections of the inner ring(s) relative to the CS_2 shaft axes. The static force balance for comparison with the applied forces and moments is determined from the actual force direction and location and not from the nodal geometry of the flexibility matrix.

For roller bearings, all forces are defined directly in the inertial radial direction at each azimuthal plane. The static force balance for comparison with the applied forces and moments is determined using inertial radial directions only.

In a ball bearing, Hertzian contact deflections at the ball-race contact points are not represented by the relatively coarse FEM mesh used to predict elastic deflections of the IRCCs. Using 3-D spar elements connecting IRCC nodes with nodes adjacent to the ball-race contact points generates structural deflections of the race independently of Hertzian contact deflections. Therefore, the Hertzian contact deflections for ball bearings are calculated separately by traditional bearing mechanics relations and superimposed on the IRCC elastic displacements for the bearing kinematic equations.

The rolling element contact points for applied forces with cylindrical roller bearings are identical to the locations where elastic deflections are required. The radial line contact force and misalignment moment between each roller and the inner raceway is approximated by two unequal radial forces. These forces are applied at two nodes on the raceway, in each azimuthal plane, which are symmetrically located on either side of the raceway centerline a distance equal to approximately 30-percent of the roller effective length. This spacing, which *must* be considered in defining the ANSYS mesh for the inner ring model, corresponds to a uniformly loaded beam on two supports symmetrically located such that the negative moment at the support equals the maximum positive moment between the supports. This spacing is one approach for representing a continuous line contact force with two concentrated forces.

In the roller bearing model, Hertzian line contact deflections are separated from elastic ring deflections by means of a special feature in the *ANSYS* model. Along each line of contact between roller and raceway, several nodes adjacent to the retained nodes are constrained radially

by the ANSYS "couple" command. By constraining several adjacent nodes to move radially together, the Hertzian line contact force is essentially spread along the effective length of the roller instead of being concentrated at the two retained nodes. The use of this modeling technique is described and illustrated in the User's Manual.

3.3   Outer Ring/Carrier Finite-Element Models

The ANSYS structural model of the outer ring and carrier is generated in cylindrical coordinates having the *ANSYS* order $(R_A \ \theta_A \ Z_A)$. The outer ring(s) are unconstrained, but the carrier support DOFs are constrained to zero deflection. The master or retained DOFs from the ANSYS outer ring/carrier stiffness matrix must be those defined for the specific bearing/support configurations. Unnecessary DOFs not constrained at the carrier support DOFs or those coupled along the roller/raceway contact line are eliminated in ANSYS by static condensation.

For ball bearings, radial and axial gaps are defined in the ANSYS model by coincident but separate nodes on the outer ring(s) and carrier. Specified initial gap values for each potential contact are subsequently input to FEREBA. Because the outside corners of the outer ring(s) are chamfered, the corner points on the outer ring cannot contact the carrier. Radial contact can therefore occur only on a radial face, and axial contact can occur only on an axial face. Cylindrical roller bearings are defined to have only radial contact.

In FEREBA, gap closure between the outer ring(s) and carrier causes contact forces between the two bodies. These contact forces are calculated from radial/axial constraint equations in which the radial/axial displacements on both sides of a closed gap are constrained to move together. The only nonlinear aspects of this approach are identifying which gaps are closed and nulling any impossible tensile forces at the local axial preload springs for ball bearings. Once a set of gap closures is assumed, the elastic displacement analysis is linear except for liftoff of the local axial preload springs.

Contact forces between the outer ring and carrier are not calculated in terms of nonlinear Hertzian contact force/displacement relations. Such calculations require assumptions of the ideal nature of the contact which would not be appropriate for these conditions. In the radial direction, contact between convex and concave cylindrical surfaces with essentially equal diameters constitutes neither ideal point nor ideal line contact. In the axial direction, contact between two flat surfaces can not be considered Hertzian contact. Including nonlinear Hertzian contact force/displacement relations would therefore add unwarranted complexity to the analysis (including potential Newton-Raphson convergence problems) without improving the fidelity of the bearing model.

For ball bearings, the basic purpose of the ANSYS model of the outer ring and carrier is to produce elastic axial and radial deflections of each outer race curvature center (*ORCC*). Each *ORCC* point is represented in the ANSYS structural model as a node located properly relative to the raceway groove at each azimuthal position. The *ORCC* node is connected to the structural model by two 3-D spar elements (STIF8) in the azimuthal plane as with the ANSYS model of the inner ring and shaft. The spar elements connect *ORCC* nodes with nodes adjacent to the ball-race contact points. The resulting elastic deflections are essentially independent of the Hertzian contact deflections of the ball-race contact points.

As with the inner ring/shaft model for cylindrical roller bearings, the two retained nodes defining the contact points between roller and outer raceway are symmetrically located on either side of the centerline a distance equal to about 30-percent of the roller effective length. The nodes adjacent to these two retained nodes are coupled in ANSYS so that the radial DOFs move together with the retained nodes. Refer to the User's Manual for more details and examples of this modeling technique.

3.4 Coordinate Transformations

The stiffness matrices generated in ANSYS must be transformed from the ANSYS cylindrical coordinate system $\{q_A\}$ into FEREBA cylindrical coordinates $\{q_F\}$. The definitions of cylindrical and Cartesian coordinates for ANSYS and FEREBA are given in equations (3-1).

$$R_A = R_F$$

$$\theta_A = \theta_F$$

$$Z_A = X_F$$

(3-1)

where R, θ, and Z or X are the radial, azimuthal (tangential), and axial coordinates. The corresponding DOF orderings are $\{q_A\}^T = \{R_A\ \theta_A\ Z_A\}$ and $\{q_F\}^T = \{X_F\ R_F\ \theta_F\}$. Since the DOF order is not the same, a transformation matrix to convert a stiffness matrix from ANSYS to FEREBA cylindrical coordinates in matrix notation is given by

$$\begin{Bmatrix} R_A \\ \theta_A \\ Z_A \end{Bmatrix} = \begin{bmatrix} 0 & 1 & 0 \\ 0 & 0 & 1 \\ 1 & 0 & 0 \end{bmatrix} \begin{Bmatrix} X_F \\ R_F \\ \theta_F \end{Bmatrix}$$

(3-2)

which in terms of the generalized coordinates may be expressed as

$$\{q_A\} = [T]\{q_F\}$$

(3-3)

The transformation of the ANSYS stiffness matrix into FEREBA coordinates is accomplished by the matrix triple product $[T]^T*[K]*[T]$ where matrix $[T]$ is the transformation matrix of equation (3-3). This matrix operation is performed in FEREBA by subroutine TRANAF, using an efficient computational procedure to minimize storage requirements.

3–11

3.5 Constraining Free-Free Outer Ring

Subroutine ADDSTF operates on the unreduced stiffness matrix of the outer ring(s) and carrier in FEREBA cylindrical coordinates. The stiffness matrix for the outer ring(s) is connected to ground or to the carrier by soft springs (3 DOF/node) at each candidate contact point except preload spring locations and, where applicable, by axial preload springs at the preload location in each azimuthal plane. The spring stiffnesses are added to the unreduced stiffness matrix in locations specified for each of the nine bearing/support configurations.

The stiffness magnitude of the soft springs is calculated as a factor multiplied by a typical outer ring stiffness term. The factor is currently selected as 1.0×10^{-6} consistent with a similar ANSYS approximation. The typical outer ring stiffness term is the radial DOF at the first ball contact point for ball bearings and the radial DOF at the second roller contact point for cylindrical roller bearings.

For ball bearings only, the total axial preload spring stiffness input to FEREBA is divided by the number of rolling elements to give the magnitude of the individual preload spring stiffness at each azimuthal plane. The individual preload springs are uncoupled from one azimuthal plane to another. Preload springs are not allowed with a roller bearing.

3.6 Condensing and Inverting Matrices

After the stiffness matrices have been transformed to the FEREBA coordinate system, DOF that are not used in the subsequent kinematic relationships are removed either by static condensation or deletion. The unrequired DOF are listed with the 12 bearing/support combinations described in section 3.1. An efficient static condensation procedure has been incorporated into FEREBA which reduces DOF one at a time. In partitioned form, the general static condensation problem for the stiffness matrix may be stated as

$$\begin{bmatrix} [K_{jk}] & \{K_{js}\} \\ \{K_{sk}\} & K_{ss} \end{bmatrix} \begin{Bmatrix} \{x_j\} \\ x_s \end{Bmatrix} = \begin{Bmatrix} \{F_j\} \\ F_s \end{Bmatrix} \quad . \tag{3-4}$$

where x_s is the coordinate to be condensed and K_{ss} is the term to be eliminated from the stiffness matrix. Note that submatrices $\{K_{sk}\}$ and $\{K_{js}\}$ are vectors. For convenience, the DOF to be condensed is the last term in equation (3-4), practical implementation of this algorithm proceeds from the largest DOF to the smallest.

The second row of (3-4) may be written as

$$x_s = \frac{1}{K_{ss}} \left(F_s - \{K_{sk}\}\{x_j\} \right) \tag{3-5}$$

which expresses the constraint relation between x_s and $\{x_j\}$. Normally, as is the case in FEREBA, F_s is zero.

3-12

Expanding the first row of (3-4), and substituting the relation given by (3-5) results in the condensed expression for the statics problem expressed in (3-4) as

$$\left([K_{jk}] - \frac{\{K_{js}\}\{K_{sk}\}}{K_{ss}}\right)\{x_j\} = \{F_j\} - \frac{\{K_{js}\}F_s}{K_{ss}} \tag{3-6}$$

which by inspection, the reduced order stiffness matrix is obtained from (3-6) as

$$[K_{jk}^*] = [K_{jk}] - \frac{\{K_{js}\}\{K_{sk}\}}{K_{ss}} \tag{3-7}$$

where $[K_{jk}^*]$ is the condensed matrix. In FEREBA, subroutine MATRED performs this reduction by sequentially removing each required DOF and shifting the remaining rows and columns of the matrix up and over by one term.

For some of the ball bearing ring configurations, DOFs are deleted, rather than condensed. Mathematically, this procedure applies a fixed constraint to the system, thus only unrequired tangential DOF are treated in this manner. In FEREBA, deleted DOFs bypass the reduction procedure and are eliminated by row and column shifts.

Once the stiffness matrices have been reduced, compliance matrices are obtained by using standard mathematical subroutines for inversion. FEREBA uses the routine DLFIRG from the commercially available IMSL* subroutine library, however, any routine capable of inverting symmetric double precision matrices can be used instead.

3.7   Partitioning Compliance Matrices

After the stiffness matrices for the inner ring/shaft and outer ring/carrier have been reduced and inverted, the resulting flexibility influence coefficient matrices are partitioned for convenience in subsequent computations. Subroutine CIPART extracts influence coefficients from matrix [CI] which define IRCC or roller deflections in terms of rolling element forces applied to the inner raceway. Similarly subroutine COPART extracts influence coefficients from matrix [CO] required for subsequent calculations.

The four required partitions of matrix [CO] are defined as follows:

COP12 = flexibility coefficients defining ORCC or roller deflections in terms of rolling element forces applied to the outer raceway;

COP13 = flexibility coefficients defining ORCC or roller deflections in terms of constraint forces between outer ring and carrier at the candidate contact points;

COP32 = flexibility coefficients defining deflections at the candidate contact points (gaps) in terms of rolling element forces applied to the outer raceway;

COP33 = flexibility coefficients defining deflections at the candidate contact points (gaps) in terms of constraint forces between outer ring and carrier at the candidate contact points.

---

* The IMSL MATH/LIBRARY is available from Visual Numerics, Inc.

Subroutines CODIM and CIDIM perform the functions of assigning dimensions for each of the one-dimensional and two-dimensional arrays involved with the bearing flexibility computations. The array dimensions are determined as the product of the number of rolling elements times integers defined for each of the twelve bearing/support configurations. The current version of REBANS limits the number of rolling elements to 20 for a single bearing row (40 total for a duplex bearing system).

3.8 Defining Gap Clearance Vector

For seven of the nine outer ring configurations, a combination of axial and radial gaps are user specified by entering values for clearance and diameters. This data is converted to the required gap clearances (or interferences in special cases) by subroutine GAPDEF. Currently, this routine applies constant radial and/or axial clearance values at all azimuthal positions. More general versions can use nonuniform clearance values if desired.

Depending on the configuration, from two to seven gap clearances require definition. With the uniform gap limitation, only four gap values are possible, three axial and one radial. The axial gaps correspond to the distance between the outer ring and carrier/housing in the load direction for a ball or duplex bearing, denoted as C_A, the corresponding clearance on the unloaded side of the bearing, set equal to unity (1.0), and the distance between outer rings in a duplex set, referred to as C_D. The single radial gap is the radial clearance between the outer ring and carrier/housing, represented as C_R. For the seven *IBSCOR* configurations which have gaps as numbered in section 3.1, the clearances are set to the following values:

IBSCOR = 2 or 3 (ball bearing with deadband)

Gap number and direction			
1 (axial)	2 (radial)	3 (radial)	4 (axial)
1.0	C_R	C_R	C_A

IBSCOR = 4 (duplex bearing without deadband)

Only one gap is required, between the two outer rings, equal to C_D

IBSCOR = 5 or 6 (duplex bearing with deadband)

Gap number and direction						
1 (axial)	2 (radial)	3 (radial)	4 (axial)	5 (radial)	6 (radial)	7 (axial)
1.0	C_R	C_R	C_D	C_R	C_R	C_A

IBSCOR = 8 or 9 (roller bearing with deadband)

Gap number and direction	
1 (radial)	2 (radial)
C_R	C_R

4. COORDINATE SYSTEMS

This section describes the coordinate systems used to develop the kinematic relations for ball and roller bearing analysis. For both bearing types, a fixed inertia system will be defined, from which any local systems will be referenced.

4.1   Angular Contact Ball Bearing Coordinate Systems

Two separate coordinate systems are defined for the major elements of the ball bearing. One is for the inner ring; the other is for the carrier and outer ring. The coordinate system describing the outer ring and carrier is the global reference frame fixed in inertial space. The reference frame for the inner ring can move relative to the global inertial frame.

Each coordinate system consists of both right-handed Cartesian (X-Y-Z) axes and cylindrical (X-R-Φ) axes. The origins of each pair of Cartesian and cylindrical axes are coincident, and the X axes of each pair are collinear. For all axis systems, positive X is defined in the general direction of the applied axial thrust load. The transformations between each Cartesian and corresponding cylindrical coordinates are defined as follows:

$$Y = R \cdot \cos(\Phi)$$

$$Z = R \cdot \sin(\Phi)$$

$$R = Y \cdot \cos(\Phi) + Z \cdot \sin(\Phi)$$

$$\Phi = \tan^{-1}(Z/Y)$$

Note that X is identical for both Cartesian and cylindrical axes and that Φ is measured from Y with the positive sense defined by the rotation of Y into Z. It should be noted that the azimuth angles (Φ) defining ball locations are identical in both the global inertial reference frame (CS_1) and the shaft/inner ring moving reference frame (CS_2). This is because the azimuth angles for the two coordinate systems are coincident in defining the initial or reference ball locations before loading. Subsequent elastic distortions resulting from loading are measured, for the small displacements assumed in bearing mechanics theory, relative to the reference ball locations and do not involve any change in the reference azimuth angles.

4.1.1   Global inertial reference frame (CS_1)

The global reference frame CS_1 is fixed in inertial space at the center of the unmounted bearing and at the center of the carrier bore. X is directed along the unloaded shaft with positive X in the direction of the applied axial thrust load. The locus of curvature centers for both inner and outer rings is initially located in the Y-Z plane before mounting and loading.

The initial diametral clearance P_d is defined in this reference frame, where P_d is total clearance across a diameter built into the bearing by the manufacturer. Half of P_d is located on either side of the origin by definition.

The carrier and outer ring are located directly in this inertial reference frame. The carrier support points are fixed in inertial space. Any initial clearance between the outer ring and the carrier in the unloaded configuration is defined directly in this coordinate system. The general small displacements of the outer ring and carrier are determined from a flexibility matrix defined in this global inertial reference frame. The locus of outer-race curvature centers is considered part of the outer ring. All applied forces and moments, including the centrifugal force on each ball, are defined in the global inertial reference frame.

4.1.2 Shaft/inner ring reference frame (CS_2)

The origin of CS_2 is fixed at the center of the loaded shaft during operation. The axial coordinate x is directed along the loaded shaft and is positive in the general direction of the applied axial thrust load. The origin is initially translated along the X-axis in the positive X direction a distance (Δe) equal to half the "free play" of the bearing. This initial position, which has the balls in contact with both races, is the starting point for the Jones and Harris bearing analysis. The initial mounted contact angles at the inner-race and outer-race contact points are equal and given as follows for the unloaded configuration:

$$\cos(\alpha^o) = (2BD - P_d)/2BD$$

$$\Delta e = BD \sin(\alpha^o)$$

$$BD = r_o + r_i - D$$

Here r_o and r_i are the radii of curvature for the outer and inner races, respectively, and D is the unloaded ball diameter.

The origin of this shifted moving coordinate system is located in the global inertial system (X-Y-Z) by three small displacements ($\Delta x + \Delta e$, Δy, Δz) and two small angles (θ_y, θ_z). These five DOFs (excluding Δe) are the unknown independent variables in the nonlinear equations evaluated by the iterative tangent-compliance solution technique. The relationship between these two coordinate systems is illustrated in Figure 4-1.

The orthogonal transformation matrix from CS_1 to CS_2 is as follows with the small angle assumption:

$$\begin{Bmatrix} x \\ y \\ z \end{Bmatrix} = \begin{bmatrix} 1 & -\theta_z & \theta_y \\ -\theta_z & 1 & 0 \\ \theta_y & 0 & 1 \end{bmatrix} \begin{Bmatrix} X \\ Y \\ Z \end{Bmatrix}$$

This coordinate system locates all points on the inner ring including the locus of points defining the inner-race curvature centers which lie initially in the y-z plane. Note that the inner-race curvature centers move out of the y-z plane under general loading due to elastic displacements of the shaft/inner ring structure. The Hertzian contact deflections and the ball/race contact angles are also defined in CS_2. This coordinate system is the basic reference frame used by Jones and Harris for defining their internal forces and kinematic relations. This coordinate system does *not*

rotate with orbital speed, as it is not fixed to the shaft/inner ring structure. This reference frame moves only with the five DOFs defined previously.
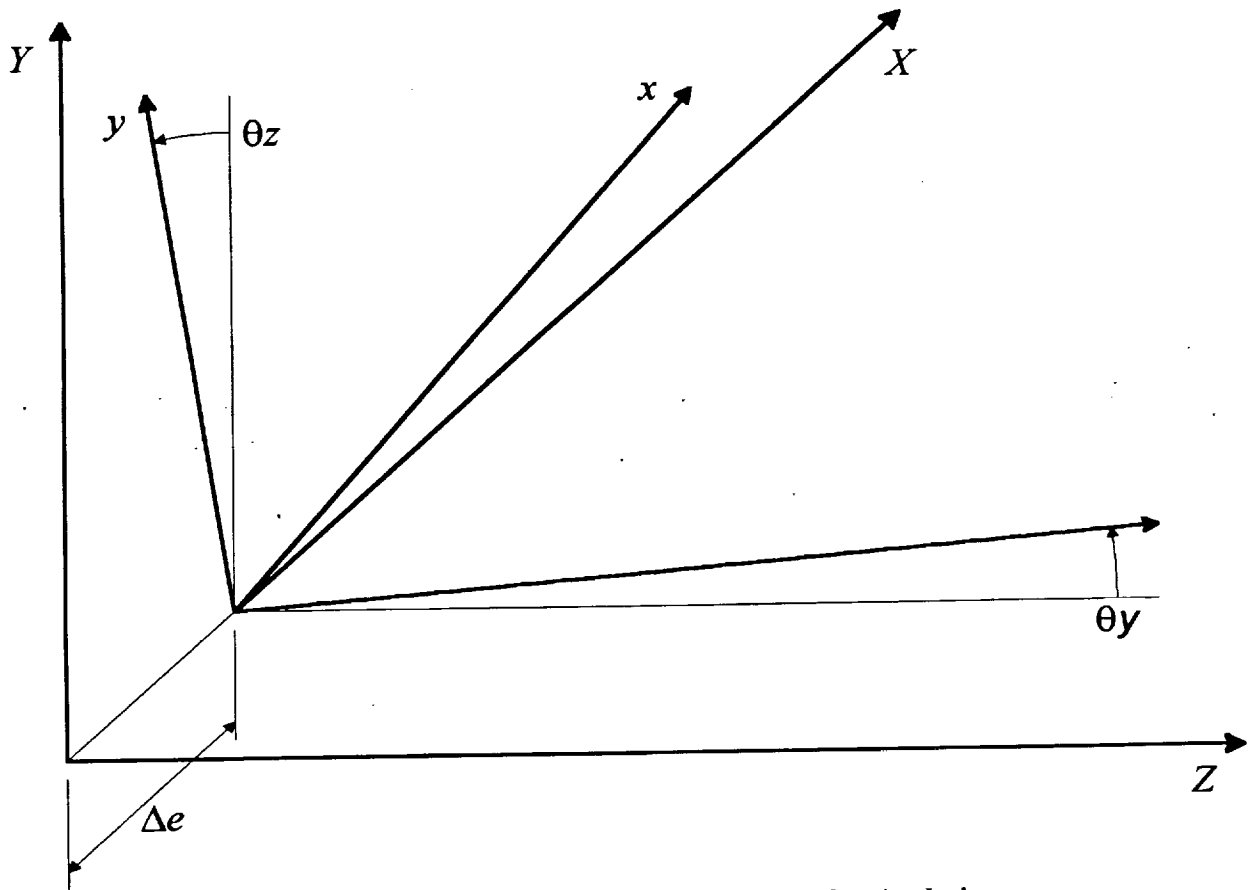
Figure 4-1 Coordinate Systems for Ball Bearing Analysis

4.1.3 Use of coordinate systems

Kinematic constraints leading to ball forces applied to inner and outer races are rigorously developed from CS_1 and CS_2. Ball forces applied to the inner race and the corresponding elastic deflections are defined in CS_2, however, total forces and moments are assumed to be in CS_1. This simplifies the structural analysis by allowing the torque from ball forces to be zero. This approximation thereby allows the bearing system to be defined by the standard five degrees of freedom instead of six.

Ball forces applied to outer race for determining elastic deflections are assumed to be in CS_1. This simplifies the structural analysis by allowing tangential forces to be zero. This approximation thereby allows the nonlinear structural analysis to be defined by radial and axial freedoms only.

These approximations are conventionally used in small-deflection structural analysis. The increased kinematic precision used to determine ball forces in CS_2 is considered necessary to evaluate the effects of structural flexibility.

4.2 Cylindrical Roller Bearing Coordinate Systems

A single inertial reference frame is used to define radial displacements and tilt rotations in the X-R azimuthal planes for all major roller bearing elements. All radial translations and tilt rotations of the inner ring and shaft, the outer ring and carrier, and the rollers are defined directly in this single inertial reference frame. The inertial reference frame consists of both right-handed Cartesian (X-Y-Z) axes and right-handed cylindrical (X-R-Φ) axes. The origins of the Cartesian and cylindrical axes are coincident, located at the center of the unloaded bearing, with half the diametral clearance on each side of the origin. The X axes of both coordinate systems are collinear. Since cylindrical roller bearings do not accept axial thrust loads, the positive X direction is defined arbitrarily to complete the right-handed coordinate system. The transformations between the Cartesian and cylindrical coordinate system are defined as follows:

$$Y = R \cos(\Phi)$$

$$Z = R \sin(\Phi)$$

$$R = Y \cos(\Phi) + Z \sin(\Phi)$$

$$\Phi = \tan^{-1}(Z/Y)$$

Note that X is identical for both Cartesian and cylindrical axes and that Φ is measured from Y with the positive sense defined by the rotation of Y into Z.

For cylindrical roller bearings, the primary load direction is radial with secondary effects of misalignment included. The quasi-static loads applied to the inner ring and shaft and the corresponding deflections are represented by four degrees of freedom defined in the inertial Cartesian coordinate system. The four displacement degrees of freedom are large Y and Z translations and small θY and θZ rotations. Thus small moments must be generated to enforce angular misalignments, but the primary loading is by radial forces.

The radial displacement of the inner ring and shaft defined in each azimuthal plane is

$$\Delta u_r = \Delta Y \cos(\Phi) + \Delta Z \sin(\Phi)$$

while the corresponding tilt rotation in each azimuthal plane is obtained from a coordinate transformation based on the small-angle assumption:

$$\Delta \theta = \theta Z \cos(\Phi) - \theta Y \sin(\Phi)$$

This equivalent small tilt angle ($\Delta \theta$) is measured with the positive sense defined by the rotation of X into R. Radial translations and tilt rotations of the outer ring and carrier and of each rolling element are defined directly in cylindrical coordinates of the inertial reference frame.

Kinematic constraints leading to rolling element forces applied to inner and outer races are developed from large-angle trigonometry in each azimuthal plane of the inertial reference frame. Roller/raceway interference is determined in the inertial radial directions leading to radial loads only. Roller crown drop is assumed to be in the inertial radial direction although actually defined normal to the roller. Maintaining the SHABERTH Hertzian contact equations, while using only inertial radial forces and displacements, simplifies the quasi-static analysis.

5. BALL BEARING KINEMATIC CONSTRAINT RELATIONS

Constraint relations for the flexibility enhanced kinematics with angular contact ball bearings will be described in this section. The kinematic constraint relations vary only slightly for the case of a duplex set. Two similar ball bearings installed back-to-back, as shown in Figure 5-1, are kinematically equivalent except for a sign change in the contact angles. For convenience in the following discussion, the bearing with the positive contact angles will be called the "primary" bearing, while the bearing with negative contact angles will be called the "duplex" bearing. As shown in Figure 5-1, the origin of the global inertial coordinate system (CS_I) is fixed at the initial location of the outer race curvature center ($ORCC$) of the primary bearing. The $ORCC$ of the duplex bearing is displaced along the inertial X axis a distance X_{cd}, which is restricted to positive values. Relative elastic deflections of the shaft between the two bearings are represented in the structural model of the shaft and inner rings.
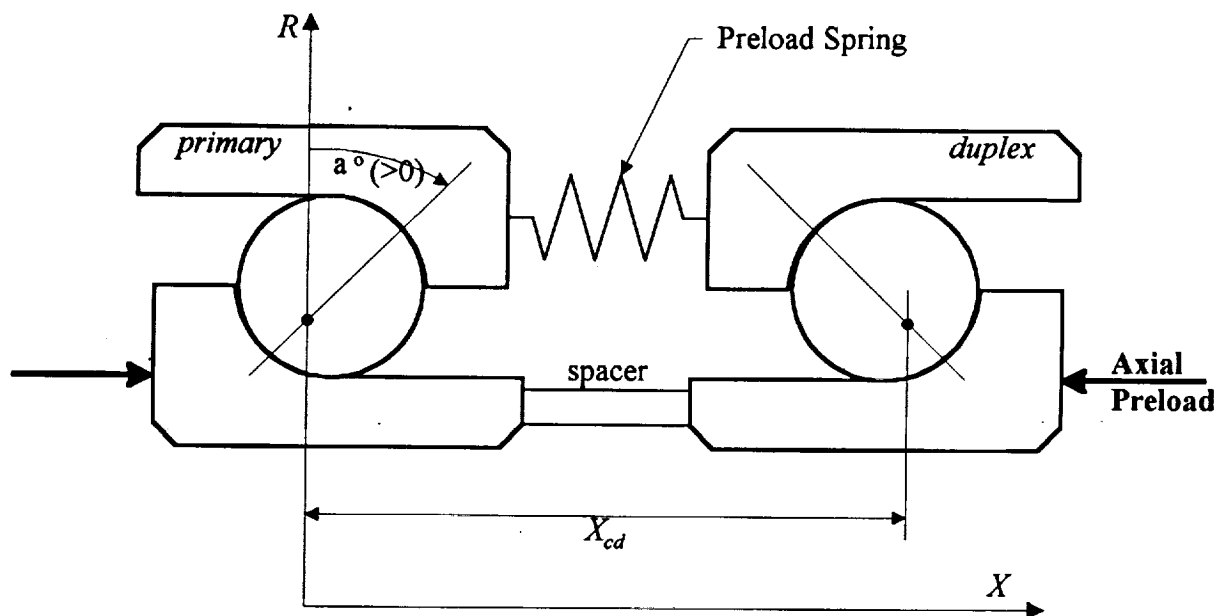
Figure 5-1 Inertial Coordinates for Duplex Bearing Set (Unloaded Condition)

The basic constraint relations for a ball in contact with both races are first developed without axial preload effects. Then modifications of the basic constraint relations to include preload effects for a duplex set are discussed.

5.1 Contact with Both Races

The following development is applicable to a single ball bearing or to the primary ball bearing of a duplex set, only because of an assumed positive initial contact angle. Otherwise the equations are equally applicable to either the primary or the duplex ball bearing.

For each ball location, the kinematic constraint relations are obtained from two different expressions for the location of the $ORCC$. One expression locates the $ORCC$ directly in CS_I. The other expression locates the $ORCC$ indirectly relative to the location of the inner race curvature

other expression locates the *ORCC* indirectly relative to the location of the inner race curvature center (*IRCC*) in the inner ring moving coordinate system (*CS₂*). Both expressions represent the *ORCC* radial and axial locations in *CS₁* when the ball is in contact with both races under load.
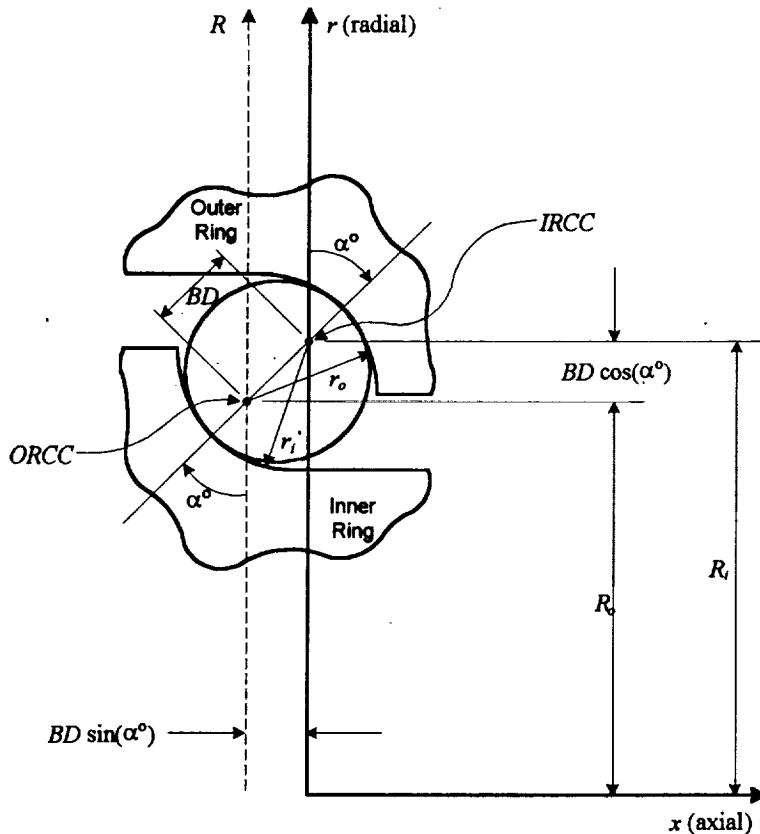
Figure 5-2 Mounted Ball-Race Configuration (Unloaded)

An auxiliary equation may be obtained from the two expressions of the *ORCC* radial inertial coordinate where the ball is unloaded but in contact with both races:

$$R_o = R_i - BD \cos(\alpha^o)$$

This expression may be rearranged as follows for a convenient identity:

$$BD \cos(\alpha^o) = R_o - R_i \qquad (5\text{-}1)$$

This kinematic relation is shown graphically in Figure 5-2.

The corresponding equation for the *ORCC* axial inertial coordinate is null, because both curvature centers are initially in the *X-R* plane and the *ORCC* does not move during mounting. The axial distance by which the *IRCC* and *CS₂* are initially displaced during mounting from the *ORCC* and *CS₁* is seen in Figure 2 to be

$$\Delta e = BD \sin(\alpha^o) \qquad (5\text{-}2)$$

The initial distance between the *ORCC* and the *IRCC* in the unloaded mounted configuration is seen in Figure 2 to be

$$BD = r_o + r_i - D \qquad (5\text{-}3)$$

And the initial (positive) contact angle for the primary bearing is related to diametral clearance by

$$\alpha^o = \cos^{-1}[(2BD - P_d - \Delta P_d)/2BD] \qquad (5\text{-}4)$$

The initial room-temperature diametral clearance is modified by thermal effects to produce a revised initial contact angle using an existing analytical method [1].

5–2

When a ball at the jth azimuthal location is loaded with applied static and centrifugal forces, the contact angles at the inner and outer races differ. The jth axial *ORCC* location under load is the axial elastic displacement determined directly in global inertial coordinates as δx_{oj}.

The same axial coordinate expressed indirectly in terms of rigid-body and elastic displacements of the inner ring and ball results in the following kinematic relation:

$$\delta x_{oj} = \Delta e + \Delta x + \delta x_{ij}$$
$$- [r_i - (D/2 - \delta d_{ij})] \sin(\alpha_{ij}) - [r_o - (D/2 - \delta d_{oj})] \sin(\alpha_{oj})$$
$$+ [\theta y \sin(\Phi j) - \theta z \cos(\Phi j)]\{R_i + \delta r_{ij}$$
$$- [r_i - (D/2 - \delta d_{ij})] \cos(\alpha_{ij}) - [r_o - (D/2 - \delta d_{oj})] \cos(\alpha_{oj})\} \tag{5-5}$$

The small angle assumption was used with θy and θz for transforming quantities defined in CS_2 into CS_1 for equation (5-5). Substituting equation (5-2) and rearranging equation (5-5) results in the basic axial kinematic relation with the loaded ball in contact with both races:

$$0 = BD \sin(\alpha^o) + \delta X_j$$
$$- [r_i - (D/2 - \delta d_{ij})] \sin(\alpha_{ij}) - [r_o - (D/2 - \delta d_{oj})] \sin(\alpha_{oj}) \tag{5-6}$$

As seen from equations (5-5) and (5-6), some of the rigid-body and elastic displacements are collected for convenience into

$$\delta X_j = \Delta x + \delta x_{ij} - \delta x_{oj}$$
$$+ [\theta y \sin(\Phi j) - \theta z \cos(\Phi j)]\{R_i + \delta r_{ij}$$
$$- [r_i - (D/2 - \delta d_{ij})] \cos(\alpha_{ij}) - [r_o - (D/2 - \delta d_{oj})] \cos(\alpha_{oj})\} \tag{5-7}$$

The corresponding kinematic relation in the radial direction is determined similarly. The jth radial *ORCC* location under load is the radial elastic displacement (δr_{oj}) added to the unloaded location (r_o). The same inertial radial coordinate expressed indirectly in terms of rigid-body and elastic displacements of the inner ring and ball results in the following kinematic relation:

$$R_o + \delta r_{oj} = R_i + \Delta y \cos(\Phi_j) + \Delta z \sin(\Phi_j) + \delta r_{ij}$$
$$- [r_i - (D/2 - \delta d_{ij})] \cdot \cos(\alpha_{ij}) - [r_o - (D/2 - \delta d_{oj})] \cos(\alpha_{oj})$$
$$+ [\theta z \cos(\Phi j) - \theta y \sin(\Phi j)] \cdot \{\delta x_{ij}$$
$$- [r_i - (D/2 - \delta d_{ij})] \sin(\alpha_{ij}) - [r_o - (D/2 - \delta d_{oj})] \sin(\alpha_{oj})\} \tag{5-8}$$

The small angle assumption was again used with θy and θz for transforming quantities defined in CS_2 into CS_1 for equation (5-8). Substituting equation (5-1) and rearranging equation (5-8) results in the basic radial kinematic relation with the loaded ball in contact with both races:

$$0 = BD \cos(\alpha^o) + \delta R_j$$
$$- [r_i - (D/2 - \delta d_{ij})] \cos(\alpha_{ij}) - [r_o - (D/2 - \delta d_{oj})] \cos(\alpha_{oj}) \tag{5-9}$$

As before, some of the rigid-body and elastic displacements are collected from equation (5-8) into

$$\delta R_j = \Delta y \cos(\Phi_j) + \Delta z \sin(\Phi_j) + \delta r_{ij} - \delta r_{oj}$$

$$+ [\theta z \cdot \cos(\Phi_j) - \theta y \sin(\Phi_j)] \{\delta x_{ij}$$

$$- [r_i - (D/2 - \delta d_{ij})] \sin(\alpha_{ij}) - [r_o - (D/2 - \delta d_{oj})] \sin(\alpha_{oj})\} \tag{5-10}$$

The planar kinematic relations given by equations (5-6) and (5-9) are expressed graphically in Figure 5-3 as done previously by Davis and Vallance [2], Harris [3] and Jones [4]. The latter terms in equations (7) and (10), not found in the literature, should be included as they may be comparable in magnitude to the *ORCC* and *IRCC* elastic displacements which are included.
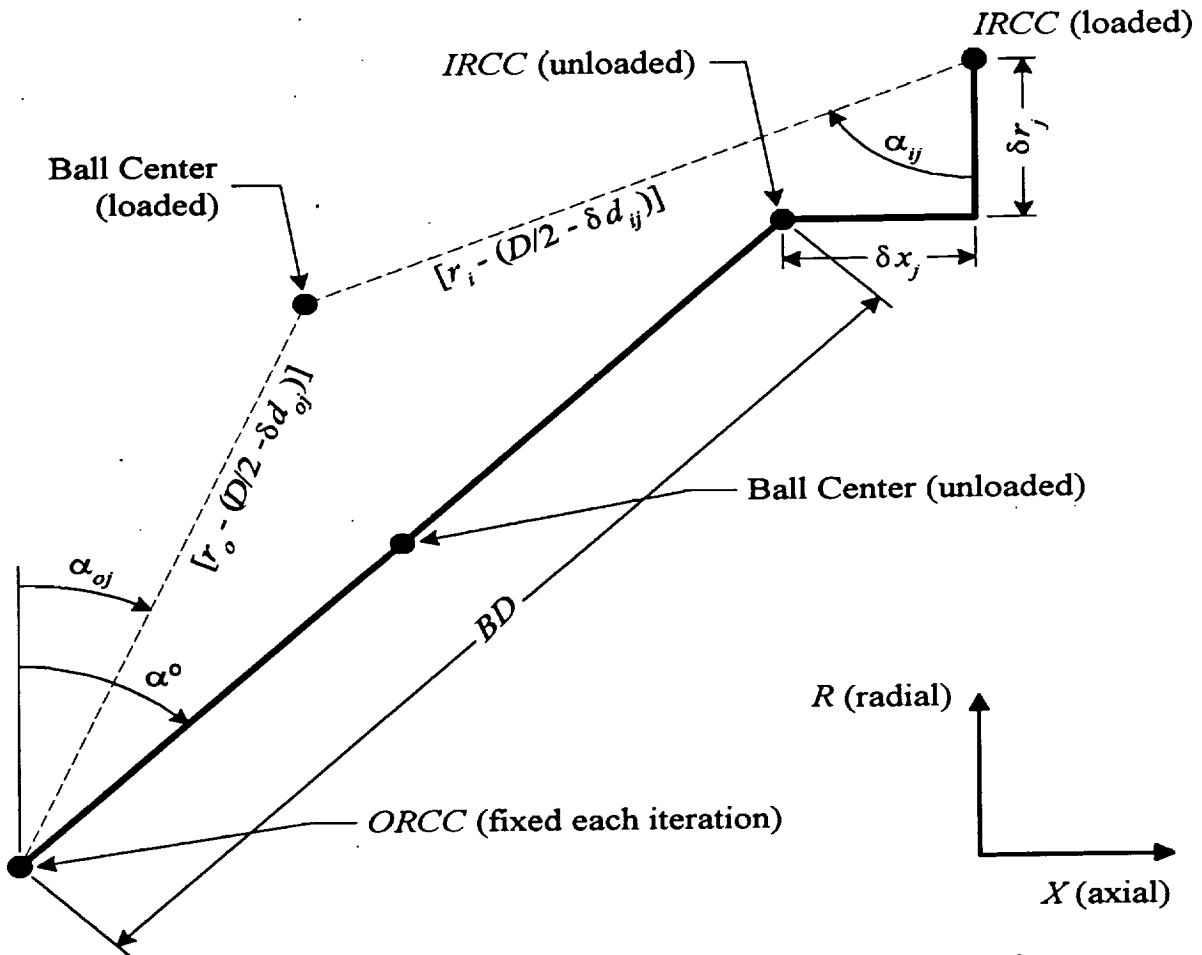
Figure 5-3 Planar Kinematic Relations for Loaded Single Ball Bearing

5.2 Contact with Outer Race Only

In the unloaded area of its orbit, the jth ball can lose contact with the inner race as it is compressed against the outer race by centrifugal force. For this condition, the Hertzian contact deflection between the jth ball and inner race (δd_{ij}) is zero. Also for this condition, the outer race contact angle (α_{oj}) and the outer race Hertzian contact deflection (δd_{oj}) can be determined directly from the centrifugal force components in CS_2. With these restrictions, equations (5-5) and (5-8) are

then the limiting relations for lost inner race contact, and the corresponding inequalities for defining lost contact in the axial direction is

$$\delta x_{oj} \geq \Delta e + \Delta x + \delta x_{ij}$$
$$- [r_i - (D/2 - \delta d_{ij})] \sin(\alpha_{ij}) - [r_o - (D/2 - \delta d_{oj})] \sin(\alpha_{oj})$$
$$+ [\theta y \sin(\Phi j) - \theta z \cos(\Phi j)]\{R_i + \delta r_{ij}$$
$$- [r_i - (D/2 - \delta d_{ij})] \cos(\alpha_{ij}) - [r_o - (D/2 - \delta d_{oj})] \cos(\alpha_{oj})\} \qquad (5\text{-}11)$$

and in the radial direction

$$R_o + \delta r_{oj} \geq R_i + \Delta y \cos(\Phi_j) + \Delta z \sin(\Phi_j) + \delta r_{ij}$$
$$- [r_i - (D/2 - \delta d_{ij})] \cos(\alpha_{ij}) - [r_o - (D/2 - \delta d_{oj})] \cos(\alpha_{oj})$$
$$+ [\theta z \cos(\Phi j) - \theta y \sin(\Phi j)] \cdot \{\delta x_{ij}$$
$$- [r_i - (D/2 - \delta d_{ij})] \sin(\alpha_{ij}) - [r_o - (D/2 - \delta d_{oj})] \sin(\alpha_{oj})\} \qquad (5\text{-}12)$$

Substituting equation (5-2) and rearranging inequality (5-11) to isolate terms involving the indeterminate inner race contact angle (α_{ij}) results in

$$X_{cj} \leq (r_i - D/2) \sin(\alpha_{ij}) + [\theta y \sin(\Phi j) - \theta z \cos(\Phi j)] (r_i - D/2) \cos(\alpha_{ij}) \qquad (5\text{-}13)$$

where

$$X_{cj} = BD \sin(\alpha^o) + \Delta x + \delta x_{ij} - \delta x_{oj} - [r_o - (D/2 - \delta d_{oj})] \sin(\alpha_{oj})$$
$$+ [\theta y \sin(\Phi j) - \theta z \cos(\Phi j)]\{R_i + \delta r_{ij} - [r_o - (D/2 - \delta d_{oj})] \cos(\alpha_{oj})\} \qquad (5\text{-}14)$$

Similarly substituting equation (5-1) and rearranging inequality (5-12) to isolate terms involving the inner race contact angle results in

$$R_{cj} \leq (r_i - D/2) \cos(\alpha_{ij}) + [\theta z \cos(\Phi j) - \theta y \sin(\Phi j)] (r_i - D/2) \sin(\alpha_{ij}) \qquad (5\text{-}15)$$

where

$$R_{cj} = BD \cos(\alpha^o) + \Delta y \cos(\Phi_j) + \Delta z \sin(\Phi_j) + \delta r_{ij} - \delta r_{oj}$$
$$- [r_o - (D/2 - \delta d_{oj})] \cos(\alpha_{oj})$$
$$+ [\theta z \cos(\Phi j) - \theta y \sin(\Phi j)] \{\delta x_{ij} - [r_o - (D/2 - \delta d_{oj})] \sin(\alpha_{oj})\} \qquad (5\text{-}16)$$

Squaring both sides of inequalities (5-13) and (5-15) and adding the two inequalities eliminates the indeterminate inner race contact angle and results in the desired constraint relation:

$$X_{cj}^2 + R_{cj}^2 \leq (r_i - D/2)^2 \{1 + [\theta y \sin(\Phi j) - \theta z \cos(\Phi j)]^2\} \qquad (5\text{-}17)$$

When this inequality is satisfied, the jth ball has lost contact with the inner race.

The centrifugal force F_{cj} on the jth ball is defined in CS_1 and directed along the positive r-axis. When this force is transformed into CS_2, using the small angle assumption, the axial and radial components are

$$F_{cxj} = F_{cj} [\theta_z \cos(\Phi_j) - \theta_y \sin(\Phi_j)] \quad (5\text{-}18)$$

$$F_{crj} = F_{cj} \quad (5\text{-}19)$$

For the condition when the ball loses contact with the inner race, the outer race contact angle is obtained directly from

$$\tan(\alpha_{oj}) = F_{cxj}/F_{crj} = \theta_z \cos(\Phi_j) - \theta_y \sin(\Phi_j) \quad (5\text{-}20)$$

Similarly, when the ball loses contact with the inner race, the Hertzian contact deflection between the jth ball and the outer race is obtained directly from

$$\delta d_{oj} = (F_{cj}/K_{oj})^{2/3} \quad (5\text{-}21)$$

Because of the small angle assumption used in the coordinate transformations, the magnitude of the centrifugal force is slightly larger in CS_2 than it is in CS_1. The resulting error is considered insignificant.

5.3 Modifications for Duplex Bearings

As discussed previously, the primary modification in the constraint relations for the duplex bearing is the change in sign of the contact angles. Note that the subscript d is used for variables related to the duplex bearing.

Ordinarily, des-criptive geometrical and mass data for the two bearings in a duplex set are identical. Thus the initial (negative) contact angle for the duplex bearing is obviously identical to equation (5-4) except for a sign change, and is determined from

$$\alpha_d^o = -\cos^{-1}[(2BD_d - P_{dd} - \Delta P_{dd})/2BD_d] \quad (5\text{-}22)$$

The negative initial contact angle for the duplex bearing in equation (5-22) results in a negative value for the mounting axial displacement defined as the axial distance between $ORCC$ and $IRCC$ and given by

$$\Delta e_d = BD_d \sin(\alpha_d^o) \quad (5\text{-}23)$$

This equation is, of course, identical to equation (5-2) except that the data relates to the duplex bearing. Note that α_d^o and Δe_d are both negative.

The only other modification besides contact angle and descriptive data regards the lateral rigid-body displacements for the $IRCC$ of the duplex bearing. The five DOFs describing the rigid-body translations and rotations of the CS_2 origin are Δx, Δy, Δz, θy and θz. The axial translation and two rotations are identical for the two bearings. However, the $IRCC$ of the duplex bearing is displaced in the axial direction relative to the CS_2 origin.

Therefore, the lateral displacements of the duplex *IRCC* differ from Δy and Δz as follows:

$$\Delta y_d = \Delta y + (X_{cd} - \Delta e + \Delta e_d)\,\theta z \qquad (5\text{-}24)$$

$$\Delta z_d = \Delta z - (X_{cd} - \Delta e + \Delta e_d)\,\theta y \qquad (5\text{-}25)$$

With α^o_d, Δy_d, Δz_d and descriptive data for the duplex bearing, the kinematic constraint relations described previously relative to the primary bearing are completely valid for the duplex bearing. Based on α^o_d the loaded contact angles, α_{odj} and α_{idj}, are both negative.

5.4 Axial Preload Effects

The extension of the preceding development to account for axial preload effects for a duplex set follows the approach of Harris [3] in which all ball forces and contact angles for a bearing are assumed equal. Note that the axial components of the preload ball forces in the primary and duplex bearings must be equal and opposite, but the radial ball force components and preload contact angles could differ. It may also be noted that axial preload effects for single ball bearings are accommodated merely by adding the preload force to the applied axial thrust force. For duplex sets, an assumption of equal ball forces and contact angles would be valid for the usual case where the primary, duplex, and carrier supports are "mirror images" as shown in Figure 5-1. The two limitations of the present preload analysis are that the number of rolling elements in the primary and duplex bearings are equal and that interference fits are not permitted between outer ring(s) and carrier.

The two expressions of *ORCC* radial location, including elastic deflections due to axial preload, produce the following constraint equation for the primary ball bearing:

$$R_o + \delta r_{po} = R_i + \delta r_{pi} - (BD + \delta n)\cos(\alpha_p) \qquad (5\text{-}26)$$

Similarly, the two expressions of *ORCC* axial location after axial preload application produce the following constraint equation with elastic structural deflections included:

$$\delta x_{po} = BD\sin(\alpha^o) + \Delta p + \delta x_{pi} - (BD + \delta n)\sin(\alpha_p) \qquad (5\text{-}27)$$

The ball Hertzian contact deflection (δn) due to axial preload is related to the specified total preload force by the following expression developed by Jones and presented by Harris [3]:

$$\frac{F_{pre}}{n\,\sin(\alpha_p)} = K_d\,D^{0.5}\left(\frac{\delta_n}{B}\right)^{1.5} \qquad (5\text{-}28)$$

For convenience, the axial deflection constant (K_d), in units of psi, can be expressed in terms of total curvature (B) and elastic constants of the raceway and ball by the following relation where C_d is determined from a least-squares fit of the data presented by Harris:

$$K_d = \left\{\frac{B}{C_d}\left[\frac{(1-\mu_w^2)}{E_w} + \frac{(1-\mu_b^2)}{E_b}\right]^{2/3}\right\}^{1/2} \qquad (5\text{-}29)$$

where $C_d = 0.61884472 + 20.261267B - 286.15792B^2$
$$+ 2306.1467B^3 - 9258.9168B^4 + 14472.024B^5$$

Here B is allowed to vary from 0.0 to 0.2. Note that the elastic constants for both raceways must be identical for this representation to be valid.

Solving equation (5-26) for ball deflection and substituting into equation (5-28) results in the following expression involving preload contact angle as the only unknown:

$$\frac{F_{pre}}{n\,K_d\,B^3\left(D\!/\!B\right)^{\frac{1}{2}}} = \sin(\alpha_p)\left(\frac{\delta u_{rp}}{\cos(\alpha_p)} - BD\right)^{\frac{3}{2}} \qquad (5\text{-}30)$$

where, with the identity of equation (5-1),

$$\delta u_{rp} = BD\cos(\alpha^{\circ}) + \delta r_{pi} - \delta r_{po} \qquad (5\text{-}31)$$

Equation (5-30) may be solved iteratively using the Newton-Raphson procedure for given values of elastic structural deflections. In closed form, the equation to be satisfied is

$$\alpha_p' = \alpha_p - f(\alpha_p)/f'(\alpha_p) \qquad (5\text{-}32)$$

where

$$f(\alpha_p) = \frac{F_{pre}}{n\,K_d\,B^3\left(D\!/\!B\right)^{\frac{1}{2}}} - \sin(\alpha_p)\left(\frac{\delta u_{rp}}{\cos(\alpha_p)} - BD\right)^{\frac{3}{2}}$$

$$f'(\alpha_p) = -\cos(\alpha_p)\left(\frac{\delta u_{rp}}{\cos(\alpha_p)} - BD\right)^{\frac{3}{2}} - 1.5\delta u_{rp}\tan^2(\alpha_p)\left(\frac{\delta u_{rp}}{\cos(\alpha_p)} - BD\right)^{\frac{1}{2}}$$

A value of α_p is determined from equation (32) when α_p' equals α_p with sufficient accuracy. For a given α_p, the corresponding axial and radial ball force components due to axial preload can be calculated directly:

$$F_{xp} = F_{pre}/n \qquad (5\text{-}33)$$

$$F_{rp} = F_{xp}/\tan(\alpha_p) \qquad (5\text{-}34)$$

The elastic structural deflections of the inner and outer race curvature centers are calculated from the appropriate linear elastic flexibility influence coefficient matrices using the ball force components given by equations (5-33) and (5-34). Since the fundamental assumption of the axial preload calculation is that all balls behave the same under the applied axial preload, the desired elastic structural deflections (i.e., δr_{po}, δr_{pi}, δx_{po}, δx_{pi}) are defined as the average values of the corresponding deflections calculated from the flexibility influence coefficient matrices. The average radial structural deflections are used to update δu_{rp} (equation 5-31) for the next iterative solution of α_p (equation 5-32). When the preload contact angle has been determined with

sufficient accuracy, the axial displacement of the inner ring due to preload can be determined from equation (5-27) using the expression for ball deflection from equations (5-26) and (5-31):

$$\Delta p = \delta x_{po} - \delta x_{pi} + \delta u_{rp}\tan(\alpha_p) - BD\sin(\alpha°) \tag{5-35}$$

The axial displacement (Δp) of the primary bearing due to axial preload is the essential result of the preload calculations described with equations (5-26) through (5-35). The only change in the basic kinematic constraint relations is the redefinition of the initial axial distance between CS_2 and CS_1. Analogous to equation (5-2), this initial axial distance due to mounting and preload is

$$\Delta e_p = BD \sin(\alpha°) + \Delta p \tag{5-36}$$

The kinematic constraint relations, when the ball is in contact with both races under load, are once again obtained from two different expressions for the inertial location of the *ORCC*. With axial preload, the *ORCC* is, of course, initially displaced axially by the distance δx_{po} due to preload, whereas the *IRCC* is displaced the additional distance δx_{pi}. However, if the axial elastic displacements (δx_{oj} and δx_{ij}) are calculated with ball forces which include the preload force components, then the preload elastic structural deflections (δx_{po} and δx_{pi}) will be included in δx_{oj} and δx_{ij}. And the gap values defined initially, prior to preload, may be used unchanged with the application of axial preload, since changes in the gaps due to preload deflections are determined automatically. Similarly, the radial elastic displacements calculated with total ball forces will include the preload radial structural deflections (δr_{po} and δr_{pi}) as well.

Accordingly, the only change in the previously developed kinematic constraint relations, for the primary bearing of a duplex set, is to replace Δe (equation 2) with Δe_p (equation 5-36). Equation (5-6) remains unchanged while equation (5-7) has only one added term (Δp) to account for the preload axial displacement:

$$\delta X_j = \Delta x + \Delta p + \delta x_{ij} - \delta x_{oj}$$
$$+ [\theta y \sin(\Phi j) - \theta z \cos(\Phi j)]\{R_i + \delta r_{ij}$$
$$- [r_i - (D/2 - \delta d_{ij})] \cos(\alpha_{ij}) - [r_o - (D/2 - \delta d_{oj})] \cos(\alpha_{oj})\} \tag{5-36}$$

The radial kinematic relations given by equations (5-9) and (5-10) are unchanged.

For a primary bearing, the analogous discussion applies to the constraint relation for a ball contacting the outer race only (inequality 5-17). For the axial component, Δe is replaced by Δe_p so that equation (5-14) becomes

$$X_{cj} = BD \sin(\alpha°) + \Delta x + \Delta p + \delta x_{ij} - \delta x_{oj} - [r_o - (D/2 - \delta d_{oj})] \sin(\alpha_{oj})$$
$$+ [\theta y \sin(\Phi j) - \theta z \cos(\Phi j)]\{R_i + \delta r_{ij} - [r_o - (D/2 - \delta d_{oj})] \cos(\alpha_{oj})\} \tag{5-37}$$

Equation (5-16) for the radial component and inequality (5-17) are unchanged. When inequality (5-17) is satisfied, the jth ball has lost contact with the inner race.

Similar modifications are required to incorporate axial preload effects for the duplex bearing. With negative contact angles and with reversed axial ball force components for the duplex

bearing, the magnitude of the axial displacement of the inner ring due to axial preload becomes analogous to equation (35):

$$\Delta p_d = \delta x_{pdo} - \delta x_{pdi} + \delta u_{rpd} \tan(\alpha_{pd}) - BD \sin(\alpha_d^o) \qquad (5\text{-}38)$$

Here δu_{rpd} and α_d^o are obtained from equations (5-28) through (5-32) using descriptive geometrical and mass data for the duplex ball bearing set. Ordinarily, both bearings of a duplex set will be identical, but the only limitations in the preload calculation, as noted, are that both bearings have the same number of rolling elements and that outer ring(s) and carrier have no interference fit.

Analogous to equation (5-23), the initial axial distance between CS_{2d} and CS_l increases by the quantity

$$\Delta e_{dp} = BD_d \sin(\alpha_d^o) + \Delta p_d \qquad (5\text{-}39)$$

Of course, for the duplex ball bearing, Δe_{dp} (equation 5-39) must replace Δe in equations (5-2) and (5-14) to give kinematic relations for the duplex bearing analogous to equations (5-36) and (5-37) for the primary bearing.

Also, for the duplex bearing, equations (5-24) and (5-25) must be changed to redefine the lateral displacements of the duplex $IRCC$ (Δy and Δz) as follows:

$$\Delta y_{dp} = \Delta y + (X_{cd} - \Delta e_p + \Delta e_{dp})\,\theta z \qquad (5\text{-}40)$$

$$\Delta z_{dp} = \Delta z - (X_{cd} - \Delta e_p + \Delta e_{dp})\,\theta y \qquad (5\text{-}41)$$

These kinematic constraint relations are consistent with the prescribed axial preload force. Therefore, ball forces resulting from these constraint relations will properly include the corresponding preload force components. The radial preload force components are self-equilibrating as are axial preload force components for duplex bearings. For single ball bearings, as noted previously, the axial preload force is merely added to the externally applied axial force component.

5.4.1 Requirements

Use of the preload spring option in FEREBA must conform to the following requirements:

1. Axial preload springs may be selected for most ball bearing configurations (IBSCOR = 2,3,...,6) to represent distributed macroscopic preload effects. For the single ball bearing, an axial preload spring is installed between the outer ring and carrier on one side of the outer ring. For the duplex ball bearing set, an axial preload spring is installed between the two ball bearings. For both configurations, the axial preload force on the outer ring is transmitted through the rolling elements to the inner ring and shaft as shown in the attached sketch. Note that there is positive clearance between the outer ring and carrier for the bearings being considered. An interference fit is permitted only between inner ring and shaft, not between outer ring and carrier when axial preload is involved.

2. The following local loading capabilities are required for the idealized preload spring:

   a. completely unloaded locally such that no force is developed;

   b. compressed locally within a linear range such that a compressive force is developed;

   c. completely bottomed locally such that the full compressive constraint force is developed.

3. The main function of the preload spring is to impose an axial force and two moments on the outer ring. These applied macroscopic preloads remove all bearing free play and increase the bearing stiffness. In addition to these effects of discrete axial forces applied to the outer ring, corresponding Coulomb friction forces are developed which minimize outer ring tangential rotation.

5.4.2 Modeling Approach

The modeling approach is the simplest preload spring model which meets the above requirements: uncoupled axial linear springs at each ball location. This model provides the three required loading capabilities (unloaded, loaded and bottomed) as well as the macroscopic preload total force and moments. The total preload spring force is simply the sum of the individual forces, and the total moments are simply the products of the individual forces times their respective moment arms. An individual force could be zero, the linear spring force, or the appropriate constraint force, depending on local (and global) kinematic conditions.

This model does not represent theoretical stiffness coupling occurring around the circumference in some types of actual preload springs, nor does it represent nonlinear behavior resulting from Belleville springs. Since actual preload springs under consideration have stiffness terms on the order of one percent of the outer ring stiffnesses, any error in the outer ring deflection due to stiffness coupling or nonlinear behavior would be negligible. Local deflections of the preload spring will be defined essentially by the axial displacement and tilt of the outer ring relative to the carrier or to the other outer ring. The relatively soft preload spring linear stiffnesses will have a small effect on outer ring deflection so long as bottoming of the preload spring is properly represented.

The basic assumptions used in representing the preload spring forces are as follows:

   a. The continuous preload spring is divided into n independent axial springs contacting the outer ring at the n ball azimuthal locations. These separate springs are combined with the finite-element model of the outer ring and carrier generated by ANSYS. This combination of preload spring stiffnesses with the ANSYS stiffness matrix is accomplished in FEREBA prior to the matrix condensation and inversion operations.

   b. The prescribed total preload force, which is user specified, is developed by the individual axial preload springs being compressed equally in their linear range.

   c. The configuration corresponding to the mounted, preloaded ball bearing system has inner ring, shaft and spacer all rigidly connected with no gaps separating these components. This configuration results from an interference fit of the inner ring on the

5-11

shaft and from the axial locking of the inner ring and spacer against the shaft shoulder during preloading.

d. All initial clearances between the outer ring and carrier, including the gaps at the preload spring locations, are defined before the preload is applied. By definition, the initial gap separation distance at a preload spring is the minimum distance consistent with zero initial force. Axial displacements required to generate the specified preload are used to define the net axial clearances after mounting. Ball forces and bearing outer ring radial structural flexibility are used to define the net radial clearances after mounting. For single ball bearings, the specified initial preload force is simply added to the applied axial thrust force. For duplex ball bearing sets, a preliminary preload analysis is performed. This preliminary preload analysis determines ball forces, elastic deflections of the inner and outer rings, and initial mounted contact angle; but the basic result is simply the axial displacement of the inner ring relative to the outer ring due to initial axial preload.

After mounting, the force in the preload spring is allowed to vary in response to the externally applied forces and moments. The specified constant preload force is distributed to the n ball azimuthal locations and applied as equal-and-opposite external forces. Preload force changes in the linear range due to structural displacements are obtained with the basic solution procedure, since the individual axial preload springs are included in the ANSYS model. The basic solution procedure also determines the constraint forces when the preload spring bottoms locally. Additional logic is required to monitor local lift-off of the preload spring and to cancel the small incremental tensile force incorrectly generated by the ANSYS linear model.

6. ROLLER BEARING KINEMATIC CONSTRAINT RELATIONS

The basic assumption of the quasi-static roller bearing analysis is that only forces in the inertial radial direction are applied by each roller to the inner and outer raceways. Thus, although small moments may be applied to the inner ring and shaft corresponding to angular (tilt) misalignment, the primary loads are radial, and axial thrust loads are not permitted.

The classical roller bearing analysis by Jones [2] permits only radial loads and displacements with no angular misalignment. Subsequent developments by SKF, as published by Harris [3] and Liu [6], include the effects of angular misalignment (tilt) in approaches similar to that employed by the SHABERTH computer code [7]. More comprehensive analyses, such as that recently developed by SKF [8], include the axial degree of freedom for all types of roller bearings in a formulation similar to that previously used for ball bearings. However, the scope of the present frictionless quasi-static analysis for cylindrical roller bearings is limited to the radial and tilt freedoms consistent with SHABERTH, which serves as the development platform for this effort.
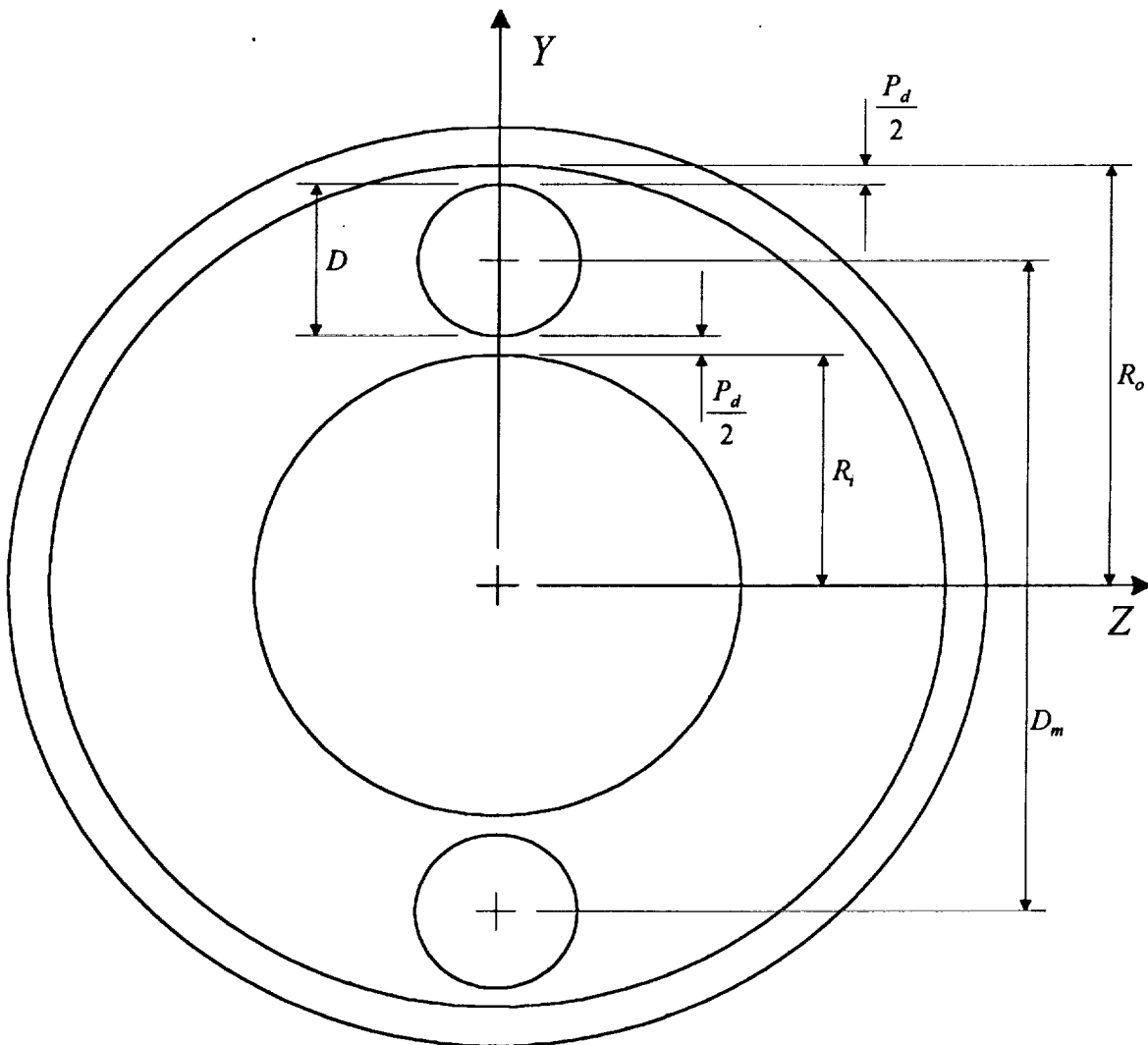
Figure 6-1 Unmounted Roller-Race Configuration

A definition of basic geometrical relations is provided in Figure 6-1 for the unmounted roller bearing configuration. As shown, the radial distance from the unmounted bearing center to the outer raceway is

$$R_o = D_m/2 + D/2 + P_d/2 \qquad (6\text{-}1)$$

The radial distance from the bearing center to the inner raceway is

$$R_i = R_o - D - P_d/2 \qquad (6\text{-}2)$$

As used in SHABERTH, the analytical expressions for roller/raceway contact forces are defined in terms of kinematic interference between roller and raceway. These kinematic constraint relations are defined in terms of inertial radial displacements and inertial tilt rotations of the roller centroid at each azimuthal roller position. Due to the shaft/bearing system modeling approach used by SHABERTH, axial displacements of the roller centroid in a rigid body sense were permitted. In the present development, the analysis of a single roller bearing eliminates the need to consider rigid-body axial motion. Consistent with precluding axial roller displacements, the raceway widths are assumed large compared with the roller lengths.

6.1 Interference Between Roller and Outer Raceway

The initial mounted (unloaded) position of roller and outer raceway at the jth azimuthal plane has contact between roller and raceway such that points A_O and B_O, shown in Figure 6-2 for the loaded condition, are initially coincident. Under applied load, the outer raceway in the jth azimuthal plane translates in the radial direction a distance δu_{oj} and rotates in the tilt direction through a small angle θ_{oj}. Simultaneously, the roller centroid translates radially a distance Δr_j, and rotates through a small angle ϕ_j. For each roller, $\Delta r_j = X(2)$ and $\phi_j = X(3)$ are the independent variables in the FEREBA equilibrium solution. The radial interference between point A_O on the roller and the radially adjacent point C_O on the outer raceway is δr_{oj}, shown negative for clarity in Figure 6-2 as a separation rather than an interference.
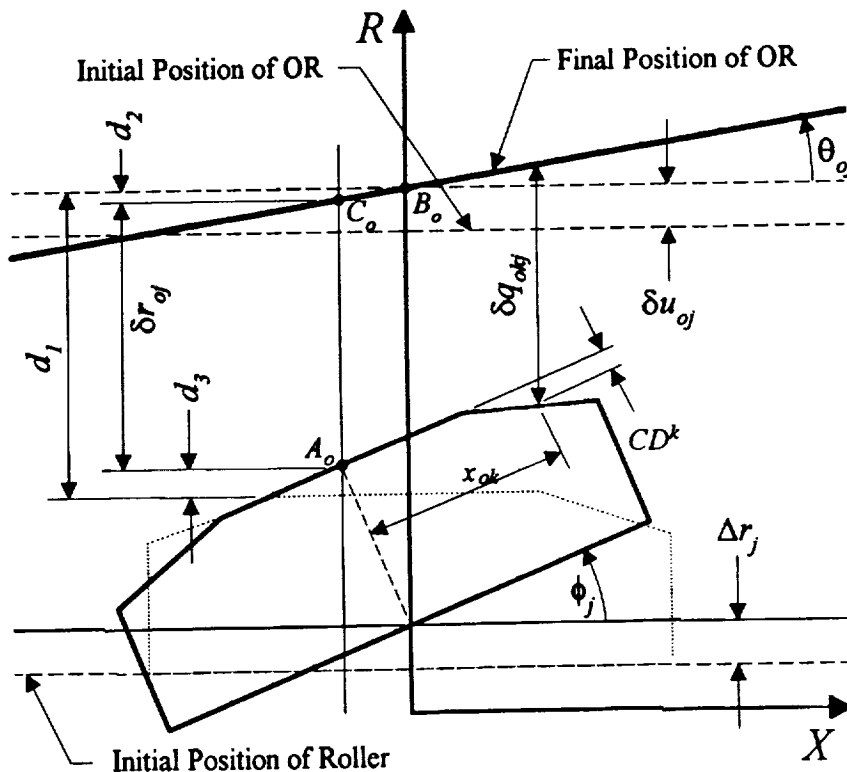
With radial translation but no rotation, the radial separation at point A_o is the distance d_1 in Figure 6-2 given by

$$d_1 = \delta u_{oj} - \Delta r_j$$

The radial increments associated with the two inertial rotations are shown in Figure 6-2 as d_2 and d_3 and are given analytically by

$$d_2 = D/2 \, \sin(\phi_j) \, \tan(\theta_{oj})$$

$$d_3 = D/2 \, [1 - \cos(\phi_j)]$$

The total radial interference between points A_o and C_o is then

$$\delta r_{oj} = d_2 - d_1 - d_3 = \Delta r_j - \delta u_{oj} - D/2[1 - \cos(\phi_j - \theta_{oj})/\cos(\theta_{oj})] \qquad (6\text{-}3)$$

The radial interference at the center of the kth slice of the jth roller (δq_{okj}) is shown negative in Figure 6-2 as a separation rather than an interference for clarity. An analytical expression for this interference, which includes a slight approximation for crown drop, is

$$\delta q_{okj} = \delta r_{oj} + x_{ok} \sin(\phi_j - \theta_{oj})/\cos(\theta_{oj}) - CD_k \qquad (6\text{-}4)$$

The crown drop approximation for the incremental decrease in radial interference is

$$CD_k \approx CD_k \cos(\phi_j - \theta_{oj})/\cos(\theta_{oj}) \qquad (6\text{-}5)$$

This simplifying approximation is, for the small angles expected, accurate to several significant digits. Probably the crown drop data, which can include raceway crown in addition to roller crown, has significantly greater variability than the error due to this approximation.

The basic kinematic constraint relations for radial interference, equations (6-3) and (6-4), are subsequently used to determine the Hertzian contact forces between the roller and outer ring.

6.2 Interference Between Roller and Inner Raceway

The initial mounted (unloaded) position of roller and inner raceway at the jth azimuthal plane has maximum radial clearance between roller and raceway at points A_i and B_i, shown in Figure 6-3 for the loaded condition. Under applied load, the roller centroid in the jth azimuthal plane translates radially a distance Δr_j, and rotates through a small angle ϕ_j. As with the outer ring, Δr_j, $= X(2)$ and $\phi_j = X(3)$ are the independent variables in the FEREBA equilibrium solution.

Simultaneously, the inner raceway translates in the radial direction a distance Δu_{rj} and rotates in the tilt direction through a small angle $\Delta \theta_j$. These two displacements of the inner raceway combine the imposed inertial translations and rotations of the inner ring and shaft with elastic distortions of the inner raceway in the jth azimuthal plane

$$\Delta u_{rj} = \Delta Y \cos(\Phi_j) + \Delta Z \sin(\Phi_j) + \delta u_{ij} \qquad (6\text{-}6)$$

$$\Delta \theta_j = \theta Z \cos(\Phi_j) - \theta Y \sin(\Phi_j) + \theta_{ij} \qquad (6\text{-}7)$$

The radial interference between point A_i on the roller and the radially adjacent point C_i on the inner raceway is δr_{ij}, shown negative in Figure 6-3 as a separation rather than an interference for clarity. With radial translation but no rotation, the radial separation at point A_i is the distance d_4 in Figure 6-3 given by

$$d_4 = \Delta r_j - \Delta u_{rj} + P_d/2 + \Delta P_d$$

The radial increments associated with the two inertial rotations are shown in Figure 6-3 as d_5 and d_6 and are given analytically by

Figure 6-3 Interference Between Roller and Inner Raceway (Loaded)

$$d_5 = D/2 \cdot (1 - \cos(\phi_j))$$

$$d_6 = R_i \cdot [1 - \cos(\theta_j)]/\cos(\theta_j) + D/2 \, \sin(\phi_j) \cdot \tan(\theta_j)$$

The total radial interference between points A_i and C_i is then

$$\delta r_{ij} = d_6 - d_4 - d_5 = \Delta u_{rj} - \Delta r_j - P_d/2 - \Delta P_d$$
$$+ R_i \, [1 - \cos(\theta_j)]/\cos(\theta_j) - D/2 \cdot [1 - \cos(\phi_j - \theta_j)/\cos(\theta_j)] \qquad (6\text{-}8)$$

The radial interference at the center of the kth slice of the jth roller (δq_{ikj}) is shown negative in Figure 6-3 as a separation rather than an interference. An analytical expression for this interference, which includes basically the same approximation for crown drop as used for the outer raceway, is

$$\delta q_{ikj} = \delta r_{ij} + x_{ik} \sin(\theta_j - \phi_j)/\cos(\theta_j) - CD_k \qquad (6\text{-}9)$$

The basic kinematic constraint relations for radial interference, equations (6-3) and (6-4) for the outer raceway and equations (6-8) and (6-9) for the inner raceway, are subsequently used to determine the roller Hertzian contact forces. The equations for roller forces and moments, required to calculate elastic deflections of the outer and inner raceways, are developed in the following section.

6-4

6.3   Roller Forces and Elastic Displacements

The roller/outer race Hertzian line contact force on the kth slice of the jth roller is

$$Q_{okj} = K_{oj} (\delta q_{okj})^{10/9} \qquad (6\text{-}10)$$

and the corresponding force at roller/inner race contact is

$$Q_{ikj} = K_{ij} (\delta q_{ikj})^{10/9} \qquad (6\text{-}11)$$

Each slice along each roller is checked independently for interference with both raceways. With positive interference, the Hertzian contact force is positive in compression. With negative interference (separation), the Hertzian contact force is zero. Q_{okj} may be defined as the radial force applied to the outer raceway by the roller. Q_{ikj} may be defined as the radial force applied to the roller by the inner raceway.

The total radial forces in the jth azimuthal plane are obtained by summing the contact forces at each slice:

$$P_{oj} = \Sigma \, Q_{okj} \qquad (6\text{-}12)$$

$$P_{ij} = \Sigma \, Q_{ikj} \qquad (6\text{-}13)$$

Here, again, P_{oj} is positive for a compressive force applied radially outward by the jth roller to the outer raceway, while P_{ij} is positive for a compressive force applied radially outward by the inner raceway to the jth roller.

The total tilt moments applied to the jth roller by the two raceways are similarly obtained by summing the contributions of the contact forces at each slice:

$$M_{oj} = - \Sigma \, Q_{okj} \, x_{ok} \qquad (6\text{-}14)$$

$$M_{ij} = \Sigma \, Q_{ikj} \, x_{ik} \qquad (6\text{-}15)$$

These tilt moments are defined positively, by the rotation of X into R, about the roller centroid.

Radial forces and tilt moments applied to the outer and inner raceways are converted to two statically equivalent radial forces on each raceway. These two forces are separated by a constant distance defined as a percentage of the roller effective length. The two forces applied to the outer raceway in the jth azimuthal plane for the right and left nodes of the outer ring finite-element model are given as follows:

$$F_{orj} = P_{oj}/2 - M_{oj}/(\lambda_o L_o) \qquad (6\text{-}16)$$

$$F_{olj} = P_{oj} - F_{orj} \qquad (6\text{-}17)$$

Similarly, the two forces applied to the inner raceway are given by

$$F_{irj} = - P_{ij}/2 - M_{ij}/(\lambda_i L_i) \qquad (6\text{-}18)$$

$$F_{ilj} = - P_{ij} - F_{irj} \qquad (6\text{-}19)$$

The two dimensionless constants λ_o and λ_i in equations (6-16) and (6-18) are set to values of 0.60, making the length of the moment arm ($\lambda_i L_i$) in equation (6-18) equal to 60 percent of the effective roller length. This value was chosen such that the maximum and minimum bending moments are approximately equal for a uniformly loaded beam on two supports. The finite element model master raceway nodes must be defined at locations established by this distance.

The forces applied to the inner and outer raceways (equations 6-16 through 6-19) produce corresponding elastic deflections at the same locations when applied to the appropriate finite-element model. These elastic deflections are then converted to the quantities required for the kinematic constraint relations (equations 6-3 through 6-9) as follows:

$$\delta u_{oj} = (\delta r_{orj} + \delta r_{olj})/2 \tag{6-20}$$

$$\theta_{oj} = (\delta r_{orj} - \delta r_{olj})/(\lambda_o L_o) \tag{6-21}$$

$$\delta u_{ij} = (\delta r_{irj} + \delta r_{ilj})/2 \tag{6-22}$$

$$\theta_{ij} = (\delta r_{irj} - \delta r_{ilj})/(\lambda_i L_i) \tag{6-23}$$

This complete set of equations results in a consistent system of forces and compatible displacements. The following sections outline the implementation of these equations into the FEREBA code.

7. NONLINEAR ELASTIC DEFLECTIONS OF OUTER RING AND CARRIER

The general finite-element model of the outer ring and carrier for single or duplex ball bearings contains soft springs to accommodate deadband and preload springs to accommodate axial preload effects. The corresponding flexibility matrix is partitioned as follows after the ANSYS stiffness matrix is transformed from ANSYS cylindrical coordinates to FEREBA cylindrical coordinates and reduced to eliminate the unnecessary DOFs:

$$
\begin{Bmatrix} U_1 \\ U_2 \\ U_3 \end{Bmatrix} = \begin{bmatrix} CO_{11} & CO_{12} & CO_{13} \\ CO_{21} & CO_{22} & CO_{23} \\ CO_{31} & CO_{32} & CO_{33} \end{bmatrix} \begin{Bmatrix} 0 \\ F_{bo} \\ F_c \end{Bmatrix} \tag{7-1}
$$

where $\{U_1\}$ = elastic axial (X) and radial (R) deflections of $ORCC$s, or for a roller bearing, the raceway contact points,.

$\{U_2\}$ = elastic X and R deflections of rolling element/outer race contact points where rolling element forces are applied,

$\{U_3\}$ = elastic X or R deflections of candidate contact points or gaps between the outer ring(s) and carrier,

$\{F_{bo}\}$ = X and R rolling element contact forces applied to the outer race, and

$\{F_c\}$ = X or R compressive constraint forces applied to contact points between the outer ring(s) and carrier when the gaps are closed.

Note that vectors $\{U_1\}$, $\{U_2\}$ and $\{F_{bo}\}$ have nodes in specific order for each of the outer ring/carrier support configurations defined by the index *IBSCOR*. Each of the nodes specified at the *ORCC* and ball/race contact points has an X and R DOF. The vectors $\{U_3\}$ and $\{F_c\}$ also have specific nodes for a given configuration, but each node has either an X DOF or an R DOF but not both. Note that the ball forces $\{F_{bo}\}$ and the flexibility coefficients (CO_{ij}) are known, but all the elastic deflections and the *mc* constraint forces $\{F_c\}$ are unknown.

Equation (7-1) may be written as follows with the unused partitions omitted:

$$
\begin{Bmatrix} U_1 \\ U_3 \end{Bmatrix} = \begin{bmatrix} CO_{12} & CO_{13} \\ CO_{32} & CO_{33} \end{bmatrix} \begin{Bmatrix} F_{bo} \\ F_c \end{Bmatrix} \tag{7-2}
$$

In this form, the flexibility matrix is directly applicable to the three roller bearing support configurations as well as to the six ball bearing configurations. The variables in equation (7-2) are now defined more generally as follows:

$\{U_1\}$ = elastic bearing deflections required for subsequent kinematic relations

$\{U_3\}$ = elastic deflections of candidate contact points or gaps between the outer ring and carrier

$\{F_{bo}\}$ = rolling element applied force vector

$\{F_c\}$ = compressive constraint forces applied to contact points between the outer ring and carrier when the gaps are closed

7-1

$[CO_{12}]$ = flexibility coefficients relating desired bearing deflections $\{U_l\}$ to rolling element forces $\{F_{bo}\}$

$[CO_{13}]$ = flexibility coefficients relating desired bearing deflections $\{U_l\}$ to constraint forces $\{Fc\}$ at closed gaps

$[CO_{32}]$ = flexibility coefficients relating gap deflections $\{U_3\}$ to rolling element forces $\{F_{bo}\}$

$[CO_{33}]$ = flexibility coefficients relating gap deflections $\{U_3\}$ to constraint forces $\{F_c\}$

It may be noted that the partitions of equation (7-2) comprise the entire flexibility matrix for the roller bearing configurations. This is because the desired bearing deflections $\{U_l\}$ are the same as the deflections $\{U_2\}$ of the points at which the rolling element forces are applied.

Each gap closure involves only a single axial or radial force magnitude which is normal to the contact surface. Friction forces in the plane of the contact surface are neglected, and the *DOFs* corresponding to friction forces have previously been reduced out of the flexibility matrix.

The constant contribution to $\{U_3\}$ is the displacement vector $\{U_{3b}\}$ corresponding to the known rolling element forces

$$\{U_{3b}\} = [CO_{32}]\{Fbo\} \tag{7-3}$$

where matrix $[CO_{32}]$ is of order *mc* by *mbo*. This constant deflection vector may be calculated immediately. The basic linear elastic equation relating constraint forces to the corresponding elastic deflections is

$$\{U_3\} - \{U_{3b}\} = [CO_{33}]\{Fc\} \tag{7-4}$$

where matrix $[CO_{33}]$ is of order *mc* by *mc*. From the basic matrix relation of equation (7-4), the row corresponding to the point on the outer ring at the kth gap is

$$U_3(O_k) - U_{3b}(O_k) = \sum_{j=1}^{mc} CO_{33}(O_{k,j}) * F_c(j) \tag{7-5}$$

where O_k denotes the X or R elastic deflection of the point on the outer ring at the kth gap, and j is the index of all *mc* candidate constraint forces. Similarly, the row corresponding to the adjacent point on the carrier at the kth gap is

$$U_3(C_k) - U_{3b}(C_k) = \sum_{j=1}^{mc} CO_{33}(C_{k,j}) * F_c(j) \tag{7-6}$$

where C_k denotes the X or R elastic deflection of the point on the carrier at the kth gap.

Positive faces are defined as those faces on the outer ring for which positive deflections of the outer ring initiate contact with a stationary carrier. By definition of the cylindrical coordinates, all radial faces of the outer ring are positive faces. Roller bearings are defined to have only radial DOFs. Ball bearings have both radial and axial DOFs. Axial faces on the positive X_l side of the ball bearing *ORCC* are also positive faces. Thus, for *IBSCOR = 2* in section 3.1, the gaps numbered 2, 3 and 4 are on positive faces. Axial faces on the negative X_l side of the ball bearing *ORCC* are negative faces. In the section 3.1 figure, gap number 1 is on the negative face. For

duplex ball bearing sets, the face between the primary and duplex bearing is defined as positive or negative with the same criterion as for single bearings. In all cases, positive contact forces are compressive.

7.1 Kinematic Constraints for Positive Faces

When the kth gap of a positive face is closed, the constraint forces on both sides of the gap are equal and opposite:

$$F_c(O_k) = -F_c(C_k) \tag{7-7}$$

where $F_c(C_k)$ is the positive (independent) constraint force applied by the outer ring to the carrier at the kth gap, and $F_c(O_k)$ is the negative constraint force applied by the carrier to the outer ring at the kth gap.

When the kth gap is closed, the points on both sides of the contact surface displace equally. This results in the following kinematic constraint relation based on the small deflection approximation:

$$U_3(O_k) = U_3(C_k) + G_k \tag{7-8}$$

where G_k is the input initial X or R clearance at the kth candidate contact point between outer ring and carrier. By definition, a positive value of G_k indicates clearance, whereas a negative value of G_k indicates interference.

For use in testing whether the kth gap is closed, equation (7-8) may be written as

$$\Delta g(k) = U_3(C_k) + G_k - U_3(O_k) \tag{7-9}$$

Then if $\Delta g(k) \leq 0$, gap closure may be assumed and the corresponding constraint forces must be calculated to enforce $\Delta g(k) = 0$.

A relation corresponding to equation (7-9) in terms of $\{U_{3b}\}$ is, for gaps at positive faces,

$$\Delta g_b(k) = U_{3b}(C_k) + G_k - U_{3b}(O_k) \tag{7-10}$$

The variables $\Delta g_b(k)$ may be calculated immediately since the terms are dependent only on known quantities. Subtracting equation (7-6) from equation (7-5) and substituting the relations in equations (7-8) and (7-10) gives the constraint equations in efficient computational form for positive faces:

$$\Delta g_b(k) = \sum_{j=1}^{mc} [CO_{33}(O_{k,j}) - CO_{33}(C_{k,j})] * F_c(j) \tag{7-11}$$

7.2 Kinematic Constraints for Negative Faces

When the kth gap of a negative face is closed, the constraint forces on both sides of the gap are equal and opposite but with signs reversed from equation (7-7):

$$F_c(C_k) = -F_c(O_k) \tag{7-12}$$

where $F_c(O_k)$ is now the positive (independent) constraint force applied by the carrier to the outer ring at the kth gap, and $F_c(C_k)$ is now the negative constraint force applied by the outer ring to the carrier at the kth gap.

When the kth gap is closed, the points on both sides of the contact surface displace equally. This results in the following kinematic constraint relation based on the small deflection approximation:

$$U_3(C_k) = U_3(O_k) + G_k \tag{7-13}$$

For use in testing whether the kth gap is closed, equation (7-13) may be written as

$$\Delta g(k) = U_3(O_k) + G_k - U_3(C_k) \tag{7-14}$$

Then if $\Delta g(k) \leq 0$, gap closure may be assumed and the corresponding constraint forces must be calculated to enforce $\Delta g(k) = 0$.

The relation corresponding to equation (7-14) in terms of $\{U_{3b}\}$ is, for gaps at negative faces,

$$\Delta g_b(k) = U_{3b}(O_k) + G_k - U_{3b}(C_k) \tag{7-15}$$

Subtracting equation (7-5) from equation (7-6) and substituting the relations in equations (7-13) and (7-15) gives the constraint equations in efficient computational form for negative faces:

$$\Delta g_b(k) = \sum_{j=1}^{mc} [CO_{33}(C_{k,j}) - CO_{33}(O_{k,j})] * F_c(j) \tag{7-16}$$

7.3 Solution Procedure for Assumed Gap Closures

Equations (7-11) and (7-16) may be written in matrix form as follows for only those *mcgc* gaps assumed to be closed

$$\{\Delta g_b\} = [-T_s]*[CO_{33}]*[T_s]^T*\{F_{cc}\} \tag{7-17}$$

This format relies on the fact that matrix $[CO_{33}]$ is symmetric. Matrix $[T_s]$ is of order *mcgc* by *mc* and is defined to extract vector $\{\Delta g_b\}$ from vector $\{U_{3b}\}$ using equations (7-10) and (7-15). For positive faces, matrix $[T_s]$ is a sparse matrix wherein the kth row consists of all zeros except for a -1.0 in the column corresponding to point O_k and a $+1.0$ in the column corresponding to point C_k. For negative faces, the signs of the coefficients corresponding to points O_k and C_k are reversed. Note that the sign of matrix $[T_s]$ must be reversed, as shown, for extracting the proper influence coefficients using equations (7-11) and (7-16).

The modified force vector $\{F_{CC}\}$ contains only *mcgc* non-zero independent constraint forces defined in equations (7-7) and (7-12). Note that there is only one independent constraint force

per gap and that this constraint force is positive in compression. The relationship between $\{F_{CC}\}$ and $\{F_c\}$ is expressed in matrix form as

$$\{F_c\} = [T_s]^{\text{T}}*\{F_{cc}\} \tag{7-18}$$

The independent constraint forces required to satisfy the kinematic constraints of equations (7-8) and (7-13) for the *mcgc* gaps assumed to be closed are then calculated simply by inverting equation (7-17)

$$\{F_{cc}\} = ([-T_s]*[CO_{33}]*[T_s]^{\text{T}})^{-1}*\{\Delta g_b\} \tag{7-19}$$

The inverted matrix is generally not positive definite, but it is non-singular. The validity of the set of assumed gap closures could be assessed by checking for impossible negative (tensile) independent constraint forces $\{F_{cc}\}$ and impossible negative (overlapping) gap separation distances $\{\Delta g\}$. Equation (7-20) for $\{\Delta g\}$ is the matrix formulation of equations (7-9) and (7-14):

$$\{\Delta g\} = [T_f](\{U_{3b}\} + [CO_{33}]\{F_c\}) + \{G\} \tag{7-20}$$

where $[T_f]$ is the full matrix $[T_s]$. The check relation actually used is slightly more complex than equation (7-20) because of the nonlinear preload spring which has zero force when unloaded.

7.4 Preload Spring Unloading

For single ball bearings or duplex ball bearing sets which admit axial preload, the preload spring is represented by appropriate axial stiffness terms at each azimuthal plane. These local preload springs are treated like the fictious soft springs required to convert the stiffness matrix of the outer ring(s) and carrier into a flexibility influence coefficient matrix. Therefore, the basic analysis procedure will properly represent the preload force in each local spring both in the linear spring range and after the preload spring has bottomed. However, when the separation distance at one of the preload spring gaps exceeds the initial G_k separation, the basic analysis procedure will calculate an impossible tensile force in this local preload spring. Some modifications to the basic procedure are then required to null the preload tensile force. This modification may be summarized as follows for the conditions relating to a local axial preload spring.

At each azimuthal plane, the local preload spring is defined to have zero force when the initial spring length equals G_k. When the separation distance at a preload gap decreases from its initial value, a compressive force is properly developed in the preload spring. When the separation distance at a preload gap increases from its initial value, an impossible tensile force is developed which must be nulled by a self-equilibrating pair of externally applied constraint forces with magnitude F_{prei}. When the relative deflection between the two surfaces of a preload gap exceeds zero $\Delta g_p > 0$, the required compressive constraint force required to null the impossible tensile force is

$$F_{prei} = K_{prei} * \Delta g_p \tag{7-21}$$

where K_{prei} is the linear stiffness coefficient of each local preload spring. For each ball bearing configuration which accepts axial preload, the appropriate signs are given to F_{prei} to form the pair of external constraint forces contained in vector $\{F_{cp}\}$. These additional constraint forces are then included in the solution procedure along with those constraint forces due to closed gaps obtained from equation (7-18).

8. PROGRAMMING IMPLEMENTATION

This section is provided as a guide to installing and maintaining the FEREBA software. Sections are also included that describes the nonlinear iteration methodology incorporated in the program. For reference, a flowchart is provided which lists all the subroutines in the code.

8.1 Flowchart

A flowchart displaying the subroutine names and execution hierarchy is contained in Figures 8-1 and 8-2. In the first figure, routines that read the analysis file (READAF module), perform problem initialization (CALCON module), and create the compliance matrices (FEMFLX module) are listed.

```
FEREBA
 ├─DBLSET    sets double precision arrays to a constant (used in many routines)


 ├─READAF    reads analysis variables and bearing data from analysis file written by PREBAN
 │   └─GETARG   returns command line arguments (note - system specific routine)


 ├─DATOUT    prints analysis summary - geometry, loads, fits, materials, temperatures
 │   ├─FDATE    writes analysis time and date to output file (note - system specific routine)
 │   └─ROLDAT   prints data on rolling elements specific to ball or roller bearing


 ├─CALCON    calculates general constants relevant to all bearing types
 │   ├─BCON   defines parameters specific to ball bearings
 │   │   └─ABDEL    calculates dimensions and elastic constants for point contact
 │   ├─CRCON   defines parameters specific to roller bearings
 │   │   ├─SLICES    calculates slice constants and crown drops for cylindrical roller bearing
 │   │   ├─SETGAP    sets gap between roller flange and roller end depending on flange type
 │   │   └─ABDEL    calculates dimensions and elastic constants for line contact
 │   ├─SPRING   determines approximate spring compliances for axial, radial, and angular loads
 │   ├─INDEL    makes initial guess on inner ring global deflections
 │   └─TMPFIT    calculates change in clearances due to differential temperature effects


 ├─FEMFLX    reads finite element substructures and converts to reduced flexibility matrices
 │   ├─ETIME    elapsed time counter (note - system specific routine)
 │   ├─RD8ASC   reads ASCII format ANSYS substructure matrices, storing stiffness only
 │   ├─MATPRT   prints out matrices 12 columns per page (for diagnostics)
 │   ├─TRANAF   reorders DOFs in stiffness matrices to FEREBA system
 │   ├─ADDSTF   adds 'dummy' springs for preload & deadband
 │   ├─MATRED   condenses DOF out of cylindrical stiffness matrices
 │   │   └─SHIFTS    shifts rows and columns of stiffness matrices over removed DOF
 │   ├─DLFIRG   IMSL routine to obtain solution to linear equation set
 │   ├─DLFTRG   IMSL routine that computes LU factor of a matrix
 │   ├─CODIM   sets dimensions of outer ring/carrier flexibility matrix
 │   ├─COART   stores required partitions of outer ring/carrier flexibility matrices
 │   ├─CIDIM   sets dimensions of inner ring/shaft flexibility matrix
 │   └─CIPART   stores required partitions of inner ring/shaft flexibility matrices
```

continues

Figure 8-1 FEREBA Flowchart (Initialization & Matrix Manipulation Routines)

```
[FEREBA]

 ├─QSTATE    drives solution of quasi-static equilibrium problem
```

```
─ETIME      elapsed time counter (note - system specific routine)
─GAPDEF     sets values of gaps depending on ring configurations
─PRELOD     determines axial displacement of inner ring due to axial preload
      ─NRSOLV     determines axial preload contact angle using a Newton-Raphson iteration
      ─DEFLOP     calculates average linear elastic ORCC deflections due to axial preload
      ─DEFLIP     calculates average linear elastic IRCC deflections due to axial preload
─DO 1, NITER    iteration loop on elastic displacements (NITER set by user)
      ─SLVBEQ     directs solution of bearing inner ring force equilibrium equations
            ─DO 1, NITRF    iteration loop on inner ring force equilibrium (NITRF set by user)
                  ─DO 1, NBRG    loop on each bearing (maximum of 2) to get loads or deflections
                        ─GUESS      get initial guesses of cage and ball/roller unknowns
                              ─GROLLB     sets roller positions, rotational and orbital speeds
                              ─GBALLB     sets ball positions, rotational and orbital speeds
                              ─GUESCG     estimates cage-ring relative motion & assigns cage DOFs*
                        ─BRGFOR     determines bearing loads to match assumed or given deflections
                              ─PREPAR     initialize rolling element, cage variables, and arrays
                                    ─BALLIN     calculates curvature center distances (ball bearing)
                                    ─UNLODB     determines if ball is out of contact with inner race
                                    ─UNLODR     determines if roller is out of contact with inner race
                                    ─MAXMIN     sets max/min values for cage and rolling element variables
                              ─DNEQNF     IMSL solution for nonlinear equations with numerical partials
                                    ─BEAREQ     sets up equilibrium equations depending on bearing type
                                          ─BALLEQ     defines ball bearing equilibrium equations
                                                ─FMIX       calculates frictional load components*
                                                ─BDRAG      calculates drag coefficient*
                                          ─ROLLIN     transforms coordinates for interference calculations
                                                ─FLNDEF     calculates roller/flange interference
                                                ─ROLLEQ     defines roller bearing equilibrium eqns
                                                      ─TPNORM     calculates loads about roller CG
                                                      ─FLNORM     determines flange loads
                                                      ─FMIXR      calculates frictional load components*
                                                      ─FLMIX      calculates flange frictional loads*
                                          ─BRGAX      calculates rolling element acceleration terms*
                                          ─CAGEEQ     defines cage-element interaction*
                              ─CALFOR     calculates forces acting on outer ring
                              ─SUMFIR     sums forces and moments acting on inner ring
                        ─DLSLRG     IMSL routine to solve set of linear force equilibrium equations
                  ─GUESS      get final values of cage and ball/roller deflections and speeds
            ─DEFLOR     calculates elastic deflections of outer ring/carrier
                  ─CNCLSD     produces a set of assumed gap closures (based on current deflections)
                  ─CNSTIF     computes constraint transformation matrix (for gap closures)
                  ─LFTOFF     modifies constraint forces to null tension
                  ─DLINRG     IMSL routine to invert constrained flexibility matrix
            ─DEFLIR     calculates elastic deflections of inner ring/shaft
            ─ERRCAL     checks values of elastic deflections, revises if necessary
      ─LIFE       calculates bearing fatigue life
            ─FLMFAC     lubrication film factor for life adjustment*

─OUTRSP     writes solution data to print file
      ─RELOUT     writes rolling element output
      ─REFLOT     writes output for roller bearing flanges
```

Figure 8-2 FEREBA Flowchart (Main Calculation Section Routines)

In Figure 8-2, which illustrates the primary quasi-static equilibrium modules, several routines are marked with an asterisk (*). These routines are not required for the current version of FEREBA, and were included for future editions which intended to add friction to the calculations. In the present code, these routines are simple shells, and perform no functions.

8.2 Nonlinear Elastic Deflection Implementation

The nonlinear elastic deflection solution is one of the more significant features of FEREBA. The solution procedure described in section 7 is implemented in subroutine DEFLOR using rolling element forces $\{F_{bo}\}$ and initial gap separation distances $\{G\}$ input from subroutine QSTATE and using flexibility influence coefficient partitions. The output of DEFLOR is the elastic deflections $\{U_{lb}\}$, designated $\{U_l\}$ in equations (7-1) and (7-2), of the ORCC or roller bearing desired for subsequent use in the kinematic constraint relations. Subroutine DEFLOR is called iteratively until the rolling element forces $\{F_{bo}\}$ and the corresponding elastic deflections $\{U_{lb}\}$ are consistent with the kinematic constraint relations.

The solution procedure leading to outer ring elastic deflections with deadband is accomplished in subroutine DEFLOR with the following 13 steps:

1. Calculate the constant elastic deflection vector $\{U_{3b}\}$, using equation (7-3) with given $\{F_{bo}\}$ and $[CO_{32}]$, for all candidate contact points or gaps.

2. Obtain the full constraint transformation matrix $[T_f]$ for all gaps from subroutine CNSTIF. The elements of sparse matrix $[T_f]$, (i.e., 0, -1, +1), are obtained immediately from the definitions of the various possible bearing support configurations. Matrix $[T_s]$, used primarily in equations (7-18) and (7-19), is a subset of $[T_f]$ corresponding only to the trial set of assumed gap closures.

3. Calculate the full vector of gap separation distances $\{\Delta g_f\}$ from equations (7-10) and (7-15) using matrix $[T_f]$. $\{\Delta g_f\}$ relates to all gaps, opened and closed, whereas $\{\Delta g_b\}$ is the subset of $\{\Delta g_f\}$ corresponding only to the trial set of assumed gap closures.

4. Assume the first trial set of assumed gap closures using subroutine CNCLSD. All radial gaps in the azimuthal plane nearest to the resultant applied radial force are initially assumed closed for both ball bearings and roller bearings. For the first pass with ball bearings, all axial gaps corresponding to the direction of the resultant axial load are assumed closed. Thus, for a positive axial load, gaps at positive outer ring faces are closed while gaps at negative faces remain open.

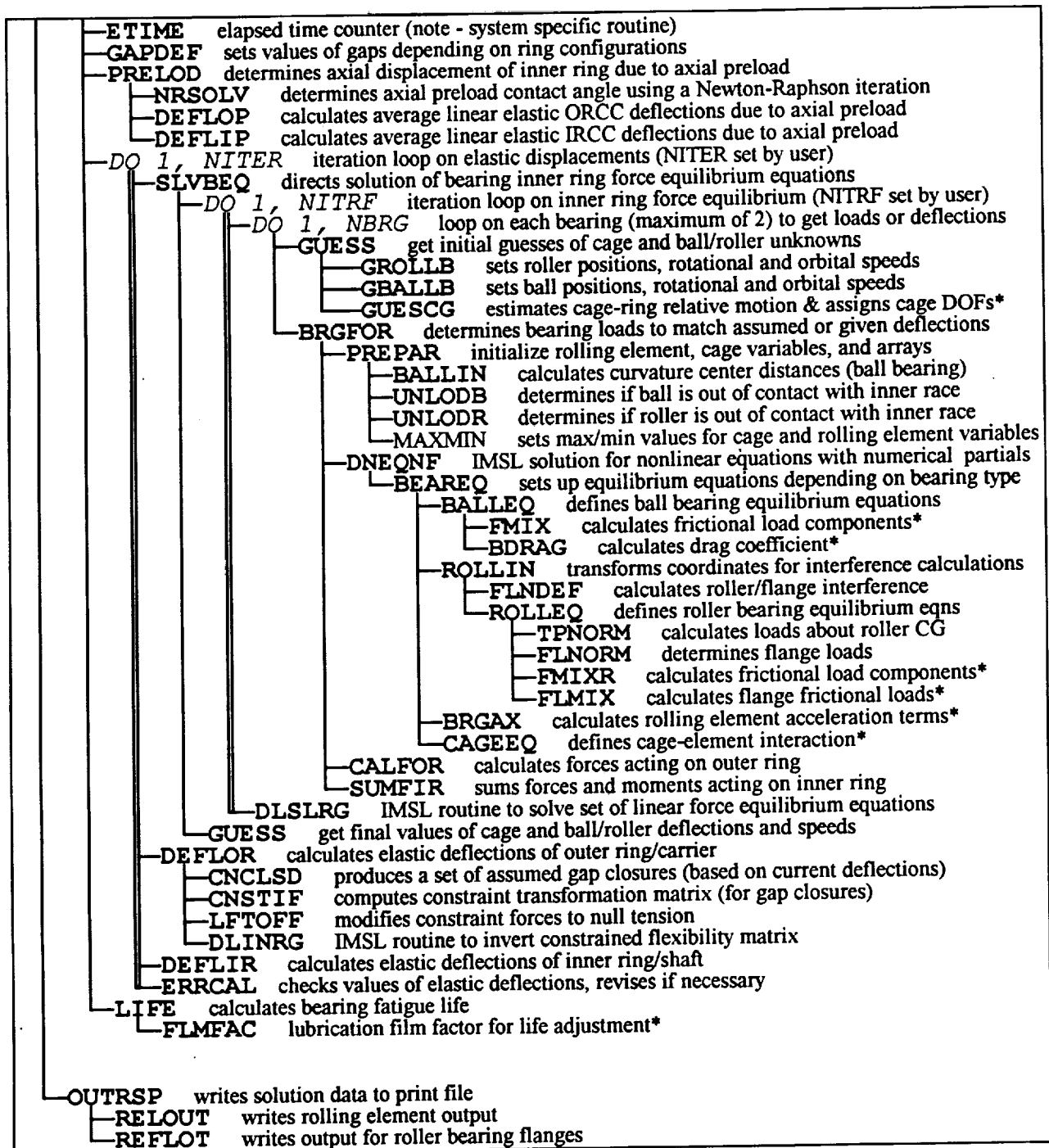5. Given the trial set of assumed gap closures, select the corresponding elements from matrix $[T_f]$ to form matrix $[T_s]$. Using the same procedure, select the appropriate elements from vector $\{\Delta g_f\}$ to form vector $\{\Delta g_b\}$. Thus matrix $[T_s]$ and vector $\{\Delta g_b\}$ correspond to closed gaps only.

6. Solve for the constraint forces $\{F_{cc}\}$ at each gap assumed closed using equation (7-19). Note that some of these constraint forces could be tensile (negative) if gaps are incorrectly assumed closed. This situation is corrected subsequently when a new set of assumed gap closures is defined. Note that equation (7-19) produces the exact linear solution for the given set of assumed gap closures.

7. Expand the independent constraint force vector $\{F_{cc}\}$ into the full vector $\{F_c\}$ using equation (7-18). Note that $\{F_{cc}\}$ and $\{F_c\}$ could contain the effects of impossible tensile preload spring forces.

8. Calculate total gap separation distances $\{\Delta g\}$ from equations (7-9) and (7-14) using matrix $[T_j]$ with the matrix notation of equation (7-20). This $\{\Delta g\}$ could contain the effects of impossible tensile preload spring forces.

9. Calculate $\{\Delta g_p\}$ as the relative deflections at each preload gap obtained from the preliminary $\{\Delta g\}$ calculation. Check for positive values of $\{\Delta g_p\}$ at preload gaps. If $\Delta g_p(k) > 0$, calculate additional constraint forces $\{F_{cp}\}$ required to null the impossible tensile forces in the preload spring. These operations are performed in subroutine LFTOFF using equation (7-21).

10. Recalculate $\{\Delta g\}$ with the additional constraint forces $\{F_{cp}\}$ which null any preload spring tensile forces. This calculation uses the equation (8-1) below, rather than equation (7-20).

$$\{\Delta g\} = [T_j](\{U_{3b}\} + [CO_{33}]\{F_c + F_{cp}\}) + \{G\} \tag{8-1}$$

11. Determine an updated trial set of gap closures based on two criteria:

    (a) A gap is closed if $\Delta g(k)$ is less than or equal to a specified tolerance value which accommodates round-off error in calculating $\{\Delta g\}$. From equation (7-19), the constraint forces $\{F_{cc}\}$ are calculated to enforce $\Delta g(k) = 0$ at the gaps assumed closed. Because of round-off error, $\Delta g(k)$ is usually calculated as a very small positive or negative number. The tolerance value is therefore a small positive number which may be machine dependent.

    (b) The trial set of gap closures determined from test (a) is modified to open any gap which has an independent constraint force $F_{cc}(k)$ less than zero. As noted previously, impossible tensile constraint forces can be generated by equation (7-19) if gaps are incorrectly assumed closed when they are actually open.

    These two tests attempt to define as closed those gaps which are in contact and which have contact compressive forces of zero or greater.

12. Compare the updated set of assumed gap closures with the prior set of gap closures. If the two sets of gap closures differ, return to step 5 and repeat the calculations with the updated set of gap closures. When all $F_{cc}(k) \geq 0$ and all $\Delta g(k) \geq 0$, continue to step 13.

13. When the closed gaps have been properly identified, calculate elastic deflections $\{U_{lb}\}$ using $\{F_{bo}\}$ and, where applicable, $\{F_c\}$ and $\{F_{cp}\}$ using equation (8-2).

$$\{U_{lb}\} = [CO_{12}]\{F_{bo}\} + [CO_{13}]\{F_{cp} + F_{cp}\} \tag{8-2}$$

Return to QSTATE to recalculate rolling element forces consistent with the kinematic constraint relations which now include the updated outer ring deflection vector $\{U_{lb}\}$.

8.3 Iterative Solution Methodology

The outermost iteration loop, as shown in Figure 8-2, determines overall elastic deflections of the outer and inner ring configurations in response to applied loads or specified displacements. The iteration is managed by QSTATE, in conjunction with subroutine ERRCAL, which checks assumed elastic deflections against user specified limits and revises the displacements using a nonlinear solution methodology.

The methodology incorporated into ERRCAL for the solution of the system of nonlinear equations uses a scheme from [9]. This procedure is an acceleration method which does not use partial derivatives as with a Newton-Raphson approach. The calculation of partials was explicitly avoided due to the potential for large Jacobian matrices to be formed. For instance, if a configuration with an outer ring of $IBSCOR = 6$ and 15 elements was used, the Jacobian would be 22 x 15, containing 330 evaluations *per iteration step*. The procedure does calculate implicit partials, and employs a secant type estimate for the next root.

This acceleration procedure attempts to minimize the difference between assumed and calculated elastic deflections at iteration n and $n+1$ based on the following relationship:

$$\{x^{n+1}\} = \{g(\{x^n\})\} \tag{8-3}$$

which in the program, is implemented with the following algorithm

$$\{x^{n+1}\} = \{\theta^n\}\{g(\{x^n\})\} + (\{I\} - \{\theta^n\})\{x^n\} \tag{8-4}$$

where $\{I\}$ is a unity vector and $\{\theta_n\}$ is a weighting factor, which for a single term is expressed as

$$\theta_i = \frac{1}{1 - g_{ii}(\{x^n\})} \tag{8-5}$$

where $g_{ii} = \partial g_i / \partial x_i$ is the partial derivative for the term under evaluation. In FEREBA, the actual value of any θ_i is limited to 0.25, which was set to prohibit large changes in assumed values. It was found that excessive corrections in iterates resulted in non-convergence for problems with many elastic displacement DOFs.

During development testing of FEREBA, significant effort was placed in the selection of this elastic displacement iteration routine. Initially, it was theorized that setting the first loop values to zero, then calculating terms with DEFLOR and using these finite values for the second iteration would be sufficient. For linear ring configurations, this is valid, however, for the nonlinear *IBSCOR* types, the first set of displacements were "close" but not within a reasonable error amount. As such, the entire iteration problem can be stated as a refinement of the initial values determined in DEFLOR, and thus the limit on θ_i to avoid large changes.

8.4 Variable List

FEREBA uses a storage scheme similar to SHABERTH, in that all of the primary problem variables are contained in several arrays. This section lists the contents of the arrays AVAR, BVAR, and BDAT, which in conjunction with the compliance matrices, store all of the significant program variables. Terms in these matrices can be printed for diagnostic purposes using the routine SYSCON, which is supplied with the source code. The first matrix listed is AVAR, which stores analysis variables.

Variable	Description
AVAR(1)	Type of analysis requested, read in READAF
AVAR(2)	NSLOT, type of quasi-static iteration run, set in READAF
	$\quad$ = 0 -> no iteration (normally not set)
	$\quad$ = 1 -> iteration without friction
	$\quad$ = 2 -> iteration with friction
AVAR(3)	Number of requested elastic deflection iteration loops, read in READAF, used in QSTATE
AVAR(4)	Required accuracy of elastic deflection iteration, read in READAF, used in QSTATE
AVAR(5-6)	
AVAR(7)	Number of requested inner ring force iteration loops, read in READAF, used in SLVBEQ
AVAR(8)	Required accuracy of inner ring force iteration, read in READAF, used in SLVBEQ
AVAR(9)	Flag to indicate if displacements (= 0) or loads (= 1) are specified, set in READAF
AVAR(10)	NPRINT, print flag for main analysis program, read in READAF
AVAR(11)	IBSCOR, outer ring configuration (0, ..., 9), read in READAF
AVAR(12)	IBSCIR, inner ring configuration (0, ..., 3), read in READAF
AVAR(13)	MBO, outer ring force vector FBO size (defined in CODIM)
AVAR(14)	MBI, inner ring force vector FBI size (defined in CIDIM)
AVAR(15)	MC, outer ring constraint vector FC size (defined in CODIM)
AVAR(16)	MCG, total number of outer ring gaps (defined in CODIM)
AVAR(17)	Number of elastic deflection iteration loops, set in QSTATE
AVAR(18)	Obtained accuracy in outer ring elastic deflection iteration
AVAR(19)	Obtained accuracy in inner ring elastic deflection iteration

The following positions are control integers for rolling element quasi-static iteration (first five formerly stored in IBD in SHABERTH)

AVAR(20)	IBRG, current bearing number being analyzed, set in BRGFOR
AVAR(21)	ISTEP, current solution index , set in BRGFOR
AVAR(22)	NARE, number of active rolling elements, set in BRGFOR & PREPAR (normally equal to total number of rolling elements except if cage only solution desired)
AVAR(23)	IMAX, index of most heavily loaded rolling element with frictional solution, set in BRGFOR
AVAR(24)	IRE, loop variable, current rolling element being analyzed (depends on ISTEP), set in BRGFOR
AVAR(25)	Number of iterations made in SLVBEQ
AVAR(26)	Accuracy in force iteration obtained in SLVBEQ (ERRMAX)
AVAR(27)	Number of times BEAREQ called by DNEQNF
AVAR(28-30)	

The next matrix listed is BVAR, which stores specific rolling element variables. BVAR is a 3-dimension array. The first dimension is the pertinent term, as described below. The second dimension is the particular rolling element, maximum of 20. The third dimension is bearing number, maximum of 2.

Element	Description
BVAR(1)	X-component of rolling element center position
BVAR(2)	Y-component of rolling element center position
BVAR(3)	X-component (axial) of rolling element rotational velocity
BVAR(4)	Y-component of rolling element rotational velocity
BVAR(5)	Z-component of rolling element rotational velocity
BVAR(6)	Orbital speed of rolling element
BVAR(7-8)	Outer/inner race-rolling element contact load
BVAR(9-10)	For ball bearing, sine of outer/inner race rolling element contact angle. Zero for roller bearing.
BVAR(11-12)	For ball bearing, cosine of outer/inner race rolling element contact angle. Unity for roller bearing.
BVAR(13-14)	For ball bearing, constant component of raceway groove curvature center distances ACON(1) and ACON(2), calculated in BALLIN. Blank for roller bearing.
BVAR(15)	UXP in center distance calculation for duplex bearing only

BVAR(16)
BVAR(17-20)   Elastic deflections of master nodes, either axial or radial, depending on bearing type:

Element	Ball Bearing	Roller Bearing
17	ORCC axial - UXORCC	Left outer race radial - UROL
18	ORCC radial - URORCC	Right outer race radial - UROR
19	IRCC axial - UXIRCC	Left inner race radial - URIL
20	IRCC radial - URIRCC	Right inner race radial - URIR

calculated in DEFLOR & DEFLIR, checked in ERRCAL

BVAR(21-24)   Outer/Inner ring rolling element forces, (axial or radial), depending on bearing type (i refers to rolling element):

Element	Symbol	Ball Bearing	Roller Bearing
21	FBO(i)	Outer ring axial	Left outer race radial
22	FBO(i+1)	Outer ring radial	Right outer race radial
23	FBI(i)	Inner ring axial	Left inner race radial
24	FBO(i+1)	Inner ring radial	Right inner race radial

calculated in CALFOR/SUMFIR, stored in FBO/FBI in SLVBEQ.

Element	Description
BVAR(25)	FW (gyro force) for outer ring, (not used), refed in SUMFIR
BVAR(26)	ZM for outer ring, calculated in ROLLEQ, used in CALFOR
BVAR(27-30)	Friction force components acting on inner ring; FW, FZ, YM, ZM, used in SUMFIR (refed but not used)
BVAR(31-32)	EHD film thickness at most heavily loaded outer/inner raceway/slice, calculated in FMIX/FMIXR (not used)
BVAR(33-34)	Outer/inner raceway contact area, used in FMIX and FMIXR
BVAR(35-36)	PMAX - in BALLEQ, maximum hertz stress, and in FMIXR, max hertz stress at most heavily loaded slice

The main storage of problem variables is in matrix BDAT, as listed below

Variable	Description
BDAT(1)	Bearing type (0, 1, 2, for ball, roller, or duplex)
BDAT(2)	Orientation angle of first rolling element (always 0)
BDAT(3)	Rotation speed of inner ring/shaft
BDAT(4)	Rolling element diameter
BDAT(5)	Pitch diameter to rolling element center
BDAT(6)	Number of rolling elements
BDAT(7)	Diametral clearance
BDAT(8)	Initial unloaded contact angle for ball bearing, based on diametral clearance, calculated in CALCON
BDAT(9)	
BDAT(10)	Roller length end to end
BDAT(11)	Roller end sphere radius
BDAT(12)	Roller included angle

The next six items are not used in quasi-static code, but the positions are retained for use in future frictional analyses

BDAT(13)	Outer race CLA surface roughness
BDAT(14)	Inner race CLA surface roughness
BDAT(15)	Rolling element CLA surface roughness
BDAT(16)	Outer race asperity slope
BDAT(17)	Inner race asperity slope
BDAT(18)	Rolling element asperity slope

BDAT(19)	
BDAT(20)	Roller crown radius
BDAT(21)	Roller flat length or ball bearing outer race curvature
BDAT(22)	Ball bearing inner race curvature or number of roller/raceway axial slices (maximum of 20, set in READAF)
BDAT(23)	Roller outer raceway effective length
BDAT(24)	Roller inner raceway effective length
BDAT(25)	Roller outer raceway crown radius
BDAT(26)	Roller inner raceway crown radius
BDAT(27-30)	
BDAT(31)	Cylindrical roller bearing outer ring flange angle
BDAT(32)	Cylindrical roller bearing inner ring flange angle
BDAT(33)	Cylindrical roller bearing outer ring end play
BDAT(34)	Cylindrical roller bearing inner ring end play
BDAT(35)	Cylindrical roller bearing flange inversion flag

The next six items are not used in quasi-static code, but the positions are retained for use in future frictional analyses

BDAT(36)	Cage type (-1, 0, +1) for outer ring land, inner ring land, or rolling element riding
BDAT(37)	Cage rail land diameter
BDAT(38)	Cage single rail width
BDAT(39)	Cage rail land diametral clearance
BDAT(40)	Rolling element cage pocket diametral clearance
BDAT(41)	Cage weight

Contents of main problem variable storage matrix BDAT, continued

Variable	Description
BDAT(42-43)	Input (42) and output (43) values of cage degrees of freedom, set in PREPAR
BDAT(44-45)	Life multipliers for outer/inner ring
BDAT(46-50)	Input values of applied displacements (x-trans, y-trans, z-trans, y-rot, z-rot)
BDAT(51)	Inner ring mean outer diameter
BDAT(52)	Outer ring mean inner diameter
BDAT(53)	Outer ring mean outer diameter
BDAT(54)	Carrier mean inner diameter
BDAT(55)	Axial gap between outer ring and carrier
BDAT(56)	Initial axial distance between duplex ball bearing centers
BDAT(57)	Initial axial gap between duplex bearing outer rings
BDAT(58-65)	
BDAT(66-70)	Elastic Moduli for shaft, inner ring, rolling elements, outer ring, and housing
BDAT(71-75)	Poisson's ratio for shaft, inner ring, rolling elements, outer ring, and housing
BDAT(76-80)	Density for shaft, inner ring, rolling elements, outer ring, and housing
BDAT(81-85)	Thermal Expansion Coefficient for shaft, inner ring, rolling elements, outer ring, and housing
BDAT(86-87)	
BDAT(88-92)	Input values of applied forces (Fx, Fy, Fz, My, Mz)

The next eighteen items are not used in quasi-static code, but the positions are retained for use in future frictional analyses

Variable	Description
BDAT(93)	Lubricant code - if = 0, implies no friction = ±1 to ±9 lubricant codes (friction) = ±10 implies dry friction the ± refers to traction mod (see SHABERTH manual)
BDAT(94)	Kinematic viscosity at 100° F
BDAT(95)	Kinematic viscosity at 210° F
BDAT(96)	Density at 15.5° C
BDAT(97)	Lubricant coefficient of thermal expansion
BDAT(98)	Lubricant thermal conductivity
BDAT(99-101)	Calculated data from LUPROP and LUBCON
BDAT(102)	Outer raceway lubricant replenishment layer thickness
BDAT(103)	Inner raceway lubricant replenishment layer thickness
BDAT(104)	Percent lubricant in bearing cavity
BDAT(105)	BDAT(104)/100, also XCAV in BCON & CRCON
BDAT(106)	Raceway-Rolling element asperity friction coefficient
BDAT(107)	Cage friction coefficient
BDAT(108)	Outer race flange replenishment layer thickness
BDAT(109)	Inner race flange replenishment layer thickness
BDAT(110)	Flange-Roller end friction coefficient
BDAT(111)	Inner ring speed in rad/sec, calculated in CALCON
BDAT(112-113)	
BDAT(114)	Rolling element y-axis inertia, calculated in CRCON
BDAT(115)	Rolling element x-axis inertia, calculated in BCON

Contents of main problem variable storage matrix BDAT, continued

Variable	Description
BDAT(116)	Rolling element mass, calculated in BCON
BDAT(117)	Sine of initial contact angle BDAT(8) calculated in CALCON
BDAT(118)	Total curvature of ball bearing (B), calculated in CALCON, used for contact angle calculation and in PRELOD
BDAT(119)	
BDAT(120-121)	Storage for variable EMOD in SHABERTH s/r CONS, calculated in CALCON, used in FMIX et al routines
BDAT(122)	RMS values of surface roughness, array RMS in CRCON
BDAT(123)	Sum of BDAT(127) and BDAT(128), variable CRVS in BCON (= A or BD), RMS(2) in CRCON
BDAT(124)	Cosine of initial contact angle BDAT(8) calculated in CALCON
BDAT(125-126)	Sine of roller bearing flange angles, array SINF in CRCON
BDAT(127-128)	Osculation parameters, array CRV in BCON; Cosine of roller bearing flange angles, array COSF in CRCON
BDAT(129-130)	Array ZEMA in BCON (See Jones 13.189 & 13.190); Flange height parameter, array ARMS in CRCON
BDAT(131-132)	Raceway/rolling element contact moduli calculated in CALCON
BDAT(133)	Variable Z10 defined in CALCON
BDAT(134)	Variable GP = BDAT(4) / BDAT(5) calculated in BCON & CRCON
BDAT(135-136)	
BDAT(137)	Variable Y calculated in BCON (initial IRCC radius, eqn 13.177 in Jones); WN2 = BDAT(22)/2 in READAF
BDAT(138)	Ball drag constant Z1, used in BALLEQ
BDAT(139)	Ball drag constant Z2, calculated in BCON & CRCON
BDAT(140)	Ball drag constant Z3, used in BALLEQ
BDAT(141-142)	Array W in CRCON, slice width
BDAT(143-144)	Ratio involving raceway curvatures, array RDEF in BCON
BDAT(145-146)	Ratio involving raceway curvatures, array REX in BCON; raceway array C2 in CRCON
BDAT(147)	Delta angular position of each rolling element
BDAT(148-152)	Contact deformation values CDEF(3,2), calculated in ABDEL
BDAT(153)	
BDAT(154-155)	Array RX in CRCON
BDAT(156)	Variable PREF in BCON, equal to .05 * rolling element dia
BDAT(157)	Relative inner ring speed (WREF), calculated in CALCON
BDAT(158-159)	Variable TF & TM in CALCON (see BRGAX for more details)
BDAT(159)	Variable TM in CALCON
BDAT(160)	Variable WREFYZ in BCON & CRCON, .2 * WREF (BDAT(157))
BDAT(161-163)	Equated to BSC(1-3) in SPRING
BDAT(164)	
BDAT(165)	Variable RPZ in CALCON, used in GUESCG
BDAT(166-167)	
BDAT(168)	Variable CRP in GUESCG, could be number of cage DOF
BDAT(169)	Variable DELYZ in GUESCG, vector sum of cage radial displacements
BDAT(170)	Variable THETA in GUESCG, angle of cage radial displacement
BDAT(171-175)	Calculated 5-axis inner ring displacements (x-trans, y-trans, z-trans, y-rot, z-rot)
BDAT(176-180)	Calculated 5-axis inner ring forces (Fx, Fy, Fz, My, Mz)

Contents of main problem variable storage matrix BDAT, continued

Variable	Description
BDAT(181-184)	
BDAT(185)	Change in bearing diametral clearance due to temperature, calculated in TMPFIT, used in CALCON, GROLLB, ROLLIN
BDAT(186)	Operating diametral clearance = BDAT(7) + BDAT(185) [not used]
BDAT(187)	Change in clearance between outer ring OD and housing for IBSCOR configurations with deadband, calculated in TMPFIT, used in GAPDEF
BDAT(188-189)	
BDAT(190)	Specified axial preload force, used only with duplex bearings
BDAT(191)	Specified axial preload spring stiffness, used with ball bearings
BDAT(192)	Resulting elastic axial displacements due to preload (UXP2), used only with duplex bearings

BDAT(193-200)
The next thirty items are not used in quasi-static code, but the positions are retained for use in future frictional analyses

Variable	Description
BDAT(201-202)	Maximum EHD film thickness HMAX defined in FMIXR
BDAT(203-204)	Miniscus distance variable DIST defined in FMIX & FMIXR
BDAT(205-206)	EHD reduction starvation factor PHIS defined in FMIX & FMIXR
BDAT(207-208)	EHD reduction thermal factor PHIT defined in FMIX & FMIXR
BDAT(209-210)	Outer/inner raceway lubrication life factor
BDAT(211-213)	Outer/inner raceway and overall bearing fatigue life
BDAT(214)	Equated to BDAT(215) in GUESCG
BDAT(215)	Variable WCAGE in GUESCG, angular speed of cage
BDAT(216-218)	
BDAT(219-220)	Array XCGF in CRCON
BDAT(221-222)	Composite raceway surface roughness, calculated in CALCON
BDAT(223-224)	Composite raceway asperity slope, calculated in CALCON
BDAT(225)	Outer ring flange CLA surface roughness (array SIGF in BCON/CRCON)
BDAT(226)	Inner ring flange CLA surface roughness
BDAT(227)	Rolling element end CLA surface roughness
BDAT(228)	Outer ring flange asperity slope (array SGF in BCON/CRCON)
BDAT(229)	Inner ring flange asperity slope
BDAT(230)	Rolling element end asperity slope
BDAT(231-232)	Array HT in CRCON
BDAT(233-234)	Array RACE in CRCON
BDAT(235-236)	Array RCFY in CRCON
BDAT(238)	Variable XLCG in CRCON (half roller length)
BDAT(239-240)	
BDAT(241-242)	Array RRFY in CRCON
BDAT(243-244)	Array RRF in CRCON
BDAT(245-246)	Array RCFX in CRCON
BDAT(247-248)	Array GAP in SETGAP, roller end gap
BDAT(249-270)	

Contents of main problem variable storage matrix BDAT, continued

Variable	Description

The next thirty items are not used in quasi-static code, but the positions are retained for use in future frictional analyses

BDAT(271-274)   Variable FLFAC(1) in ROLLEQ passed to FLMIX as DISTH, miniscus diatance variable

BDAT(275-278)   Variable FLFAC(5) in ROLLEQ passed to FLMIX as PHISH, EHD film reduction starvation factor

BDAT(279-282)   Variable FLFAC(9) in ROLLEQ passed to FLMIX as PHITH, EHD film reduction thermal facor

BDAT(283-286)   Variable FLFAC(13) in ROLLEQ passed to FLMIX as RATIOH, QASP/QTOT for roller bearing

BDAT(287-294)

BDAT(295-298)   Flange/roller conductivity terms

BDAT(299-300)   Outer/inner film thickness to surface roughness ratio, calculated in LIFE

BDAT(301-330)   Sine of rolling element angular position, set in CALCON

BDAT(331-360)   Cosine of rolling element angular position, set in CALCON

In the next six items, the first 20 positions refer to the roller bearing *outer* race, the last 20 positions refer to the *inner* race

BDAT(361-400)   Array DK in SLICES, roller slice radius

BDAT(401-440)   Roller bearing crown drops CD, calculated in SLICES

BDAT(441-480)   Slice half width constant BMI, calculated in SLICES

BDAT(481-520)   Array HM in SLICES, called from CRCON

BDAT(521-560)   Product of terms used to calculate film thickness (not used)

BDAT(561-600)   Array RK in SLICES

BDAT(601-605)   Temperatures of shaft, inner ring, rolling elements, outer ring, and carrier/housing. Note that flange and lube temperatures used in SHABERTH are not defined here. SHABERTH initially stores temperatures in an array TB, then transfers to these locations in routine SHABE.

BDAT(606)   Reference temperature for fit calculations, set to 70°F in CALCON, used in TMPFIT

BDAT(607-650)

BDAT(651-690)   Variable HZ in ROLLEQ, hertz contact stress, first 20 are for outer raceway, second 20 are for inner raceway

BDAT(691-750)

9. REFERENCES

The following references are specified in this manual by number:

1. Crecelius, W. J., and Milke, D. R., "Dynamic and Thermal Analysis of High Speed Tapered Roller Bearings Under Combined Loading," NASA CR-121207, (SKF Report No. AL73P010), March 1973.

2. Jones, A. B., "A General Theory for Elastically Constrained Ball and Radial Roller Bearings Under Arbitrary Load and Speed Conditions," Journal of Basic Engineering, ASME Transactions, Volume 82, pp. 309-320, June 1960.

3. Harris, T. A., Rolling Bearing Analysis, 2nd Edition, John Wiley, 1984.

4. Davis, R. R., and Vallance, C. S., "Incorporating General Race and Housing Flexibility and Deadband in Rolling Element Bearing Analysis", Rotordynamic Instability Problems in High-Performance Turbomachinery - 1988, NASA CP 3026, May 1980.

5. DeSalvo, G.J., and Gorman, R.W., "ANSYS Engineering Analysis System User's Manual," Swanson Analysis Systems, Inc., 1 August 1989.

6. Liu, J.Y., "The Effect of Misalignment on the Life of High Speed Cylindrical Roller Bearings," Journal of Lubrication Technology, ASME Transactions, Jan 1971, pp. 60-68

7. Hadden, G.B., R.J. Kleckner, M.A. Ragen, and L. Sheynin, "Steady State and Transient Thermal Analysis of a Shaft Bearing System Including Ball, Cylindrical and Tapered Roller Bearings," NASA CR No. 165365, May 1981.

8. deMul, J.M., J.M. Vree, and D.A. Maas, "Equilibrium and Associated Load Distribution in Ball and Roller Bearings Loaded in Five Degrees of Freedom While Neglecting Friction--Part II: Application to Roller Bearings and Experimental Verification," Journal of Tribology, ASME Transactions, Vol. 111, Jan 1989, pp. 149-155.

9. Isaacson, E., and H. B. Keller, Analysis of Numerical Methods, John Wiley, 1966.

The following references are not explicitly discussed in this manual, and are included for additional sources of information in the area of bearing analysis.

Conry, T. F., "Transient Dynamic Analysis of High Speed Lightly Loaded Cylindrical Roller Bearings, Parts I and II," NASA Technical Reports 3334 and 3335, NASA/Lewis, 1981.

Crecelius, W. J., and Pirvics, J., "Computer Program Operation Manual on SHABERTH, A Computer Program for the Analysis of the Steady-State and Transient Thermal Performance of Shaft Bearing Systems," USAF Technical Report AFAPL-TR-76-90, U. S. Aero Propulsion Lab, Wright Paterson AFB, 1976.

Filetti, E. G. and Rumbarger, J. H., "A General Method for Predicting the Influence of Structural Support Upon Rolling Element Bearing Performance", Journal of Lubrication Technology, ASME Trans, Vol 92, pp 121-128, 1970.

Gupta, P. K., "Transient Ball Motion and Skid in Ball Bearings," Journal of Lubrication Technology, ASME Trans, Vol 97, pp 261-269, 1975.

Gupta, P. K., "Dynamics of Rolling Element Bearings, Parts I, II, III, and IV," Journal of Lubrication Technology, ASME Trans, Vol 101, pp 293-326, 1979.

Gupta, P. K., "A Review of Computerized Simulations of Roller Bearing Performance," Computer-Aided Design of Bearings and Seals, Proc. AMSE Annual Meeting, Dec 1976.

Hadden, G. B., Kleckner, R. J., Ragen, M. A., and Sheynin, L., "Steady State and Transient Thermal Analysis of a Shaft Bearing System Including Ball, Cylindrical, and Tapered Roller Bearings (SHABERTH User's Manual)," NASA Technical CR 165365, NASA/Lewis, 1981.

Harris, T. A. and Mindel, M. H., "Rolling Element Bearing Dynamics," Wear, Vol 23, pp 311-337, 1973.

Jones, A. B., "The Mathematical Theory of Rolling-Element Bearings," Mechanical Design and Systems Handbook, Chapter 13, Rothbart, Ed., McGraw-Hill, 1963.

Kleckner, R. J., Pirvics, J. and Castelli, V., "High-Speed Cylindrical Rolling Element Bearing Analysis CYBEAN - Analytical Formulation," Journal of Lubrication Technology, ASME Trans, Vol 102, pp 380-390, 1980.

Kleckner, R. J. and Pirvics, J., "High-Speed Cylindrical Rolling Element Bearing Analysis Computer Program CYBEAN - Volumes I and II," NASA CR 159460, NASA Lewis Research Center, 1978.

Kleckner, R. J. and Pirvics, J., "Spherical Roller Bearing Analysis," Journal of Lubrication Technology, ASME Trans, Vol 104, pp 99-108, 1982.

Rumbarger, J. H., Filetti, E. G., and Gubernick, D., "Gas Turbine Engine Mainshaft Roller Bearing-System Analysis," Journal of Lubrication Technology, ASME Trans, Vol 95, pp 401-416, 1973.

Sibley, L. B. and Pirvics, J., "Computer Analysis of Roller Bearings," Computer-Aided Design of Bearings and Seals, Proc. AMSE Annual Meeting, pp 95-115, Dec 1976.

Walters, C. T., "The Dynamics of Ball Bearings," Journal Lubrication Technology, ASME Trans, Vol 93, pp 1-10, 1971.

STATIC LOAD-DISPLACEMENT TEST OF SINGLE BALL BEARING

D. H. Merchant   23 July 1994

TEST DESCRIPTION AND RESULTS:

A discussion of the special relations between forces applied to the test rig and the statically equivalent forces and moments input to FEREBA is provided in Attachment 1. Attachment 2 is a listing of the FEREBA input data file used for the pretest analysis for the no-deadband configuration. The axial preload spring stiffness of 73,400 lb/in represents the slope of the nonlinear load-displacement curve for small loads. This Belleville spring bottoms with a maximum load of about 3800 lb at a maximum stroke ("Outer Ring/Hsg Axial Gap") of 0.093 in. For the deadband test configuration, the carrier inner diameter exceeds the outer ring outer diameter by 0.0002 in; this results in a measured radial deadband of 0.0001 in.

Attachment 3 comprises the informal notes, for both bearing tests, prepared by the Test Engineer. Raw data consisting of applied forces, measured by four load cells, and corresponding displacements, measured by four Bently probes, are listed on page 3-4 for Test 1 and on page 3-7 for Test 2. The XF-YF-ZF coordinates for the transducer locations listed in Table 1 apply to the FEREBA analysis. To order the test rig locations for consistency with those for the FEREBA analysis, it is necessary to interchange the values for B2 and B3 and for L2 and L3.

As noted in Attachment 1, the forces applied to the test rig are the carrier support reactions in the FEREBA analysis. The FEREBA input loads must thereforce be calculated from the applied test rig loads (plus distributed carrier weight) by appropriate transformation relations. These equations are coded, for example, in Attachment 4a for Case 6 of the deadband configuration (Test 2). The corresponding forces and moments input to FEREBA for this case are listed in Attachment 4b. A complete set of test-rig applied forces and statically equivalent FEREBA forces and moments are listed in Tables 2 and 3 for both tests. Forces for the five runs for each load case are averaged.

For comparison with FEREBA calculated displacements, the test rig displacements must be converted to equivalent translations and rotations relative to the shaft inner ring. This conversion is accomplished by the transformation equations coded, for example, in Attachment 5a for Case 1 of the no-deadband configuration (Test 1). The corresponding equivalent shaft displacements for the case are listed in Attachment 5b. A complete set of these test rig "measured" displacements are listed in Tables 4 and 5 for both tests. Displacements for the five runs for each load case are averaged.

The displacements measured on the test rig by the Bently probes do not include the initial axial displacement due to the carrier weight of 24 lb. For comparison with test rig "measured" displacements, the axial displacement due to preload (Ux = 0.0006 in) must be subtracted from the FEREBA displacements calculated with applied loads plus 24-lb axial preload. The resulting relative shaft displacements are listed in Tables 4 and 5 as FEREBA output displacements.

CONCLUSIONS:

1. The forces applied to the test rig for both tests show very small run-to-run variations from the intended forces.

2. The displacements measured for the no-deadband configuration show acceptably small run-to-run variations. In particular, the four runs without applied load (Case 0) show excellent repeatability.

3. The displacements measured for the 0.0001-inch deadband configuration show rather large run-to-run variations. In particular, the six runs without applied load (Case 0) show poor repeatability. This probably indicates stiction in the bearing load path.

4. One variable which could not be accounted for between test and analysis is the alignment of radial force relative to ball locations. The potential magnitude of this effect was not evaluated.

5. FEREBA did not converge to input forces and moments for several cases. Correlation between test "measured" displacements and FEREBA output displacements is difficult to assess because of the relative errors in translation and rotational displacements.

6. An alternate procedure is available with FEREBA to correlate measured and calculated data. It is possible to input "measured" displacements to FEREBA and calculate corresponding shaft forces to compare with test values designated as FEREBA input forces. This procedure would avoid the previously noted convergence problems since no convergence is involved with the displacement input option. Whether assessing correlation becomes easier with this procedure was not determined.

REPRESENTATION OF TEST RIG FOR FEREBA PRETEST ANALYSIS

Version 1   D. H. Merchant   12-15-93

COORDINATE SYSTEM AND CONSTRAINTS:

In FEREBA, the thrust force is applied in the + X direction to the inner ring and shaft at the center of the unmounted bearing. This corresponds to the + Z direction in the ANSYS finite-element model. FEREBA then automatically transforms the ANSYS reduced stiffness matrix in cylindrical coordinates from the ANSYS coordinate system (RA-θA-ZA) to the required FEREBA cylindrical coordinate system (XF-RF-ΦF). The constraints applied to the ANSYS carrier model must be consistent with the FEREBA coordinate system.

The solution procedure in FEREBA is predicated on a bearing system which has the carrier fixed in inertial space and which has forces or displacements prescribed at the inner ring and shaft. Whether forces or displacements are prescribed, the inner ring/shaft undergoes five independent small displacements to result in rolling element forces. For the test rig, the inner ring and shaft are fixed in inertial space and forces are applied to the carrier to result in rolling element forces.

To represent the bearing and carrier of the test rig using the FEREBA solution procedure, it is necessary to replace the forces applied to the test rig carrier by reaction forces at the carrier supports of the ANSYS/FEREBA model. By constraining six degrees of freedom on the ANSYS carrier in a statically determinate manner and by applying appropriate forces and moments at the center of the unmounted bearing, the reaction forces on the FEREBA carrier can be made identical to the forces applied to the test rig carrier. Four of the six constrained degrees of freedom in the ANSYS model must be exactly those at which the three axial forces and one radial force are applied to the test rig carrier. And the forces and moments applied at the center of the FEREBA bearing must exactly equilibrate the forces applied to the test rig carrier.

The deflections measured by the test rig are relative deflections between the fixed inner ring and the movable carrier. The measured deflections are therefore equivalent to those calculated by FEREBA so long as there is negligible elastic deflection of the test rig's shaft connecting the inner ring to ground. Since this shaft is solid steel with diameter exceeding that of the inner ring, the shaft elastic deflections are justifiably neglected.

FEREBA INPUT DATA FOR PRETEST ANALYSIS (CASE 6)

Rig Ball Bearing, IBSCOR/IBSCIR = 3/1, Fa = 828, Fr = 600

Date this analysis file written: Thu Feb 3, 1994

Time this analysis file written: 10:36:50

fembor.asc   fembir.asc

CONTROL
1	Analysis Type
0	Bearing Type (0, 1, or 2)
0	Analysis Units
50.00000	Ring Disp Iteration Loops
0.001000000	Ring Disp Iteration Error (%)
100.0000	Force Iteration Loops
1.000000E-04	Force Iteration Error (%)
2.000000	Analysis Print Flag
3.000000	Outer Ring Configuration
0.0000000E+00	Inner Ring Configuration

GENERAL
0.0000000E+00	Shaft Speed
3.366000	Bearing Pitch Diameter
14.00000	Number of Rolling Elements
1.000000	Outer Ring Life Multiplier
1.000000	Inner Ring Life Multiplier
2.974000	Inner Ring Outer Diameter
3.784000	Outer Ring Inner Diameter
4.331000	Outer Ring Outer Diameter
4.331000	Carrier/Hsg Inner Diameter
9.3000002E-02	Outer Ring/Hsg Axial Gap
73400.00	Preload Spring Stiffness

BALL BRG
0.6250000	Ball Diameter
2.0000001E-03	Diametral Clearance
0.5300000	Outer Raceway Curvature
0.5200000	Inner Raceway Curvature

MATL PROP
440C	Shaft Material
52100	Inner Ring Material
52100	Elements Material
52100	Outer Ring Material
52100	Car/Hsng Material
3.0000000E+07	Shaft Elastic Modulus
3.0000000E+07	Inner Ring Elastic Modulus
3.0000000E+07	Elements Elastic Modulus
3.0000000E+07	Outer Ring Elastic Modulus
3.0000000E+07	Car/Hsng Elastic Modulus
0.3000000	Shaft Poisson Ratio
0.3000000	Inner Ring Poisson Ratio
0.3000000	Elements Poisson Ratio
0.3000000	Outer Ring Poisson Ratio
0.3000000	Car/Hsng Poisson Ratio
0.2830000	Shaft Density
0.2830000	Inner Ring Density
0.2830000	Elements Density
0.2830000	Outer Ring Density
0.2830000	Car/Hsng Density
8.0000000E-06	Shaft Thermal Exp Coeff
8.0000000E-06	Inner Ring Thermal Exp Coeff
8.0000000E-06	Elements Thermal Exp Coeff
8.0000000E-06	Outer Ring Thermal Exp Coeff
8.0000000E-06	Car/Hsng Thermal Exp Coeff

TEMP DATA
70.00000	Shaft Temperature
70.00000	Inner Ring Temperature
70.00000	Elements Temperature
70.00000	Outer Ring Temperature
70.00000	Car/Hsng Temperature

LOADS
828.0000	X-Axis (Thrust) Force
0.0000000E+00	Y-Axis Force
600.00000	Z-Axis Force
1500.000	XZ-plane Moment (About Y)
0.0000000E+00	XY-plane Moment (About Z)

The two bearing tests were conducted at A zone in Ed Mack's lab. The first one on 6-17-94, the second on 6-21-94.

Calibration of load cells by using voltage substition. 0 mvdc and 1800 lbf eqivalent voltage were sent to the DATRONIC adc set up. A PC was used to capture test data. After 0 and 1800 lbf cal, with all load off - zero all load channels. 1800 lbf cal voltage = load cell sensitivity / 3000 X 1800 with exitation adjusted to 10.00vdc.

Calibration of Bently probes by applying various thickness of shims and record output voltages. Shims used : 0.010", 0.015", 0.020", 0.029", 0.039" 0.048" and 0.059".

Test data were taken 5 times on each load condition(case). Loads were applied incrementally to improve repeatability. Light taps were made to cable, supports to release any stiction. Max load was reduced from 3000 to 1800 lbf due to cable yielding at about 2000 lbf.

Dave Merchant and ~~Wilt wax~~ Wil Holzmann reviewed the raw Bently voltage outputs on each case after the 1st bearing test. It was determined that the data seemed to consistant enough that we will go into the 2nd bearing test.

Removal of 1st bearing was difficult. LN2 was used to freeze the center shaft but not conduct enough to the bearing mounting area. 3 screws were used in the fixture to force the outter race of the bearing. Eventually the outter race broke off with the inner race not responding. Finally a hub puller was found and used to pull off the rest of the bearing.

The 2nd bearing was installed after freezing the mounting shaft in LN2 for 30 minutes. The bearing slided into place with no apparent effort.

Calibration of the load cells went smoothly just like the first one. But the calibration of the Bently was not successful. It was determined that the probe when back off close to its mounting location would induced interference in calibration. Thinner target disc was used to minimize backing when cal to thicker shims. This approach seemed to improve reading except the 0.048" and 0.059" cals looked "round off". With the probes set at about 0.029" to begin testing - the probes are stationary with respect to their mounting environments. This condition was later discussed with Wilt and agreed that the last 2 calibration points would normalized to the 1st bearing cal, then process the test data.

It is discoverred that the two bearing test set up were slightly different. There was no aluminum retaining ring on the first bearing. Pointing the Bently probes directly at the alunimum ring resulted in very large step voltage output, e.g. at 0.020" read 12.27V and at 0.029" read 16.16V. There for the thin target discs were used.

The following is the brief description of files generated:

READ.ME - This file.
BENTCAL.WQ1 - The Quarttro file of the 2 bearing test's Bently probe cals.
RAWBEAR1.DAT - Raw data taken on PC for bearing test 1.
BEARING1.DAT - Raw data "clean up" to just one data entry per load case sin
               data is very stable during each case load. Test 1.
LINBEAR1.FRN - Linearized data after ran through Russ Miller's BENT_LIN.bas
               program using calibration file BCAL.cal. Test 1.
BCAL1.CAL - Bently cal. Test 1.
BEARING1.WQ1 - Quattro file with LINBEAR1.FRN imported with headings. Test
BCAL2.CAL - Bently cal. Test 2 with the last two thickness shim output
            reading "normalized" from the first calibration.

10-6

```
5,7
0.01 ,  0.015 ,   0.02 ,  0.029 ,  0.039 ,   0.048 ,   0.059
5.61 ,   6.70 ,   7.96 ,  10.03 ,  12.12 ,   13.89 ,   15.31
5.47 ,   6.65 ,   7.90 ,  10.26 ,  12.26 ,   14.00 ,   15.72
4.45 ,   5.56 ,   6.83 ,   9.37 ,  11.42 ,   12.96 ,   14.50
1.56 ,   2.37 ,   3.44 ,   5.50 ,   7.41 ,    9.26 ,   11.38
```

57613.4 ,	0.0293 ,	0.0261 ,	0.0281 ,	0.0340 ,	62 ,	61 ,	61 ,	
58178.7 ,	0.0241 ,	0.0287 ,	0.0328 ,	0.0267 ,	59 ,	59 ,	59 ,	60
58692.9 ,	0.0213 ,	0.0296 ,	0.0341 ,	0.0237 ,	61 ,	61 ,	61 ,	180
59503.0 ,	0.0457 ,	0.0221 ,	0.0227 ,	0.0502 ,	600 ,	116 ,	116 ,	60
62755.1 ,	0.0230 ,	0.0257 ,	0.0291 ,	0.0280 ,	301 ,	300 ,	302 ,	60
63128.2 ,	0.0197 ,	0.0272 ,	0.0317 ,	0.0238 ,	301 ,	301 ,	301 ,	180
63377.7 ,	0.0292 ,	0.0280 ,	0.0313 ,	0.0318 ,	0 ,	0 ,	0 ,	
63954.9 ,	0.0236 ,	0.0289 ,	0.0335 ,	0.0260 ,	61 ,	60 ,	59 ,	60
64485.8 ,	0.0207 ,	0.0299 ,	0.0347 ,	0.0231 ,	60 ,	59 ,	59 ,	180
65201.4 ,	0.0459 ,	0.0220 ,	0.0226 ,	0.0505 ,	599 ,	114 ,	114 ,	60
66303.3 ,	0.0229 ,	0.0257 ,	0.0293 ,	0.0279 ,	301 ,	301 ,	300 ,	5=
66790.8 ,	0.0198 ,	0.0272 ,	0.0316 ,	0.0240 ,	300 ,	300 ,	301 ,	180
66917.1 ,	0.0291 ,	0.0281 ,	0.0317 ,	0.0315 ,	0 ,	0 ,	0 ,	
67328.5 ,	0.0233 ,	0.0293 ,	0.0335 ,	0.0258 ,	61 ,	60 ,	59 ,	60
68044.3 ,	0.0204 ,	0.0302 ,	0.0349 ,	0.0226 ,	61 ,	60 ,	60 ,	17=
68425.8 ,	0.0452 ,	0.0221 ,	0.0227 ,	0.0499 ,	600 ,	113 ,	114 ,	60
69455.8 ,	0.0231 ,	0.0258 ,	0.0289 ,	0.0282 ,	300 ,	299 ,	299 ,	60
69764.4 ,	0.0197 ,	0.0273 ,	0.0316 ,	0.0239 ,	301 ,	302 ,	301 ,	180
70216.0 ,	0.0237 ,	0.0291 ,	0.0332 ,	0.0261 ,	60 ,	60 ,	59 ,	60
70426.0 ,	0.0207 ,	0.0301 ,	0.0345 ,	0.0230 ,	59 ,	58 ,	60 ,	180
70754.3 ,	0.0453 ,	0.0221 ,	0.0227 ,	0.0499 ,	602 ,	115 ,	114 ,	6=
71145.6 ,	0.0232 ,	0.0257 ,	0.0289 ,	0.0282 ,	300 ,	300 ,	301 ,	6=
71434.0 ,	0.0196 ,	0.0273 ,	0.0317 ,	0.0238 ,	301 ,	301 ,	301 ,	180
71572.7 ,	0.0292 ,	0.0281 ,	0.0316 ,	0.0316 ,	0 ,	0 ,	0 ,	
71837.0 ,	0.0240 ,	0.0289 ,	0.0330 ,	0.0265 ,	61 ,	60 ,	60 ,	60
72361.7 ,	0.0212 ,	0.0298 ,	0.0342 ,	0.0235 ,	60 ,	60 ,	61 ,	180
72795.8 ,	0.0456 ,	0.0221 ,	0.0227 ,	0.0501 ,	599 ,	115 ,	115 ,	6=
73355.2 ,	0.0238 ,	0.0253 ,	0.0287 ,	0.0289 ,	301 ,	298 ,	298 ,	5=
73831.5 ,	0.0201 ,	0.0271 ,	0.0312 ,	0.0244 ,	302 ,	299 ,	301 ,	180
73961.0 ,	0.0292 ,	0.0280 ,	0.0316 ,	0.0317 ,	0 ,	0 ,	0 ,	

NO DEADBAND

BEARING TEST NO. 1 @ A ZONE 6-17-94

(5 runs were performed on each case.)

B1....B4 converted to INCH

L1....L4 in LBf

VIEW LOOKING DOWN
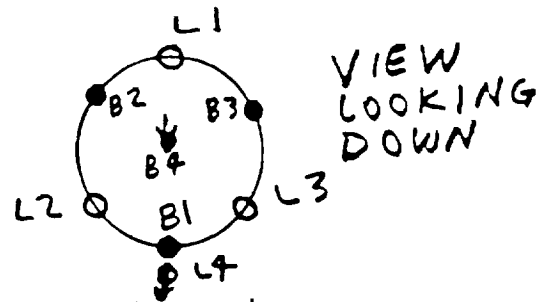
L → load cells
B → deflection gages

TIME	B1	B2	B3	B4	L1	L2	L3	L4	CASE
~~57619.4~~	~~0.0293~~	~~0.0261~~	~~0.0281~~	~~0.0340~~	~~62~~	~~61~~	~~61~~	~~0~~	
58178.7	0.0241	0.0287	0.0328	0.0267	59	59	59	600	5
58692.9	0.0213	0.0296	0.0341	0.0237	61	61	61	1801	4
59503.0	0.0457	0.0221	0.0227	0.0502	600	116	116	602	6
62755.1	0.0230	0.0257	0.0291	0.0280	301	300	302	600	2
63128.2	0.0197	0.0272	0.0317	0.0238	301	301	301	1803	1
63377.7	0.0292	0.0280	0.0313	0.0318	0	0	0	0	0
63954.9	0.0236	0.0289	0.0335	0.0260	61	60	59	601	5
64485.8	0.0207	0.0299	0.0347	0.0231	60	59	59	1802	4
65201.4	0.0459	0.0220	0.0226	0.0505	599	114	114	604	6
66303.3	0.0229	0.0257	0.0293	0.0279	301	301	300	599	2
66790.8	0.0198	0.0272	0.0316	0.0240	300	300	301	1800	1
66917.1	0.0291	0.0281	0.0317	0.0315	0	0	0	0	0
67328.5	0.0233	0.0293	0.0335	0.0258	61	60	59	601	5
68044.3	0.0204	0.0302	0.0349	0.0226	61	60	60	1798	4
68425.8	0.0452	0.0221	0.0227	0.0499	600	113	114	601	6
69455.8	0.0231	0.0258	0.0289	0.0282	300	299	299	600	2
69764.4	0.0197	0.0273	0.0316	0.0239	301	302	301	1802	1
70216.0	0.0237	0.0291	0.0332	0.0261	60	60	59	600	5
70426.0	0.0207	0.0301	0.0345	0.0230	59	58	60	1801	4
70754.3	0.0453	0.0221	0.0227	0.0499	602	115	114	600	6
71145.6	0.0232	0.0257	0.0289	0.0282	300	300	301	602	2
71434.0	0.0196	0.0273	0.0317	0.0238	301	301	301	1800	1
71572.7	0.0292	0.0281	0.0316	0.0316	0	0	0	0	0
71837.0	0.0240	0.0289	0.0330	0.0265	61	60	60	600	5
72361.7	0.0212	0.0298	0.0342	0.0235	60	60	61	1801	4
72795.8	0.0456	0.0221	0.0227	0.0501	599	115	115	601	6
73355.2	0.0238	0.0253	0.0287	0.0289	301	298	298	599	2
73831.5	0.0201	0.0271	0.0312	0.0244	302	299	301	1800	1
73961.0	0.0292	0.0280	0.0316	0.0317	0	0	0	0	0

```
5,7
0.01  ,  0.015 ,   0.02  ,  0.029 ,  0.039 ,  0.048 ,  0.059
5.87  ,   6.71 ,   7.85  ,  10.02 ,  11.92 ,  13.69 ,  15.11
5.53  ,   6.60 ,   7.80  ,   9.96 ,  11.70 ,  13.44 ,  15.16
4.45  ,   5.56 ,   7.09  ,   9.08 ,  10.77 ,  12.31 ,  13.85
1.69  ,   2.61 ,   3.61  ,   5.18 ,   6.98 ,   8.94 ,  11.23
```

|								
49121.9 ,	0.0250 ,	0.0272 ,	0.0305 ,	0.0275 ,	0 ,	0 ,	0 ,	0
49533.3 ,	0.0239 ,	0.0252 ,	0.0280 ,	0.0252 ,	61 ,	60 ,	59 ,	1800
49978.6 ,	0.0233 ,	0.0260 ,	0.0271 ,	0.0228 ,	61 ,	61 ,	59 ,	1800
50536.8 ,	0.0462 ,	0.0107 ,	0.0000 ,	0.0000 ,	601 ,	113 ,	114 ,	601
51267.6 ,	0.0345 ,	0.0189 ,	0.0155 ,	0.0438 ,	302 ,	298 ,	299 ,	600
51886.9 ,	0.0244 ,	0.0247 ,	0.0207 ,	0.0289 ,	301 ,	298 ,	298 ,	1800
52012.0 ,	0.0260 ,	0.0268 ,	0.0275 ,	0.0292 ,	0 ,	0 ,	0 ,	0
52324.3 ,	0.0228 ,	0.0271 ,	0.0257 ,	0.0254 ,	61 ,	59 ,	59 ,	601
52855.0 ,	0.0225 ,	0.0275 ,	0.0254 ,	0.0229 ,	60 ,	59 ,	60 ,	1802
53242.1 ,	0.0460 ,	0.0114 ,	0.0000 ,	0.0000 ,	602 ,	115 ,	113 ,	601
54257.9 ,	0.0299 ,	0.0209 ,	0.0166 ,	0.0401 ,	303 ,	297 ,	299 ,	601
54648.6 ,	0.0230 ,	0.0254 ,	0.0205 ,	0.0278 ,	299 ,	299 ,	299 ,	1799
54765.9 ,	0.0265 ,	0.0260 ,	0.0276 ,	0.0301 ,	0 ,	0 ,	0 ,	C
55085.9 ,	0.0229 ,	0.0270 ,	0.0260 ,	0.0257 ,	61 ,	60 ,	59 ,	599
55427.0 ,	0.0227 ,	0.0274 ,	0.0257 ,	0.0232 ,	60 ,	60 ,	59 ,	1801
55797.6 ,	0.0459 ,	0.0102 ,	0.0000 ,	0.0000 ,	599 ,	115 ,	114 ,	601
56398.3 ,	0.0316 ,	0.0197 ,	0.0164 ,	0.0416 ,	302 ,	300 ,	299 ,	601
56782.1 ,	0.0239 ,	0.0245 ,	0.0206 ,	0.0288 ,	301 ,	301 ,	300 ,	1801
56931.3 ,	0.0282 ,	0.0280 ,	0.0233 ,	0.0335 ,	0 ,	0 ,	0 ,	C
57141.6 ,	0.0234 ,	0.0265 ,	0.0259 ,	0.0264 ,	61 ,	60 ,	59 ,	599
57460.7 ,	0.0224 ,	0.0273 ,	0.0256 ,	0.0230 ,	61 ,	59 ,	61 ,	1800
57748.7 ,	0.0461 ,	0.0108 ,	0.0000 ,	0.0000 ,	600 ,	115 ,	115 ,	602
58041.7 ,	0.0316 ,	0.0203 ,	0.0159 ,	0.0415 ,	302 ,	300 ,	300 ,	600
58216.6 ,	0.0217 ,	0.0257 ,	0.0208 ,	0.0262 ,	301 ,	300 ,	298 ,	1802
58338.6 ,	0.0252 ,	0.0281 ,	0.0265 ,	0.0291 ,	0 ,	0 ,	0 ,	C
58734.0 ,	0.0238 ,	0.0267 ,	0.0257 ,	0.0267 ,	61 ,	60 ,	59 ,	601
58873.3 ,	0.0249 ,	0.0270 ,	0.0254 ,	0.0256 ,	60 ,	60 ,	59 ,	1802
59283.9 ,	0.0458 ,	0.0118 ,	0.0000 ,	0.0000 ,	602 ,	113 ,	114 ,	603
59657.1 ,	0.0385 ,	0.0177 ,	0.0127 ,	0.0486 ,	302 ,	300 ,	299 ,	599
60050.6 ,	0.0289 ,	0.0240 ,	0.0183 ,	0.0353 ,	302 ,	300 ,	301 ,	1803
60181.3 ,	0.0294 ,	0.0253 ,	0.0243 ,	0.0350 ,	0 ,	0 ,	0 ,	C

0.0001" DEAD BAND

BEARING TEST NO. 2 @ A ZONE 6-20-94
(5 runs were performed on each case.)
B1....B4 converted to INCH
L1....L4 in LBf

VIEW LOOKING DOWN
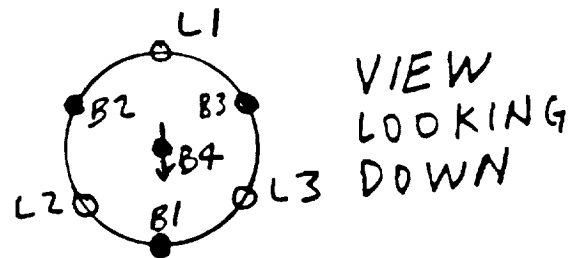
L → load cells
B → deflection gages

TIME	B1	B2	B3	B4	L1	L2	L3	L4	CASE
49121.9	0.0250	0.0272	0.0305	0.0275	0	0	0	0	0
49533.3	0.0239	0.0252	0.0280	0.0252	61	60	59	600	5
49978.6	0.0233	0.0260	0.0271	0.0228	61	61	59	1800	4
50536.8	0.0462	0.0107	0.0000	0.0000	601	113	114	601	6
51267.6	0.0345	0.0189	0.0155	0.0438	302	298	299	600	2
51886.9	0.0244	0.0247	0.0207	0.0289	301	298	298	1800	1
52012.0	0.0260	0.0268	0.0275	0.0292	0	0	0	0	0
52324.3	0.0228	0.0271	0.0257	0.0254	61	59	59	601	5
52855.0	0.0225	0.0275	0.0254	0.0229	60	59	60	1802	4
53242.1	0.0460	0.0114	0.0000	0.0000	602	115	113	601	6
54257.9	0.0299	0.0209	0.0166	0.0401	303	297	299	600	2
54648.6	0.0230	0.0254	0.0205	0.0278	299	299	299	1799	1
54765.9	0.0265	0.0260	0.0276	0.0301	0	0	0	0	0
55085.9	0.0229	0.0270	0.0260	0.0257	61	60	59	599	5
55427.0	0.0227	0.0274	0.0257	0.0232	60	60	59	1801	4
55797.6	0.0459	0.0102	0.0000	0.0000	599	115	114	601	6
56398.3	0.0316	0.0197	0.0164	0.0416	302	300	299	601	2
56782.1	0.0239	0.0245	0.0206	0.0288	301	301	300	1801	1
56931.3	0.0282	0.0280	0.0233	0.0335	0	0	0	0	0
57141.6	0.0234	0.0265	0.0259	0.0264	61	60	59	599	5
57460.7	0.0224	0.0273	0.0256	0.0230	61	59	61	1800	4
57748.7	0.0461	0.0108	0.0000	0.0000	600	115	115	602	6
58041.7	0.0316	0.0203	0.0159	0.0415	302	300	300	600	2
58216.6	0.0217	0.0257	0.0208	0.0262	301	300	298	1802	1
58338.6	0.0252	0.0281	0.0265	0.0291	0	0	0	0	0
58734.0	0.0238	0.0267	0.0257	0.0267	61	60	59	601	5
58973.3	0.0249	0.0270	0.0254	0.0256	60	60	59	1802	4
59283.9	0.0458	0.0118	0.0000	0.0000	602	113	114	603	6
59657.1	0.0385	0.0177	0.0127	0.0486	302	300	299	599	2
60050.6	0.0289	0.0240	0.0183	0.0353	302	300	301	1803	1
60181.3	0.0294	0.0253	0.0243	0.0350	0	0	0	0	0

10-12

BENTLY PROBE CALIBRATION
6-17-94

Legend: B1, B2, B3, B4

X-axis: POSITION (INCH)
Y-axis: OUTPUT VOLTAGE (VOLTS)

BENTLY PROBE CALIBRATION
6-20-94

Legend: B1, B2, B3, B4

X-axis: POSITION (INCH) — 0.01, 0.015, 0.02, 0.025, 0.03, 0.035, 0.04, 0.045, 0.05, 0.055, 0.06

Y-axis: OUTPUT VOLTAGE (VOLTS) — 0, 2, 4, 6, 8, 10, 12, 14, 16

10-14
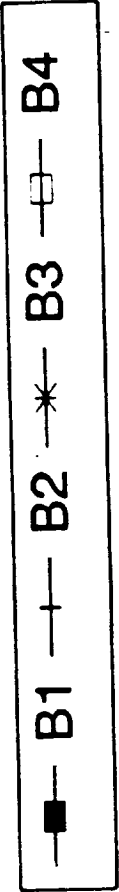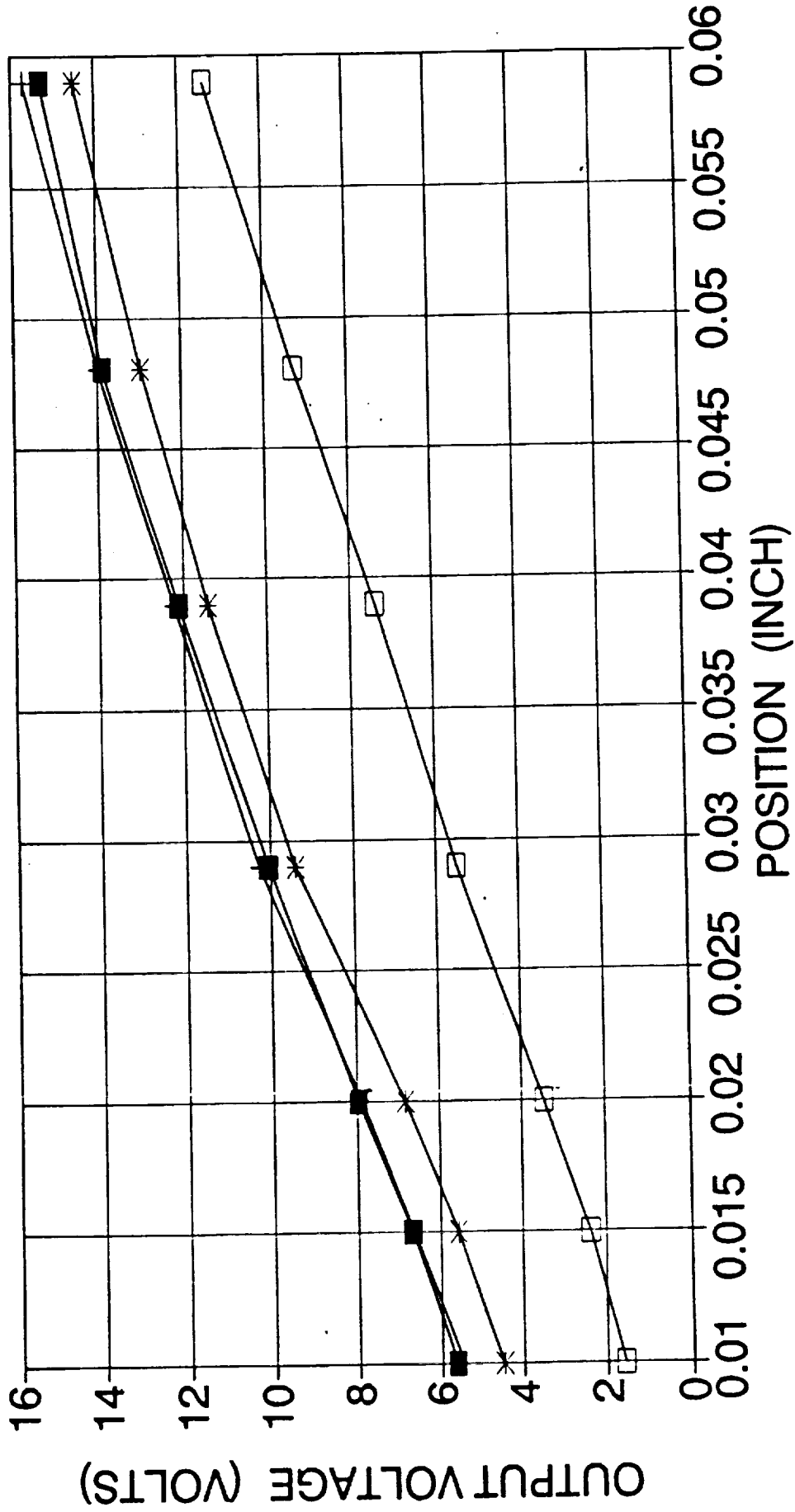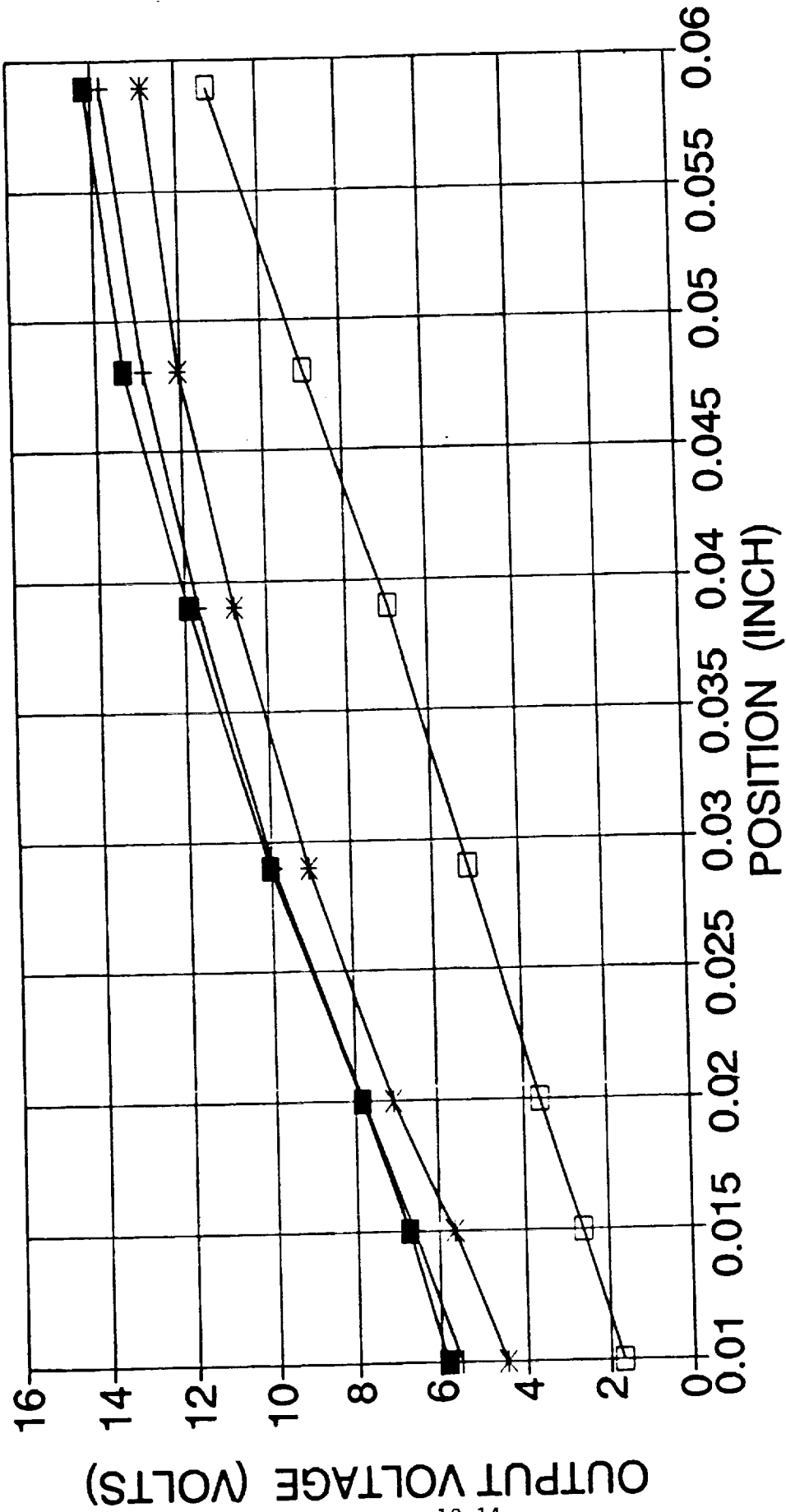
Bearing Test

F.S. w/ E = 10.00V , 3000 lbs

Load		
1	168.6 mV	
2	187.6 mV	
3	208.2 mV	
4	180.1 mV	
5	not used	

1	0.1012V
2	0.1126V
3	0.1249V
4	0.1081V

Calibrate load cells at zero & 1800 lbf

Bently (displacement) Calibration

	0.010	0.015	0.020	0.029	0.039	0.048	0.059
B1	5.61	6.70	7.96	10.03	12.12	13.89	15.31
B2	5.47	6.65	7.90	10.26	12.26	14.00	15.72
B3	4.45	5.56	6.83	9.37	11.42	12.96	15.02 14
B4	1.56	2.37	3.44	5.50	7.41	9.26	11.38

Bearing 1 test data : C:\Bearing\Bearing1.D:

Case

	60	60	60	Ø
5	✓	✓	✓	✓
4	✓	✓	✓	✓
6	✓	✓	✓	✓
2	✓	✓	✓	✓
1	✓	✓	✓	✓
Ø	✓	✓	✓	✓

All Ø → Ø

Bearing 2 test data : C:\Bearing\Bearing2.DAT

Bentley probe Calibration (6-20-94)

	0.010	0.015	0.020	0.029	0.039	0.048	0.059
B1	3.94	4.38	4.90	5.16			
B2	4.15	4.85	5.13	5.99			
B3	3.65	4.65	5.56	6.14	7.10		
B4	1.69	2.61	3.61	5.18	6.98	8.94	11.23

		0.010	0.015	0.020	0.029	0.039	0.048	0.059
	B1	5.87	6.71	7.85	10.02	11.92	13.36 13.69	14.15 15
	B2	5.53	6.60	7.80	9.96	11.70	12.89 13.14	13.87 15.1
mAl:	B3	9.01	10.53	12.27	16.16			
	B3	4.02	4.78	5.66	7.17	7.67	12.31	13
New shim thinner	B3	4.45	5.66	7.09	9.08	10.77	12.03	12.79

2nd Bearing Test

∅   ✓ ✓ ✓ ✓ ✓ ✓
Case 5   ✓ ✓ ✓ ✓ ✓
4   ✓ ✓ ✓ ✓ ✓
6   ✓ ✓ ✓ ✓ ✓
2   ✓ ✓ ✓ ✓ ✓
1   ✓ ✓ ✓ ✓ ✓

GAUSS CODE TO CALCULATE FEREBA INPUT LOADS

```
/*
           file BFORCE.PRC        DHM        7-16-94

This GAUSS code transforms the forces applied to the bearing
tester to FEREBA forces and moments at the inner ring/shaft
for post-test correlation as part of the ROLLING ELEMENT
BEARING MECHANICS contract with MSFC.

INPUT
*/

        R = ZEROS(4,4);
        R[1,1]  =   1.0;
        R[1,2]  =   1.0;
        R[1,3]  =   1.0;
        R[2,4]  =   1.0;
        R[3,1]  =   3.600;
        R[3,2]  =  -1.800;
        R[3,3]  =  -1.800;
        R[3,4]  =  -0.15;
        R[4,2]  =  -3.118;
        R[4,3]  =   3.118;

        L = ZEROS(4,1);
        L[1,1]  = 608.8;   /* AVG L1 FORCE FOR CASE 6 TEST 2 */
        L[2,1]  = 122.0;   /* AVG L3 FORCE FOR CASE 6 TEST 2 */
        L[3,1]  = 122.2;   /* AVG L2 FORCE FOR CASE 6 TEST 2 */
        L[4,1]  = 601.6;   /* AVG L4 FORCE FOR CASE 6 TEST 2 */

/*
CALCULATE FEREBA FORCES AND MOMENTS
*/
        FFM = R*L;
/*
OUTPUT DATA
*/
        OUTPUT FILE = BFORCE.OUT;
        OUTPUT RESET;
        FORMAT /M1 /RD 12,4;

        PRINT FFM;
        PRINT;
        PRINT;
        PRINT;
        PRINT R;
        PRINT;
        PRINT L;
        OUTPUT OFF;
```

CALCULATED FEREBA INPUT LOADS FROM GAUSS CODE

FILE BFORCE.OUT   DHM   7-18-94

FEREBA APPLIED FORCES AND MOMENTS FOR TEST 2   (CASE 6)

```
        FFM
   853.0000
   601.6000
  1661.8800
     0.6236


        R
   1.0000        1.0000        1.0000        0.0000
   0.0000        0.0000        0.0000        1.0000
   3.6000       -1.8000       -1.8000       -0.1500
   0.0000       -3.1180        3.1180        0.0000

        L
   608.8000
   122.0000
   122.2000
   601.6000
```

GAUSS CODE TO CALCULATE "MEASURED" SHAFT DISPLACEMENTS

```
/*

        file BDEFLA1.PRC        DHM        7-16-94

This GAUSS code calculates the inner ring/shaft deflections
in FEREBA coordinates from positions measured in the bearing
static test performed as part of the ROLLING ELEMENT BEARING
MECHANICS contract with MSFC.

This program is hardwired for load case 1 of test A without
deadband.

INPUT
*/
      R = ZEROS(4,4);   /*  MRDV = R*FDEFL  */
      R[1,1] = 1.0;
      R[2,1] = 1.0;
      R[3,1] = 1.0;
      R[4,2] = 1.0;
      R[1,3] = - 1.993;
      R[2,3] =   0.997;
      R[3,3] =   0.997;
      R[4,3] = - 2.10;
      R[2,4] = - 1.726;
      R[3,4] =   1.726;
       RINV = INV(R);

      B = ZEROS(4,5);   /*  LOADED POSITIONS FOR 5 TRIALS IN
           LOAD CASE 1 IN FEREBA COORDINATES  */
      B[1,1] = 0.0197;  /*  POSITION AT GAGE B1   */
      B[1,2] = 0.0198;
      B[1,3] = 0.0197;
      B[1,4] = 0.0196;
      B[1,5] = 0.0201;
      B[2,1] = 0.0317;  /*  POSITION AT GAGE B2   */
      B[2,2] = 0.0316;
      B[2,3] = 0.0316;  /*  GAGE B3 IN TEST   */
      B[2,4] = 0.0317;
      B[2,5] = 0.0312;
      B[3,1] = 0.0272;  /*  POSITION AT GAGE B3   */
      B[3,2] = 0.0272;
      B[3,3] = 0.0273;  /*  GAGE B2 IN TEST   */
      B[3,4] = 0.0273;
      B[3,5] = 0.0271;
```

```
            B[4,1] = 0.0238;   /*   POSITION AT GAGE B4   */
            B[4,2] = 0.0240;
            B[4,3] = 0.0239;
            B[4,4] = 0.0238;
            B[4,5] = 0.0244;

        B0 = ZEROS(4,5);   /*   UNLOADED POSITIONS FOR 5 TRIALS
            OF ALL LOAD CASES IN FEREBA COORDINATES   */
        B0[1,1] = 0.0292;   /*   POSITION AT GAGE B1   */
        B0[1,2] = 0.0291;
        B0[1,3] = 0.02918;
        B0[1,4] = 0.0292;
        B0[1,5] = 0.0292;
        B0[2,1] = 0.0313;   /*   POSITION AT GAGE B2   */
        B0[2,2] = 0.0317;
        B0[2,3] = 0.03155;  /*   GAGE B3 IN TEST   */
        B0[2,4] = 0.0316;
        B0[2,5] = 0.0316;
        B0[3,1] = 0.0280;   /*   POSITION AT GAGE B3   */
        B0[3,2] = 0.0281;
        B0[3,3] = 0.02805;  /*   GAGE B2 IN TEST   */
        B0[3,4] = 0.0281;
        B0[3,5] = 0.0280;
        B0[4,1] = 0.0318;   /*   POSITION AT GAGE B4   */
        B0[4,2] = 0.0315;
        B0[4,3] = 0.03165;
        B0[4,4] = 0.0316;
        B0[4,5] = 0.0317;

/*
CALCULATE MEAN RELATIVE DEFLECTION VECTOR FOR THIS LOAD CASE
*/
        MRDV = ZEROS(4,1);
        i = 1;
        DO WHILE i LE 4;
            j = 1;
            SUM = 0.0;
            DO WHILE j LE 5;
                SUM = SUM + B0[i,j] - B[i,j];
                j = j + 1;
            ENDO;
            MRDV[i,1] = SUM*0.2;
            i = i + 1;
        ENDO;

/*
CALCULATE FEREBA DEFLECTIONS FOR THIS LOAD CASE
*/
        FDEFL = RINV*MRDV;
```

```
/*
OUTPUT DATA FOR THIS LOAD CASE
*/
        OUTPUT FILE = BDEFLA1.OUT;
        OUTPUT RESET;
        FORMAT /M1 /RD 12,4;

        PRINT FDEFL;
        PRINT;
        PRINT;
        PRINT B;
        PRINT;
        PRINT MRDV;
        PRINT;
        PRINT R;
        PRINT;
        PRINT B0;
        PRINT;
        OUTPUT OFF;
```

CALCULATED "MEASURED" SHAFT DISPLACEMENTS FROM GAUSS CODE

FILE BDEFLA1.OUT   DHM   7-18-94

"MEASURED" SHAFT DEFLECTIONS FOR TEST 1   (CASE 1)

FDEFL
0.0034
0.0014
-0.0030
0.0002

B				
0.0197	0.0198	0.0197	0.0196	0.0201
0.0317	0.0316	0.0316	0.0317	0.0312
0.0272	0.0272	0.0273	0.0273	0.0271
0.0238	0.0240	0.0239	0.0238	0.0244

MRDV
0.0094
-0.0000
0.0008
0.0077

R			
1.0000	0.0000	-1.9930	0.0000
1.0000	0.0000	0.9970	-1.7260
1.0000	0.0000	0.9970	1.7260
0.0000	1.0000	-2.1000	0.0000

B0				
0.0292	0.0291	0.0292	0.0292	0.0292
0.0313	0.0317	0.0316	0.0316	0.0316
0.0280	0.0281	0.0280	0.0281	0.0280
0.0318	0.0315	0.0316	0.0316	0.0317

TABLE 1

TRANSDUCER LOCATIONS FOR BEARING TEST RIG

TRANSDUCER	DIRECTION	XF LOCATION	YF LOCATION	ZF LOCATION
L1	Axial	N/A	0.000	3.600
L2	Axial	N/A	3.118	-1.800
L3	Axial	N/A	-3.118	-1.800
L4	Radial	0.15	N/A	N/A
B1	Axial	N/A	0.000	-1.993
B2	Axial	N/A	1.726	0.997
B3	Axial	N/A	-1.726	0.997
B4	Radial	2.10	N/A	N/A

Notes:

(1) Li refers to load cell while Bi refers to deflection transducer.

(2) The origin of the FEREBA coordinate system is at bearing center.

(3) YF and ZF coordinates obtained from drawings and checked on rig.

(4) XF coordinates measured from rig and subject to +/- 0.10" error.

TABLE 2

TEST RIG AND FEREBA APPLIED LOADS
TEST NO. 1 (NO DEADBAND)

CASE NO.	TEST RIG APPLIED LOADS(1)				FEREBA INPUT LOADS(2)				
	F1 (lb)	F2 (lb)	F3 (lb)	F4 (lb)	Fx (lb)	Fy (lb)	Fz (lb)	My (in-lb)	Mz (in-lb)
1	309.0	309.0	308.6	1801.0	926.6	0.0	1801.0	-269.4	-1.2
2	308.6	308.0	307.6	600.0	924.2	0.0	600.0	-87.1	-1.2
3 (3)	-	-	-	-	-	-	-	-	-
4	68.2	68.2	67.6	1800.6	204.0	0.0	1800.6	-269.0	-1.9
5	68.4	67.2	67.8	600.4	203.4	0.0	600.4	-86.8	1.9
6	608.0	122.6	122.6	601.6	853.2	0.0	601.6	1657.2	0.0

(1) F1, F2, F3 are axial forces which include 24 lb carrier weight preload; F4 is radial.

(2) Fx is axial; Fy and Fz are radial; My is moment about FEREBA Y axis; Mz is about Z.

(3) The requested radial force for Case 3 (3000 lb) could not be achieved by the test rig.

TABLE 3

TEST RIG AND FEREBA APPLIED LOADS

TEST NO. 2 (0.0001" DEADBAND)

CASE NO.	TEST RIG APPLIED LOADS[1]				FEREBA INPUT LOADS[2]				
	F1 (lb)	F2 (lb)	F3 (lb)	F4 (lb)	Fx (lb)	Fy (lb)	Fz (lb)	My (in-lb)	Mz (in-lb)
1	308.8	307.2	307.6	1801.0	923.6	0.0	1801.0	-265.1	1.2
2	310.2	307.2	307.0	600.0	924.4	0.0	600.0	-78.8	-0.6
3[3]	-	-	-	-	-	-	-	-	-
4	68.4	67.6	67.8	1801.0	203.8	0.0	1801.0	-267.6	0.6
5	69.0	67.0	68.0	600.0	204.0	0.0	600.0	-84.6	3.1
6	608.8	122.0	122.2	601.6	853.0	0.0	601.6	1661.9	0.6

(1) F1, F2, F3 are axial forces which include 24 lb carrier weight preload; F4 is radial.

(2) Fx is axial; Fy and Fz are radial; My is moment about FEREBA Y axis; Mz is about Z.

(3) The requested radial force for Case 3 (3000 lb) could not be achieved by the test rig.

TABLE 4

"MEASURED" AND FEREBA SHAFT DISPLACEMENTS

TEST NO. 1 (NO DEADBAND)

CASE NO.	TEST RIG "MEASURED" DISPLACEMENTS[1]				FEREBA OUTPUT DISPLACEMENTS[2]			
	U_x (in)	U_z (in)	θ_y (rad)	θ_z (rad)	U_x (in)	U_z (in)	θ_y (rad)	θ_z (rad)
1	0.0034	0.0014	-0.0030	0.0002	*	*	*	*
2	0.0037	0.0010	-0.0012	0.0000	*	*	*	*
4	0.0012	0.0009	-0.0036	0.0003	0.0020	0.0035	-0.0057	0.0000
5	0.0010	0.0007	-0.0022	0.0002	0.0023	0.0022	-0.0040	0.0000
6	-0.0005	-0.0018	0.0080	-0.0008	*	*	*	*

(1) Equivalent shaft displacements calculated from four measured relative displacements.

(2) Shaft displacements, calculated by FEREBA from equivalent forces applied to test rig, less the axial shaft displacement of 0.0006 inch due to the 24 lb preload. Asterisks indicate that FEREBA did not converge for these load cases.

TABLE 5

"MEASURED" AND FEREBA SHAFT DISPLACEMENTS
TEST NO. 2 (0.0001" DEADBAND)

CASE NO.	TEST RIG "MEASURED" DISPLACEMENTS [1]				FEREBA OUTPUT DISPLACEMENTS [2]			
	U_x (in)	U_z (in)	θ_y (rad)	θ_z (rad)	U_x (in)	U_z (in)	θ_y (rad)	θ_z (rad)
1	0.0036	0.0027	0.0006	-0.0013	*	*	*	*
2	0.0040	-0.0013	0.0053	-0.0011	*	*	*	*
4	0.0014	0.0050	-0.0011	-0.0003	0.0020	0.0036	-0.0059	0.0000
5	0.0014	0.0028	-0.0010	0.0000	0.0023	0.0023	-0.0042	0.0001
6 [3]	-	-	-	-	-	-	-	-

(1) Equivalent shaft displacements calculated from four measured relative displacements.

(2) Shaft displacements, calculated by FEREBA from equivalent forces applied to test rig, less the axial shaft displacement of 0.0006 inch due to the 24 lb preload. Asterisks indicate that FEREBA did not converge for these load cases.

(3) Equivalent shaft displacements can not be determined because transducer measurements B3 and B4 are not available for this case.

NASA

National Aeronautics and
Space Administration

REPORT DOCUMENTATION PAGE

1. Report No.	2. Government Accession No.	3. Recipient's Catalog No.

4. Title And Subtitle

Modeling of Rolling Element Bearing Mechanics

5. Report Date
October 1994

6. Performing Organization Code

7. Author(s)

D. H. Merchant
L. M. Greenhill

8. Performing Organization Report No.

10. Work Unit No.

9. Performing Organization Name and Address

Aerojet
P.O. Box 13222
Sacramento, CA 95813-6000

11. Contract or Grant No.
NAS 8-38607

13. Type of Report and Period Covered
Final Report - Theoretical Manual

12. Sponsoring Agency Name and Address

National Aeronautics and Space Administration
George C. Marshall Space Flight Center
Marshall Space Flight Center, Alabama 35812

14. Sponsoring Agency Code

15. Supplementary Notes

Theoretical model definition and documentation for the described rolling element bearing analysis codes were led by Aerojet, with support from Rotordynamics-Seal Research, North Highlands, CA.

The NASA technical monitor is S. Ryan, MSFC/ED14.

16. Abstract

This report documents the theoretical basis for the Rolling Element Bearing Analysis System (REBANS) analysis code which determines the quasi-static response to external loads or displacement of three types of high-speed rolling element bearings: angular contact ball bearings, duplex angular contact ball bearings, and cylindrical roller bearings. The model includes the effects of bearing ring and support structure flexibility. It is comprised of two main programs: the Preprocessor for Bearing Analysis (PREBAN) which creates the input files for the main analysis program, and Flexibility Enhanced Rolling Element Bearing Analysis (FEREBA), the main analysis program. This report addresses the input instructions for and features of the computer codes. REBANS extends the capabilities of the SHABERTH (Shaft and Bearing Thermal Analysis) code to include race and housing flexibility, including such effects as dead band and preload springs.

17. Key Words (Suggested by Author(s))

Rolling Element, Bearings, Ball, Roller, Finite Element, Stability, Mechanics, Clearance, Internal Loads, Deadband, Stiffness, Damping

18. Distribution Statement

Unclassified - Unlimited

19. Security Classif. (of this report)	20. Security Classif. (of this page)	21. No. of pages	22. Price
Unclassified	Unclassified	92	

RPT/I0062.149-RDP

NASA FORM 1626 OCT 86

C-2